약학박사학위논문

암 세포 증식과 이동에서의 Lysyl-tRNA Synthetase 와 Aminoacyl-tRNA Synthetase-Interacting Multi-functional Protein2 의 역할 규명

The Effect of Lysyl-tRNA Synthetase and Aminoacyl-tRNA Synthetase-Interacting Multi-functional Protein2 in Cancer Progression and Migration

2012 년 8 월

서울대학교 약학대학원

약학과 의약생명과학전공

김 대 규

Abstract

Aminoacyl-tRNA synthetases (ARSs) are enzymes to catalyze the ligation of amino acids to cognate tRNAs in translation. Among 20 mammalian ARSs, 9 ARSs form the multi-tRNA synthetase complex (MSC) with three non-enzymatic factors for efficient translation. The function of non-enzymatic factors, aminoacyl-tRNA synthetase-interacting multi-functional proteins (AIMPs), is a stabilization of MSC via interaction with their adjacent ARSs. Lysyl-tRNA synthetase (KRS) is the ARS ligating the lysine to $tRNA^{Lys}$. Among the AIMPs, aminoacyl-tRNA synthetase-interacting multi-functional protein2 (AIMP2) is the major scaffolding molecule to stabilize the MSC for enhancing the efficiency of translation. KRS shows the strong binding to AIMP2 in MSC.

KRS enhances the cell migration in membrane through the binding with 67kDa laminin receptor (67LR), dimerized form of p40/37LRP which is one of the ribosomal components. 67LR was well reported as a critical factor in cell migration and cancer metastasis. This study elucidates that KRS facilitates cell migration via stabilization of 67LR in normal cells, especially increases the cancer metastasis in cancer cells. Upon laminin signal, KRS, phoshprylated at threonine 52 by p38MAPK, is dissociated from

MSC and translocates to plasma membrane. In membrane, KRS binds to 67LR for inhibiting the approach of Nedd4, E3 ligase of 67LR, resulting the suppression of ubiquitination-mediated turnover of 67LR.

AIMP2, strong binding partner of KRS in MSC, shows the TGF-β signal-mediated tumor suppressor function. TGF-β is the essential antiproliferative cytokine. This study demonstrates the AIMP2 enhances the TGF-β signal, implying the function of tumor suppressor. Upon TGF-β signal, AIMP2 is phosphorylated at serine 156 by p38MAPK and translocated to nucleus from cytosol. In nucleus, AIMP2 facilitates the turnover of Smad7-Smurf2 complex, negative feedback components of TGF-β signal, resulting in stabilization of type I TGF-β receptor. AIMP2 leads to the turnover of FBP, transcription factor of c-myc, through Smurf2-mediated ubiquitination in nucleus.

Through the above two studies, the migration promoting and tumor suppressing effect of KRS and AIMP2, interaction partners in MSC for translation, was unveiled. These investigations suggest KRS and AIMP2 as innovative therapeutic targets to control the cancer metastasis and progression.

Keywords: Lysyl-tRNA synthetase (KRS)/ Laminin receptor/ Laminin signal/ Cell migration/ Aminoacyl-tRNA synthetase-interacting multi-functional protein2 (AIMP2)/ TGF-β signal/ TGF-β receptor I/ Smad7-Smurf2/ FBP/ Cell proliferation

Student number: 2007-30945

Introduction

Aminoacyl-tRNA synthetases (ARSs) are enzymes to ligate the specific amino acids to cognate tRNAs in translation. So, ARSs as a house keeping gene carry out the pivotal role to transfer the exact amino acids for protein synthesis. Among 20 mammalian ARSs, 9 ARSs form the macromolecular complex, multi-tRNA synthetase complex (MSC), with three non-enzymatic factors. Three non-enzymatic factors, aminoacyl-tRNA synthetase-interacting multi-functional proteins (AIMPs), function as a scaffolding protein of MSC via interaction with their adjacent ARSs for efficient translation.

Protein synthesis-associated molecules are well known to relate with disease, especially cancer. Many studies report the abnormal expression or mutations of translational machinery in cancer, implying the significance of translation in cancer. Since cancer cells obtain the enhanced proliferatory character, many studies focused on canonical function, catalytic activity, of translational machinery proteins. Among factors in protein synthesis, translation initiation factors and ribosomal proteins were well studied for long time to understand their function in cancer. Researches about initiation factors and ribosomal proteins in cancer are also centered on elucidating the

facilitated translation for cancer cell progression. Although relationship between many translation-associated proteins and cancer is elucidated, understanding the function of ARSs, one of the pivotal enzymes in protein synthesis, is limited in cancer. Recently, many studies uncovered the changed expression of ARSs in cancerous tissues and showed that ARSs are related with various cancer through the interaction with cancer-associated proteins. Interestingly, functions of ARSs in cancer are independent to their catalytic activity for protein synthesis. So, understanding the non-canonical functions of ARSs in cancer is important to ARS-mediated therapeutic approach to the cancer.

Aminoacyl-tRNA synthetase-interacting multi-functional protein2 (AIMP2) is the major scaffolding protein to stabilize the MSC for enhancing the efficiency of translation. In addition to the role as scaffolding protein, AIMP2 has an anti-proliferative function through the regulation of various signaling pathway. AIMP2 facilitates cell death by stabilization of p53 and degradation of TRAF2 in response to UV stress and TNF-α signal, respectively. Upon proceeding TGF-β signal, AIMP2 induces the degradation of FBP, transcription factor of c-myc, resulting in transcriptional downregulation of c-myc. Also AIMP2 heterogenous mouse shows higher susceptibility to multiple carcinogens for formation of tumor, implying that AIMP2 is a haploinsufficient tumor suppressor. Here, novel role of AIMP2 as the

positive regulator of TGF-β signal via inhibiting negative feedback loop has been proposed. Through regulating negative feedback complex of TGF-β signal, AIMP2 facilitates TGF-β signal-mediated cell cycle arrest, resulting in cell death.

Lysyl-tRNA synthetase (KRS) is the strong interaction partner with AIMP2 in MSC. Through the interaction between KRS and AIMP2, the stability of MSC is increased and translation efficiency is enhanced. The canonical function of KRS is the charging the lysine to $tRNA^{Lys}$. In addition to translation-associated function, KRS has disease-related additional function. Upon immune response, KRS moves to nucleus and binds to transcription factor, MITF, for the induction of the target genes. Also, KRS is secreted from cancer cells to induce the pro-inflammatory response. Interestingly, the expression of KRS is specifically higher in cancerous region than normal region. Although pathologically increased expression of KRS was reported, the reason why the expression of KRS is elevated in cancer is not clear. This report unveils the cancer-associated function of KRS. KRS enhances the laminin-dependent cell migration via stabilization of 67kDa laminin receptor, implying the KRS as pro-migratory proteins.

The interaction of proteins is critical to control the cell viability and mobility. Two researches show that complex forming status of KRS and AIMP2 in MSC contributes the enhanced proliferation via efficient translation. But the signal-dependent

dissociated status of KRS and AIMP2 shows opposite effect, pro-migratory and anti-proliferative function, respectively. So, fine-tuning of interaction between KRS and AIMP2 is critical point to control the disease, especially cancer.

Contents

Abstract ---------- **i**

Introduction ---------- **iv**

Contents ---------- **viii**

Chapter I.

Interaction of Two Translational Components, Lysyl-tRNA Synthetase and p40/37LRP in Plasma Membrane Promotes Cell Migration ------ **ix**

Chapter II.

Tumor Suppressor AIMP2 Regulates Smad7-Smurf2-Mediated Negative Regulation of TGF-β Signaling ---------- **x**

List of figures and tables ---------- **xi**

Abbreviations ---------- **xiii**

국문초록 ---------- **xiv**

Chapter I

Interaction of Two Translational Components, Lysyl-tRNA Synthetase and p40/37LRP in Plasma Membrane Promotes Cell Migration

Title ---------- 1

Abbreviation lists ---------- 2

Abstract ---------- 3

Introduction ---------- 4

Results ---------- 7

Discussion ---------- 42

Materials and Methods ---------- 45

References ---------- 58

Chapter II

Tumor Suppressor AIMP2 Regulates Smad7-Smurf2-Mediated Negative Regulation of TGF-β Signaling

Title ---------- 64

Abbreviation lists ---------- 65

Abstract ---------- 66

Introduction ---------- 67

Results ---------- 70

Discussion ---------- 103

Materials and Methods ---------- 107

References ---------- 114

List of figures and tables

Chapter I

Interaction of Two Translational Components, Lysyl-tRNA Synthetase and p40/37LRP in Plasma Membrane Promotes Cell Migration

Figure I-1. KRS enhances laminin-dependent cell migration ---------- 22

Figure I-2. Interaction between KRS and laminin receptor ---------- 24

Figure I-3. Laminin-induced membrane localization of KRS ---------- 26

Figure I-4. KRS enhances stability of 67LR ---------- 28

Figure I-5. Effect of KRS on transcription, acylation of 37LRP, and integrin levels -- 30

Figure I-6. p38MAPK-mediated phosphorylation is required for laminin-induced dissociation of KRS from the multisynthetase complex ---------- 31

Figure I-7. Determination of p38MAPK-induced phosphorylation site in KRS ------- 33

Figure I-8. Phosphorylation of KRS threonine 52 is too enough to membrane localization ---------- 35

Figure I-9. Nedd4 is the specific E3 ligase of 67LR ---------- 36

Figure I-10. KRS inhibits Nedd4-mediated ubiquitination of 67LR ---------- 38

Figure I-11. Proposed model for cell migration control of KRS via 67LR in plasma membrane ---------- 40

Table I-1. The phosphopeptides of KRS induced by p38MAPK ---------- 41

Chapter II

Tumor Suppressor AIMP2 Regulates Smad7-Smurf2-Mediated Negative Regulation of TGF-β Signaling

Figure II-1. AIMP2 facilitates the TGF-β signal ---------- 85

Figure II-2. Phosphorylation of AIMP2 is required for nuclear translocation ---------- 87

Figure II-3. p38MAPK phosphorylates AIMP2 ---------- 89

Figure II-4. Interaction between AIMP2 and Smad7 ---------- 91

Figure II-5. AIMP2 specifically binds to Smad7 ---------- 93

Figure II-6. Ternary complex formation of AIMP2 with negative feedback complex of TGF-β signal ---------- 94

Figure II-7. AIMP2 enhances auto-ubiquitination of Smurf2 ---------- 96

Figure II-8. Smurf2 functions as E3 ligase of FBP via AIMP2 ---------- 98

Figure II-9. AIMP2 increases TGF-β signal-mediated cell cycle arrest ---------- 100

Figure II-10. Schematic summary of AIMP2-mediated enhancement of TGF-β signal ---------- 102

Abbreviations

MSC: Multi-tRNA synthetase complex

KRS: Lysyl-tRNA synthetase

WRS: Tryptophanyl-tRNA synthetase

MRS: Methionyl-tRNA synthetase

EPRS: Glutamyl-prolyl-tRNA synthetase

67LR: 67kDa laminin receptor

37LRP: 37kDa laminin receptor precursor

AIMP2: ARS-interacting multifunctional protein2

EV: Empty vector

si-con: si-control

WCL: Whole cell lysate

Chapter I

Interaction of Two Translational Components, Lysyl-tRNA Synthetase and p40/37LRP in Plasma Membrane Promotes Cell Migration

Running title: KRS enhances cell migration via 67LR.

Keywords: Lysyl-tRNA synthetase/ 67kDa Laminin receptor/ Laminin signal/ Cell migration/ Metastasis

Abbreviations list

MSC: Multi-tRNA synthetase complex

KRS: Lysyl-tRNA synthetase

WRS: Tryptophanyl-tRNA synthetase

MRS: Methionyl-tRNA synthetase

EPRS: Glutamyl-prolyl-tRNA synthetase

67LR: 67kDa laminin receptor

37LRP: 37kDa laminin receptor precursor

EV: Empty vector

si-con: si-control

WCL: Whole cell lysate

Abstract

Although human lysyl-tRNA synthetase (KRS), an enzyme for protein synthesis, is often highly expressed in various cancer cells, its pathophysiological implications have not been understood. Here novel function of KRS, which induces cancer cell migration through the interaction with 67kDa laminin receptor (67LR) that is converted from ribosomal subunit, p40, was found. Upon laminin signal, KRS was phosphorylated at T52 residue by p38MAPK and dissociated from the cytosolic multi-tRNA synthetase complex for membrane translocation. The importance of T52 phosphorylation for membrane translocation of KRS was confirmed by site-directed mutagenesis. In the membrane, turnover of 67LR was controlled by Nedd4-mediated ubiquitination and KRS inhibited ubiquitin-dependent degradation of 67LR, thereby enhancing laminin-induced cell migration. This work thus unveiled a unique function of KRS in the control of cell migration and its pathological implication in metastasis.

Introduction

Aminoacyl-tRNA synthetases (ARSs) link cognate amino acids and tRNAs for protein synthesis. Interestingly, eukaryotic ARSs have incorporated unique functional domains into their catalytic domains, which have rendered the additional functions besides the canonical catalytic activities (1). Through these additional domains, ARSs form various functional complexes that can execute diverse cell regulatory functions (2). Owing to the functional significance of ARSs as catalysts and also as signal mediators, aberrant expression or mutations of the encoding genes can lead to various human diseases (3). Although the pathophysiological implications of ARSs in tumorigenesis have been suggested (4, 5), understanding how these enzymes are actually involved in the control of tumorigenesis is limited.

Among various protein complexes that can be formed by ARSs, most intriguing complex is a macromolecular complex consisting of nine different cytoplasmic ARSs and three non-enzymatic factors designated AIMP1, 2 and 3 (6-8). While this complex serves as one of the protein synthesis machinery, it also maintains the cellular stability of the components (9) before they are dispatched to ex-translational target sites for other functions (10). Among the components within MSC, lysyl-tRNA synthetase (KRS) is

most functionally versatile and found at various cellular locations (11). For instance, in the nucleus of activated mast cells, KRS was shown to interact with the transcriptional factors such as MITF for the induction of the target genes (12). In addition, KRS can be secreted from some inflammatory cancer cells to induce pro-inflammatory cytokines such as TNF-α (13). Although KRS was also identified in plasma membrane (11, 14-16), its functional implication has not been understood. In this work, it is found that KRS is translocated to plasma membrane in laminin-dependent manner and associates with 67kDa laminin receptor (67LR). The effect of the KRS-67LR interaction on cell behavior and also on the membrane stability of 67LR have been investigated in this work.

67LR is formed by dimerization of its precursor (37kDa laminin receptor precursor; 37LRP) although the conversion process is not completely understood (17). Interestingly, 37LRP is identical to a ribosomal component, p40 that is involved in the formation of polysome for protein synthesis (18). While its precursor works in cytosol as translational component, its dimer form, 67LR, is located in plasma membrane to mediate cell adhesion and migration through the interaction with extracellular matrix, laminin (19-22). Although 67LR is not a typical laminin receptor, it appears to be implicated in a few different pathologic processes. For instance, it serves not only as the

receptor for several pathogenic viruses (23), but is also associated with cancer metastasis (19). For this reason, understanding how its membrane turnover is regulated is important for therapeutic purposes. In this study, novel function of lysyl-tRNA synthetase (KRS), an essential enzyme for protein synthesis, as a positive regulator for the membrane stability of 67LR and cell migration was identified.

Results

KRS mediates laminin-induced cell migration

Although KRS is often highly expressed in various cancer cells and tissues, its pathophysiological meaning was not understood. To have a functional insight into the increased expression of KRS in cancer cells, the expression level of KRS was changed by exogenous supplementation and siRNA-mediated knockdown methods in lung cancer cell, A549 and breast cancer cell, 4T1, and monitored the resulting cell behavior such as proliferation, death and migration. Surprisingly, cell migration was varied depending on the expression level of KRS in the presence of extracellular matrix (ECM) (Figure I-1A). To determine which component of ECM would be specifically involved in the effect of KRS on cell migration, it is repeated the same experiments in the culture medium containing different components of ECM. The effect of KRS expression on cell migration was only apparent in the presence of laminin, but not of collagen or fibronectin (Figure I-1A). In fact, the effect of KRS on cell migration was significantly reduced when the laminin receptor expression was suppressed with its specific siRNA or without laminin (Figure I-1B). Since KRS is secreted as a pro-inflammatory cytokine (13), it was examined whether extracellular KRS would also affect cell migration. When

A549 cells were treated with purified KRS at different concentrations, migration was not affected by extracellular treatment of KRS (Figure I-1C), excluding the extracellular effect of KRS on cell migration. However, changes of KRS level gave little influence on the cell proliferation and death (data not shown).

Laminin induces cell migration via the activation of focal adhesion kinase (FAK) (24, 25). It is evaluated the effect of KRS on migration by the FAK activity (26) that is indicated by the phosphorylation of FAK at Y397 (27) and Y925 (28). The suspended EV- or KRS-transfected A549 cells in serum-free medium were divided into two groups in which one group was kept in suspension culture and the other group was reseeded on the laminin-coated culture dishes. KRS significantly enhanced the FAK activity in the cells cultivated on the laminin-coated culture dishes but not in the suspension culture (Figure I-1D), suggesting that the effect of KRS on migration required the adhesion of the cells to laminin-coated surface. It was also monitored the effect of KRS on cell migration by cell morphology and immunofluorescence staining of actin and FAK after reseeding onto laminin-coated coverslips, which are the known signatures of cell migration. KRS overexpression changed cell morphology, distribution of actin and the activated FAK to a more-branched and spread shape, reflecting the migratory cells (Figure I-1E). As laminin treatment results in the activation of MMP-2

(matrix metalloproteinase-2) (29), it was checked the effect of KRS on the laminin-dependent activation of MMP-2 using zymography. The laminin-induced MMP-2 activity was ablated when KRS was suppressed with its siRNA (Figure I-1F, left), but enhanced by overexpression of KRS (Figure I-1F, right). All of these results suggest that KRS can control laminin-dependent cell migration via 67LR.

Specific interaction of KRS and 67LR in plasma membrane

To understand the molecular mechanism for pro-migratory activity of KRS, cellular proteins that can bind to human KRS were screened by yeast two-hybrid screening using HeLa cell cDNA library. As the baits, it is used the 597aa full-length and 72aa N-terminal eukaryote-specific extension that is thought to be involved in its interactions (30). The full-length KRS bait pulled out AIMP2/p38 (Gene ID: 7965) (31) that is already known to bind KRS in multi-tRNA synthetase complex (MSC) (32) and FANCC-interacting protein (FAZF, Gene ID: 27033). The N-terminal peptide of KRS selected hypoxanthine phosphoribosyltransferase1 (HPRT1, Gene ID: 3251), RPSA (also known as ribosomal subunit p40, Gene ID: 3921) and cyclophilin B (cypB, Gene ID: 5479) as potential KRS-binding proteins. Among them, p40 was attracted attention since p40 is also called 37kDa laminin receptor precursor (37LRP) that is converted to

67kDa laminin receptor (17).

The specific interaction between the full-length KRS and 37LRP was confirmed by yeast two-hybrid assay. LexA-KRS generated blue colonies when paired with B42-37LRP as well as AIMP2, but not with AIMP1, another component of MSC (9) (Figure I-2A). The direct interaction between KRS and laminin receptor (LR) was tested by *in vitro* pull-down assay. GST-KRS and -WRS (tryptophanyl-tRNA synthetase) were reacted with radioactively synthesized 37LRP. 37LRP was co-precipitated with GST-KRS, but not with -WRS (Figure I-2B).

It was then examined whether KRS would bind either or both of 37LRP and 67LR in cells. Myc-KRS was introduced into A549 cells, fractionated plasma membrane from cytoplasm, immunoprecipitated Myc-KRS from each fraction, and subjected the precipitates to immunoblotting with anti-67LR and -37LRP antibodies. While 37LRP and 67LR were mainly detected in the cytosol and membrane fractions, respectively, (Figure I-2C, right), KRS preferentially bound to 67LR in the membrane (Figure I-2C, left). To see the interaction between endogenous KRS and 67LR in A549 cells, KRS was immunoprecipitated and co-precipitation of endogenous 67LR was determined by immunoblotting using the anti-67LR antibody specifically recognizing 67LR. 67LR was co-precipitated with KRS but not with IgG (Figure I-2D, upper).

Conversely, when endogenous 67LR was immunoprecipitated, KRS was specifically precipitated with 67LR but not with IgG (Figure I-2D, lower). Interestingly, the interaction of the two endogenous proteins appeared to be increased in the presence of laminin. To further validate this observation, exogenously introduced Myc-KRS was precipitated from A549 cells that were cultivated in the absence and presence of laminin. The amount of 67LR co-precipitated with Myc-KRS was significantly increased in the presence of laminin (Figure I-2E). It was determined the peptide regions of the two proteins that are involved in interaction. Human KRS was divided into the 219aa N-terminal anticodon-binding and extension, and 378aa C-terminal catalytic domain (33), and 37LRP consists of three functional domains of 88aa (1-88) intracellular, 13aa (89-101) transmembrane and 194aa (102-295) extracellular domains (19) (Figure I-2F). The interaction of full-length (F), N- and C-terminal domains of GST-KRS with GFP-37LRP was tested by *in vitro* pull-down assay. GST-KRS-N as well as GST-KRS-F was co-precipitated with GFP-37LRP (Figure I-2G). Conversely, different domains of GFP-37LRP were subjected to affinity-precipitation with GST-KRS-F. Among the tested LR-fragments, extracellular and transmembrane (E+T) domains bound to KRS (Figure I-2H). Combined together, the N-terminal extended domain of KRS appears to interact with the C-terminal region of LR (Figure I-2F).

Laminin-induced translocation of KRS to plasma membrane

To see whether membrane localization of KRS is induced by laminin, cells were fractionated into cytosol and plasma membrane and the KRS levels were determined by immunoblot at time interval after laminin treatment. The membrane levels of KRS were gradually increased after laminin treatment although the majority of KRS still remained in cytosol (Figure I-3A, top). On the same condition, KRS expression was not changed as determined by RT-PCR (Figure I-3A, bottom). To see the effect of laminin on KRS localization in live cells, GFP-KRS was expressed in A549 cells, treated with laminin or collagen, and monitored the change of KRS localization by fluorescence microscopy. When the cells were treated with laminin, dynamic foci formation of GFP-KRS, but not GFP alone, was observed in the plasma membrane although the majority of KRS still remained in cytosol (Figure I-3B, top and bottom). The membrane foci of GFP-KRS were not observed when the cells were treated with collagen (Figure I-3B, middle). Laminin-induced membrane enrichment of endogenous KRS was also observed by immunofluorescence microscopy (Figure I-3C).

The surface exposure of KRS was examined in A549 cells by flow cytometry with anti-Myc antibody after transfection with Myc-KRS. The amount of exposed KRS

was enhanced approximately two fold by laminin treatment (Figure I-3D, middle). In contrast, the signal was not much changed in the cells that were transfected with EV or Myc-MRS (methionyl-tRNA synthetase) regardless of laminin treatment (Figure I-3D, top and bottom). This suggests that the laminin-dependent surface exposure is specific to KRS. To determine which side of KRS is exposed out of the cells, GFP-tag was fused to the N- or C-terminal end of KRS and introduced into A549 cells. It was incubated the transfected cells in the presence and absence of laminin, labeled unpermeabilized cells with QD625-conjugated to anti-GFP antibody, and visualized by fluorescence. GFP fused to the N-terminal end of KRS gave fluorescence from the laminin-treated cells (Figure I-3E), suggesting that the N-terminal end of KRS should be exposed from the cell membrane.

KRS enhances membrane stability of 67LR

To understand the functional implication for the interaction of KRS with 67LR in membrane, cells were separated into plasma membrane and cytosol, and the changes of 67LR levels in each fraction by various KRS level was examined. The 67LR level in the plasma membrane was enhanced by the increase of KRS, but reduced when KRS was suppressed with its siRNA (Figure I-4A). The positive effect of KRS on the 67LR

membrane level was also observed by flow cytometry (Figure I-4B). KRS also increased the membrane levels of 67LR in different cancer cell types (Figure I-4C), suggesting that the functional connection of KRS with 67LR in cell migration could be applicable to many different cancer cells.

It was investigated how KRS enhances membrane level of 67LR. Transfection of KRS did not increase the LR transcription as determined by semi-quantitative RT-PCR (Figure I-5A), excluding its effect on the transcription of the LR-encoding gene. It was also examined whether KRS would mediate fatty-acylation of 37LRP, known to be required for the conversion of 37LRP to 67LR (34, 35). The acylation of 37LRP was not significantly influenced by the various KRS expression (Figure I-5B). It was also checked the effect of KRS on turnover of 67LR by pulse-chase experiment. Nascent protein synthesis was labeled with radioactive methionine. Disappearance of 67LR was monitored by autoradiography at time interval. 67LR was more rapidly decreased when KRS was suppressed with its siRNA (Figure I-4D). Thus, KRS appears to extend the half-life of 67LR in the plasma membrane through its association with 67LR. Since integrins are the major receptor family of laminin (36), It was tested whether KRS can also affect the membrane levels of different integrins by flow cytometry. None of the tested integrins was influenced by the overexpression of KRS (Figure I-5C), suggesting

that the effect of KRS is specific to 67LR.

Laminin-induced phosphorylation of KRS is involved in membrane localization

Cytosolic KRS is mainly bound to MSC. To see whether the membrane translocation of KRS involves its dissociation from MSC, it was immunoprecipitated MSC from the laminin-untreated and -treated A549 cells using the antibody against EPRS (glutamyl-prolyl-tRNA synthetase), another component of MSC, and determined whether the amount of KRS bound to MSC is reduced by laminin treatment. The amount of KRS co-precipitated with EPRS was decreased by laminin treatment (Figure I-6A, left), while the portion of KRS dissociated from MSC was increased in the immuno-depleted fraction (Figure I-6A, right), suggesting that KRS located in the plasma membrane should be originated from MSC.

KRS was previously known to be translocated into nucleus via phosphorylation (12). It was examined whether phosphorylation is also involved in the laminin-induced membrane translocation of KRS. The purified GST-KRS was mixed with the protein extracts from the laminin-untreated and -treated A549 cells in the presence of [γ-^{32}P] ATP, and the reaction mixtures were subjected to autoradiography. Radioactivity of GST-KRS was detected by the incubation of the extract and significantly increased by

the incubation of laminin-treated cells (Figure I-6B). No radioactivity was observed when GST was reacted with either of the extracts. Since laminin treatment activates PI3K (37, 38), it was determined whether PI3K is involved in the phosphorylation of KRS. Phosphorylation of GST-KRS was performed as above with the protein extracts from A549 cells with and without the treatment of LY294002, the PI3K inhibitor. Laminin-induced phosphorylation of KRS was inhibited when the cells were treated with LY294002 (Figure I-6C), suggesting that KRS phosphorylation would involve PI3K. To determine the downstream kinase that can be responsible for the laminin-induced phosphorylation of KRS, each of three different MAPKs was introduced into the cells and interaction with KRS was determined by co-immunoprecipitation. Among the three kinases, p38MAPK was co-immunoprecipitated with Myc-KRS when laminin is treated (Figure I-6D). The interaction between Myc-KRS and p38MAPK was significantly increased by laminin treatment (Figure I-6E) and it was further confirmed by co-immunoprecipitation between the endogenous KRS and p38MAPK (Figure I-6F). To see whether p38MAPK can actually phosphorylate KRS, it was incubated GST or GST-KRS with purified p38MAPK as above. GST-KRS, but not GST, was indeed phosphorylated by p38MAPK (Figure I-6G). It was determined whether p38MAPK is actually necessary for laminin-induced phosphorylation of KRS using its inhibitor,

SB202190. The laminin-induced phosphorylation of GST-KRS was inhibited when the cells were treated with SB202190 (Figure I-6H), indicating the functional relevance of p38MAPK for KRS phosphorylation. The treatment of A549 cells with SB202190 inhibited translocation of KRS to membrane and also ablated laminin-dependent increase of 67LR in the membrane (Figure I-6I). All of these results suggest that laminin induces phosphorylation of KRS through PI3K and p38MAPK pathway and this process is required for membrane localization of KRS and its effect on 67LR.

Determination of laminin-induced phosphorylation site in KRS

To determine the laminin-induced phosphorylation site in KRS, Myc-KRS transfected A549 cells were incubated in different combination of SB202190 and laminin. The immunoprecipitated Myc-KRS was subjected to immunoblot with anti-p-Thr and -Ser antibodies. The phospho-Thr signal was enhanced by laminin treatment but blocked with SB202190, whereas phospho-Ser signal was not changed (Figure I-7A). To determine the phosphorylation site, GST-KRS was reacted with p38MAPK and subjected to mass analysis. The two phosphopeptides, QLSQATAAATNHTTDNGVGPEEESVDPNQYYK,

VTYHPDGPEGQAYDVDFTPPFR, were identified. Among these two peptides, S49,

T52 and T388 residues were predicted to the potential phosphorylation sites by p38MAPK (Table I-1). To validate whether any of these sites is actually phosphorylated by p38MAPK, these sites were mutated to alanine, and each of the GST-KRS mutants was subjected to *in vitro* kinase assay as above. The radioactivity of KRS was significantly reduced by the S49A or T52A mutant (Figure I-7B). To further validate the effect of these mutations, Myc-KRS mutants introduced A549 cells were incubated in the presence of laminin. Phosphorylation of immunoprecipitated KRS was determined by immunoblotting with anti-p-Thr and -Ser antibodies. Only T52A showed significantly reduced phosphorylation (Figure I-7C). Then laminin-treated A549 cells were fractionated and the membrane levels of 67LR and KRS mutants were compared. Among the three mutants, only the T52A mutant was not translocated to membrane and also did not enhance the 67LR membrane level (Figure I-7D). It was introduced each of the mutants into A549 cells with GFP-AIMP2, and compared whether their association with AIMP2 would be affected by laminin. Among the three mutants, binding of the T52A to AIMP2 was not affected by laminin treatment whereas the two other mutants as well as the wild type (WT) KRS dissociated from AIMP2 upon laminin treatment (Figure I-7E). In the Transwell chamber assay, the T52A mutant lost the ability to induce cell migration unlike the two other mutants (Figure I-7F).

The T52D mutant that can mimic the phosphorylation of KRS was also made, and it was compared the T52D and T52A mutants with the WT KRS for the laminin-dependent membrane localization and the effect on the membrane level of 67LR. Each of the GFP-KRS WT and -mutants was expressed in A549 cells and the effect of laminin on the membrane localization was monitored by fluorescence microscopy. The T52D mutant showed constitutively increased membrane localization independently of laminin whereas the membrane localization of the T52A mutant was not apparently observed (Figure I-8A). Consistently, the higher level of 67LR was detected in the membrane of the T52D mutant transfected cells regardless of laminin. In contrast, the T52A mutant was not found in the membrane and also did not increase membrane level of 67LR (Figure I-8B). Combined together, T52 appears to be the site that determines cellular localization of KRS in response to laminin stimulus.

KRS inhibits ubiquitin-mediated degradation of 67LR by Nedd4

To understand how KRS would stabilize 67LR in the membrane, it was investigated whether 67LR is subject to ubiquitin-mediated degradation system. For this, MG132, 26S proteasome inhibitor, was treated to A549 cells and determined whether the membrane level of 67LR could be stabilized. The MG132 treatment alone without

laminin treatment increased the membrane level of 67LR compared to that in the control (Figure I-9A). 67LR was previously reported to be enriched in membrane lipid raft (39) and Nedd4 was suggested as one of the E3 ligases that can ubiquitinate the target proteins in lipid raft (40). It was thus tested whether Nedd4 can control the 67LR membrane level. Ectopic expression of Nedd4 significantly reduced the 67LR membrane level in A549 cells while suppression of Nedd4 with its shRNA increased 67LR (Figure I-9B). The interaction between endogenous 67LR and Nedd4 was induced by laminin treatment (Figure I-9C). The ubiquitinated 67LR was increased by exogenous supplementation of Nedd4 WT, but not by the C894A inactive mutant (41) (Figure I-9D). When the effect of Nedd4 WT and C894A on the membrane level of 67LR was compared, the WT Nedd4, but not the mutant, reduced the 67LR level (Figure I-9E). Nedd4 is one of the HECT-type E3 ligases (42). To check the specificity of Nedd4 to degradation of 67LR, it was tested another HECT-type E3 ligase, Smurf2 (42), to see if it can also decrease 67LR in the membrane. The effect of Smurf2 on the 67LR membrane level was not apparent as strong as that of Nedd4 (Figure I-9F), suggesting that the membrane stability of 67LR is mainly controlled by Nedd4.

It was then examined how KRS would affect Nedd4-mediated ubiquitination of 67LR. Laminin-induced ubiquitination of 67LR was reduced by the exogenous

introduction of Myc-KRS and increased when KRS was suppressed with its siRNA (Figure I-10A). Exogenous introduction of Nedd4 enhanced ubiquitination of 67LR but addition of KRS reduced Nedd4-induced ubiquitination of 67LR (Figure I-10B). The binding of Nedd4 to LR was also suppressed by the ectopic expression of KRS (Figure I-10C). The exogenous supplementation of Nedd4 significantly reduced membrane level of 67LR but simultaneous introduction of KRS inhibited the membrane localization of Nedd4 and restored the membrane level of 67LR (Figure I-10D). The amount of Nedd4 in membrane was inhibited by the introduction of WT or T52D, but not by T52A KRS (Figure I-10D). All of these results suggest that the binding of KRS to 67LR in plasma membrane is important for the protection of 67LR from the Nedd4-mediated degradation.

Combined together, KRS mainly bound to MSC is phosphorylated at T52 by PI3K-p38MAPK pathway that is activated by laminin. The phosphorylated KRS is then dissociated from MSC and translocated to plasma membrane. In the membrane, KRS binds 67LR to inhibit ubiquitination of 67LR that is mediated by Nedd4. The stabilized 67LR can mediate cell migration in laminin-dependent manner (Figure I-11).

Figure I-1. KRS enhances laminin-dependent cell migration

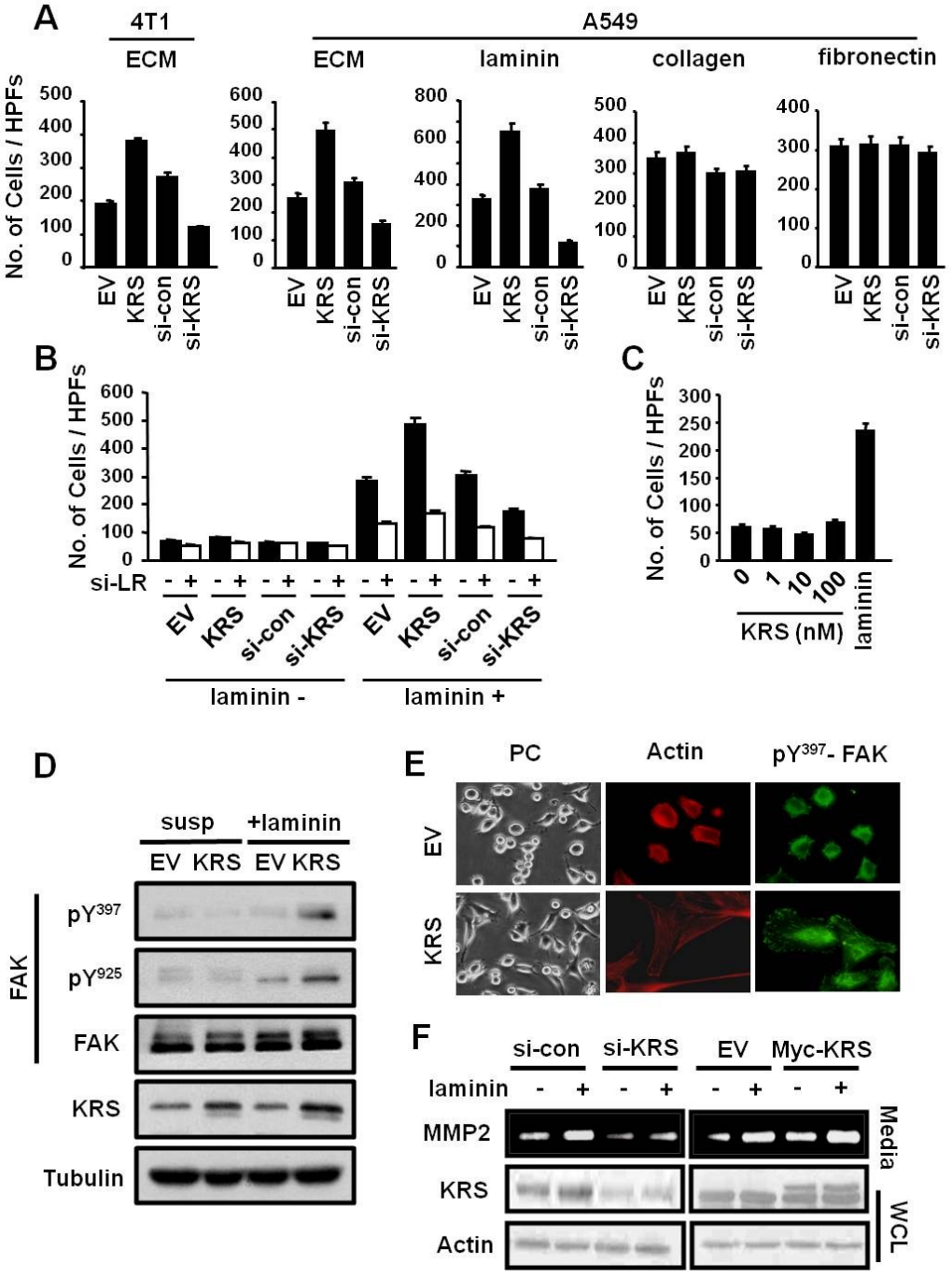

Figure I-1. KRS enhances laminin-dependent cell migration. **(A)** The effect of KRS on the migration of 4T1 and A549 cells in the presence of extracellular matrix (ECM) or different components was determined by Transwell chamber assays. KRS expression

levels were varied by transfection of Myc-KRS or its specific siRNA, and the cells migrated through the membrane were counted and presented as bar graphs. **(B)** To see whether the effect of KRS on cell migration requires laminin and laminin receptor, I monitored cell migration as above in the indicated combinations of laminin and laminin receptor using A549 cells. **(C)** To see whether extracellular KRS treatment can increase cell migration, A549 cells were treated with the indicated concentrations of purified KRS and cell migration was monitored as above. Laminin was used as a positive control. **(D)** The effect of KRS on cell migration was determined by the activation of focal adhesion kinase (FAK). The A549 cells detached from the plates were divided into two groups. One group was incubated as suspension culture and the other group was on the laminin-coated plates. The extract from the cells was subjected to immunoblotting with the antibodies specific to phospho-Tyr 397 and 925 residues. Tubulin was used as a loading control. **(E)** KRS- and EV- transfected A549 cells were observed for cell morphology by phase contrast light microscopy (left) and by immunofluorescence staining with rhodamine phalloidin for actin (red, middle) and antibody against pY^{397}-FAK (green, right). **(F)** The relationship of KRS to cell migration was also determined by MMP2 activity. KRS expression in A549 cells was varied as above. The MMP2 activity and expression of KRS were quantified by zymography (top) and immunoblotting (bottom), respectively. Actin was used as a loading control.

Figure I- 2. Interaction between KRS and laminin receptor

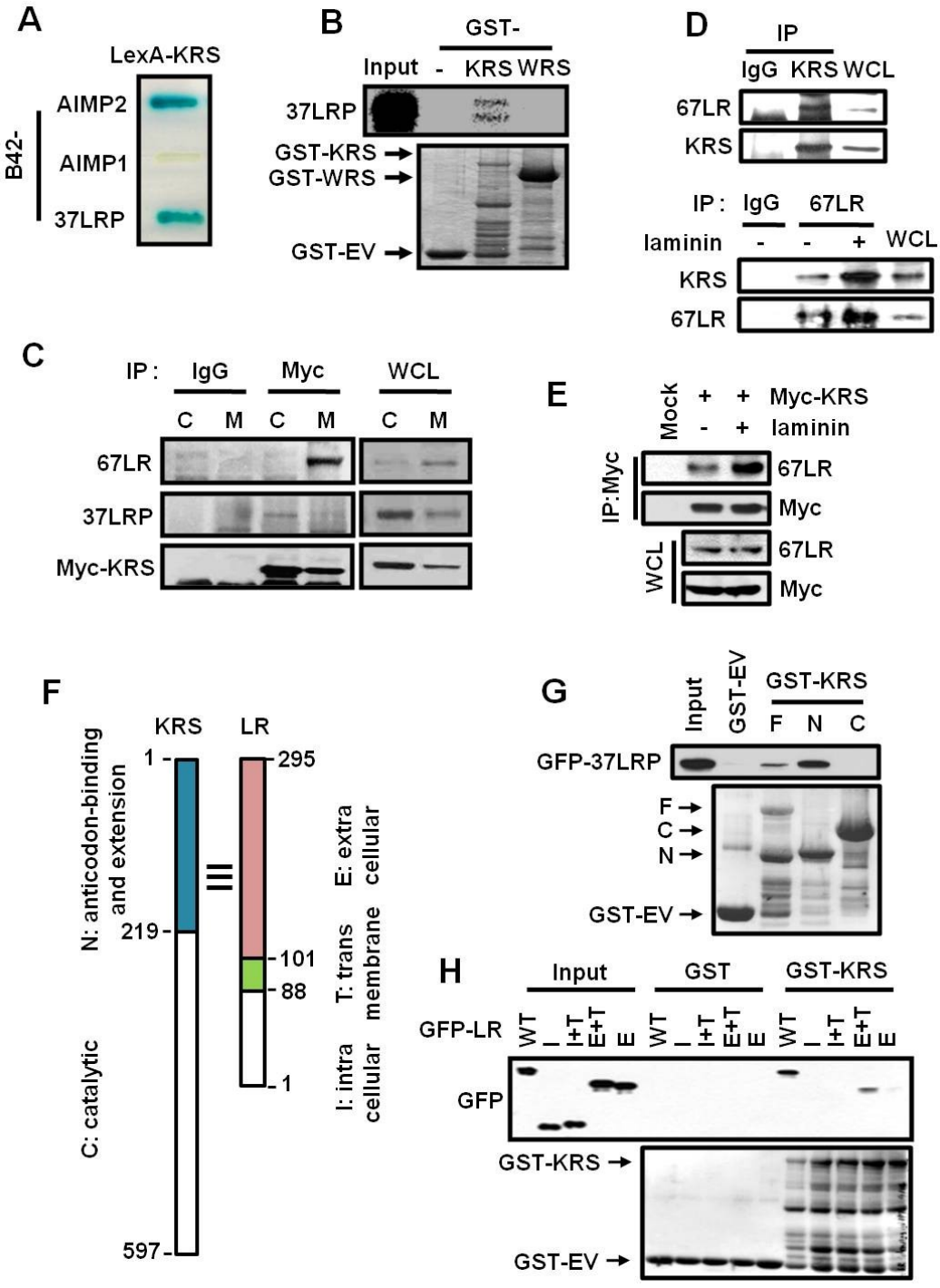

Figure I-2. Interaction between KRS and laminin receptor. **(A)** Interaction between full-length human KRS and 37LRP/p40 was determined by yeast two-hybrid assay. AIMP2

and AIMP1 were used as positive and negative controls, respectively (31). Positive interaction is indicated by a blue colony formation on yeast medium containing X-gal. **(B)** 37LRP was synthesized by *in vitro* translation in the presence of [^{35}S] methionine, and was subjected to pull-down with GST, GST-KRS and GST-WRS. 37LRP co-precipitated with GST proteins was detected by autoradiography. **(C)** Upon treating with laminin, the A549 cells transfected with Myc-KRS were separated into cytosolic (C) and membrane (M) fractions and immunoprecipitated with anti-Myc antibody. The endogenous 37LRP and 67LR that were co-precipitated with Myc-KRS were determined by immunoblotting. IgG was used as control. **(D)** Interaction of endogenous KRS with 67LR was determined by co-immunoprecipitation. Upper: Endogenous KRS was immunoprecipitated with its specific antibody and co-precipitation of 67LR was determined by immunoblotting with the corresponding antibody (F-18, Santa Cruz). Lower: Endogenous 67LR of A549 cells was immunoprecipitated with its specific antibody and co-precipitation of KRS was immunoblotted with anti-KRS antibody. **(E)** Myc-KRS in laminin-untreated and -treated A549 cells was immunoprecipitated with anti-Myc antibody, and co-precipitated 67LR was determined by immunoblotting with anti-67LR antibody. **(F)** The arrangement of functional domains in human KRS and 37LRP. Domains of KRS were divided to 219aa N- (anticodon-binding and extension domain) and 378aa C- (catalytic domain) fragments. 37LRP were separated to the indicated fragments. **(G)** GST-fused full-length, N- and C- domains of human KRS were reacted with GFP-37LRP. They were precipitated with glutathione-Sepharose beads and co-precipitated GFP-LR fragment was detected by immunoblotting with anti-GFP antibody. **(H)** GFP-fused domains of human 37LRP were reacted with GST-KRS-F. The mixture was precipitated with glutathione-Sepharose beads and co-precipitated GFP-37LRP fragments were determined by immunoblotting with anti-GFP antibody.

Figure I-3. Laminin-induced membrane localization of KRS

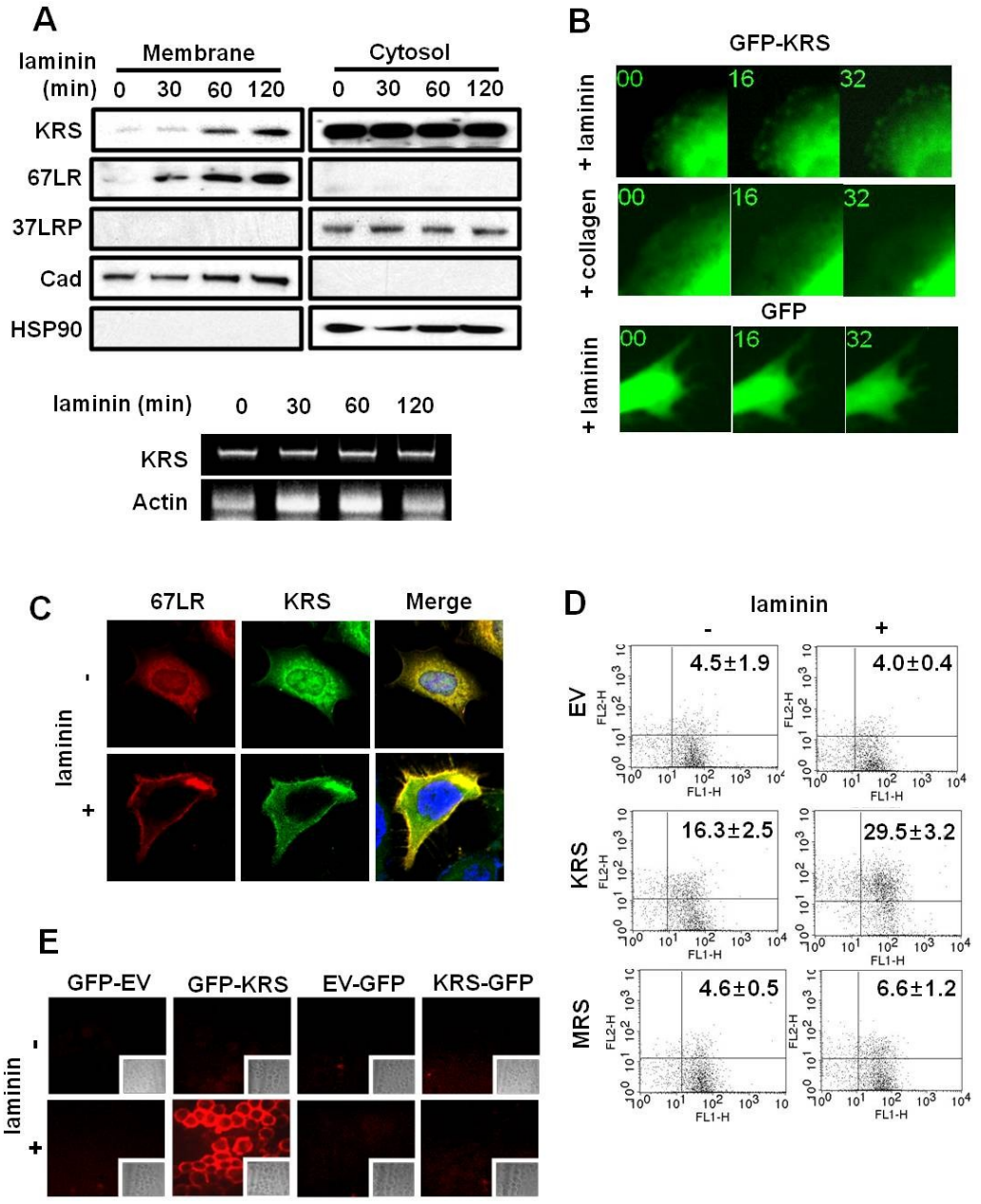

Figure I-3. Laminin-induced membrane localization of KRS. **(A)** A549 cells incubated in the presence of laminin (10μg/ml) were harvested at the indicated times and separated to the plasma membrane and cytosolic fractions. The levels of 67LR, 37LRP and KRS were determined by immunoblotting. HSP90 and Cadherin (Cad) were used as

the markers for cytosol and membrane, respectively (top). A549 cells were treated with laminin in time dependent manner and effect on transcription level of KRS via laminin was determined by RT-PCR. Actin was used as a loading control (bottom). **(B)** A549 cells transfected with GFP-KRS or GFP were treated with laminin or collagen. Cellular localization of GFP-KRS was monitored by live cell fluorescence microscopy. **(C)** Cellular localization of endogenous 67LR and KRS in A549 cells in the absence and presence of laminin was determined with the antibodies conjugated with Alexa555 (red) and 488 (green), respectively. **(D)** The amounts of surface exposed KRS and MRS were monitored by flow cytometry using anti-Myc antibodies in the laminin-untreated and -treated A549 cells transfected with Myc-KRS or -MRS. **(E)** GFP was attached to either the N- (GFP-KRS) or C- (KRS-GFP) terminal end of KRS and expressed in A549 cells. The cells were then incubated in the absence and presence of laminin, and the extracellularly exposed GFP was monitored by immunofluorescence staining with the antibody against GFP as described in experimental procedures. The insets show the cells observed by light microscope, indicating that the cells were grown to similar confluency.

Figure I-4. KRS enhances stability of 67LR

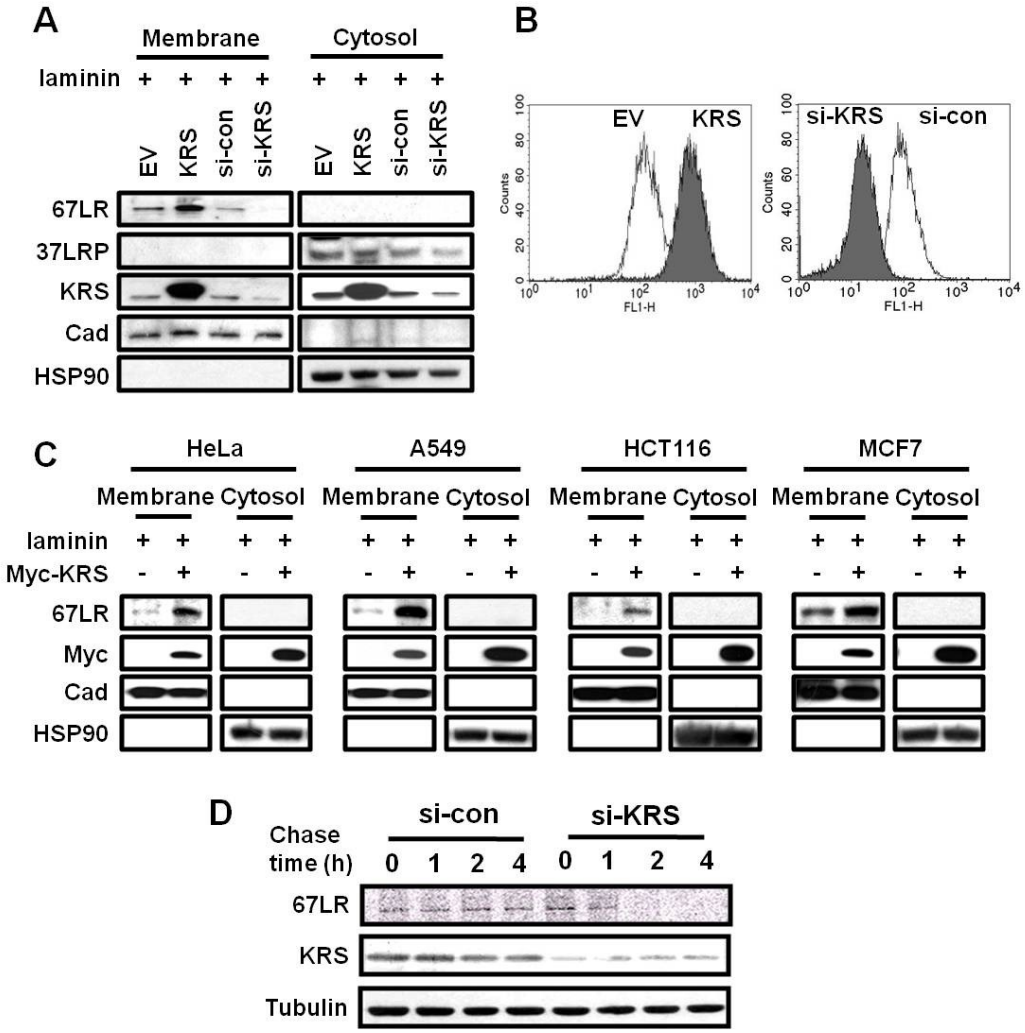

Figure I-4. KRS enhances stability of 67LR. **(A)** A549 cells were treated with laminin (10μg/ml) for 1 h, and the plasma membrane and cytosolic fractions were separated. The levels of 67LR, 37LRP and KRS were determined by immunoblotting. **(B)** Membrane level of 67LR in A549 cells was monitored by flow cytometry. The cells were transfected with EV or KRS (left) and si-KRS or si-control (right). **(C)** The Myc-KRS and EV transfected cells (HeLa, A549, HCT116 and MCF7) were incubated in the presence of laminin. The cells were fractionated into the membrane and cytosolic parts and the levels of 67LR were determined by immunoblotting. **(D)** The cellular stability of 67LR was determined by pulse-chase experiment. HEK293 cells were transfected

with si-KRS or si-control. [^{35}S] methionine was incorporated for 1 h. 67LR was immunoprecipitated with anti-67LR antibody, separated by SDS-PAGE, and autoradiographed. Suppression of KRS with its specific siRNA was confirmed by immunoblotting.

Figure I-5. Effect of KRS on transcription, acylation of 37LRP, and integrin levels

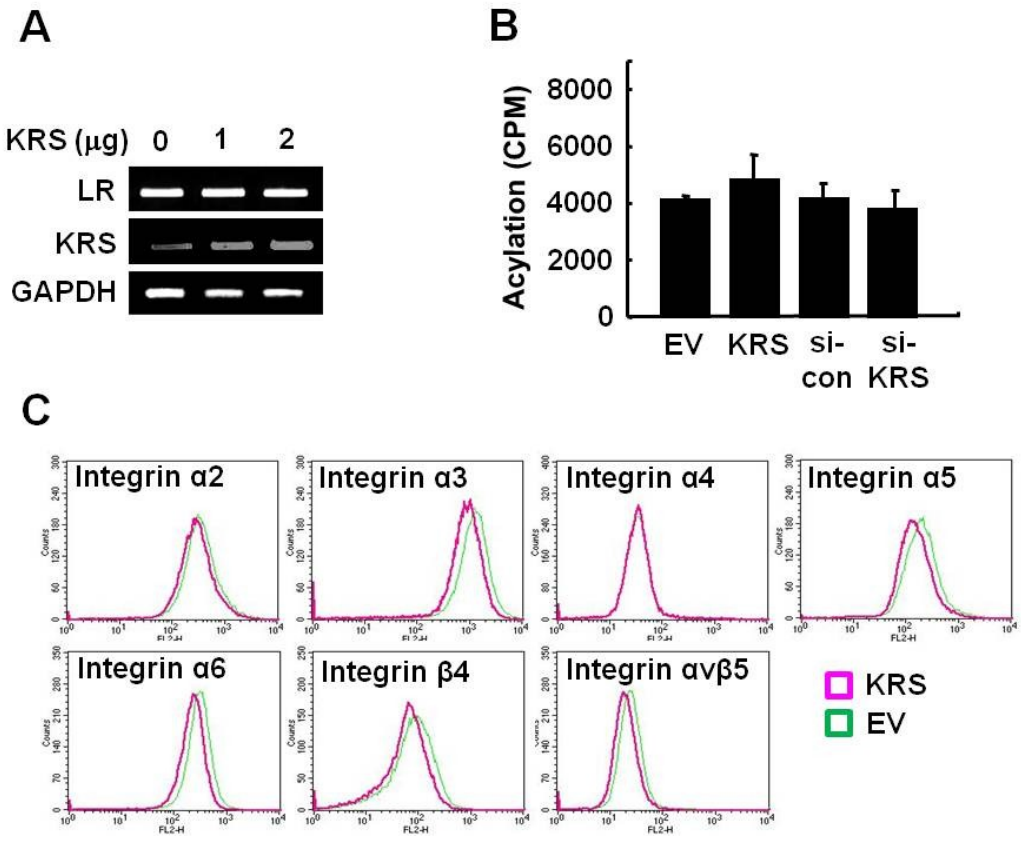

Figure I-5. Effect of KRS on transcription, acylation of 37LRP, and integrin levels. **(A)** KRS were introduced into A549 cells at the indicated concentrations and its effect on the transcription of 37LRP was determined by RT-PCR. GAPDH was used as a loading control. **(B)** The effect of KRS on acylation of laminin receptor was determined as described in experimental procedures. **(C)** The membrane levels of each integrin in the KRS overexpressed cells were compared with those in the cells transfected with EV. Purple and green lines show the KRS- and EV-transfected cells, respectively.

Figure I-6. p38MAPK-mediated phosphorylation is required for laminin-induced dissociation of KRS from the multisynthetase complex

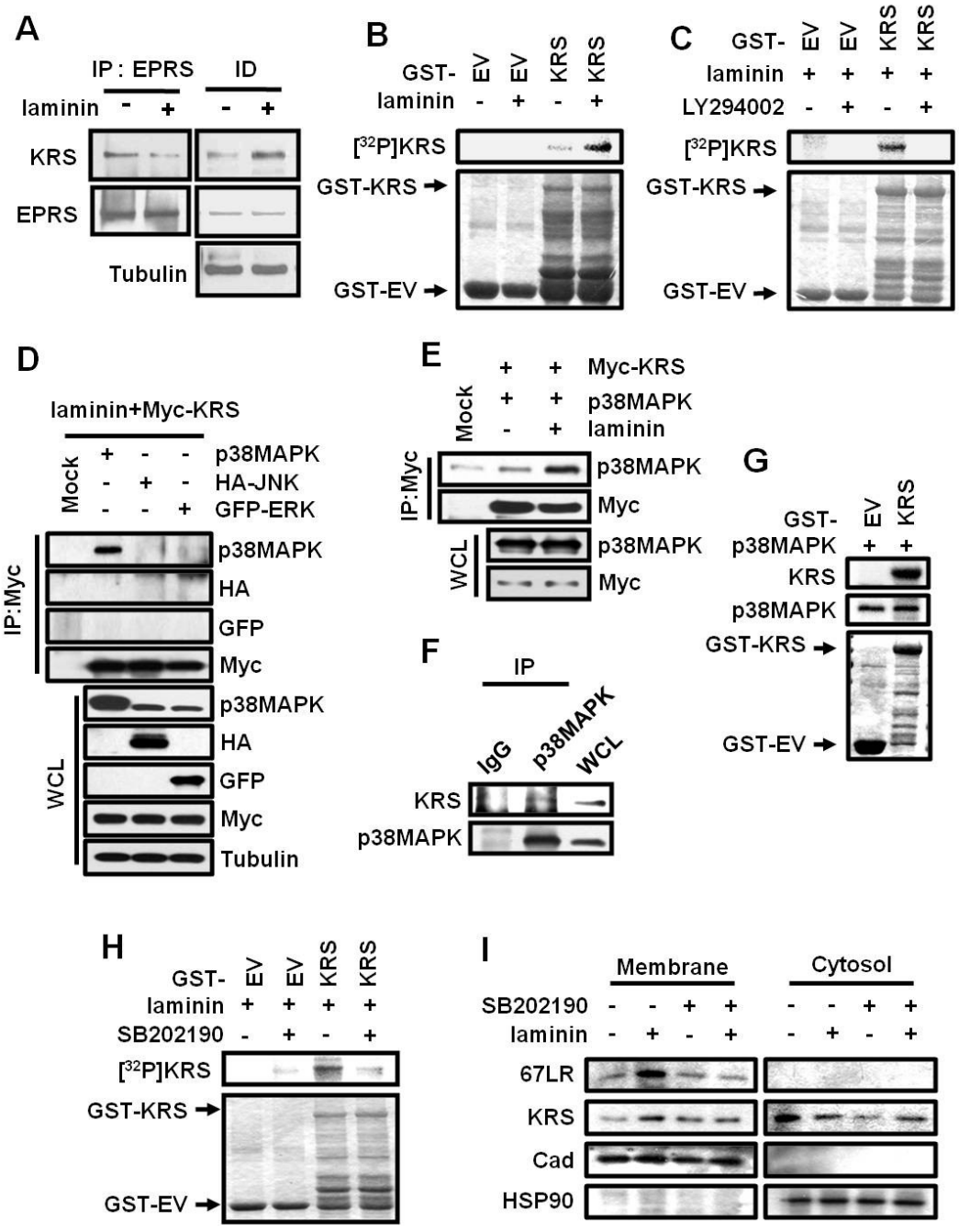

Figure I-6. p38MAPK-mediated phosphorylation is required for laminin-induced dissociation of KRS from the multisynthetase complex. **(A)** The extracts from A549

cells that were cultivated in the absence and presence of laminin were immunoprecipitated with antibody against EPRS, one of the enzyme components for MSC. The mixture was separated into immunoprecipitate (IP) and the immuno-depleted supernatant (ID), and each fraction was subjected to immunoblotting with anti-KRS and -EPRS antibodies. **(B)** GST and GST-KRS were purified and reacted with the protein extracts from A549 cells incubated in the absence and presence of laminin in the presence of [γ-^{32}P] ATP. The radioactivity of GST-KRS was determined by autoradiography. **(C)** Kinase assay was conducted as above in the absence and presence of LY294002. **(D)** KRS binding to three different MAPKs (p38MAPK, JNK and ERK) was tested by co-immunoprecipitation. p38MAPK, HA-JNK and GFP-ERK were transfected into A549 cells with Myc-KRS and the cells were treated with laminin. KRS was immunoprecipitated with anti-Myc antibody and co-precipitation of different MAPKs was determined by immunoblotting with their respective antibodies. **(E)** Myc-KRS and p38MAPK were expressed in A549 cells that were incubated in the absence and presence of laminin. KRS was immunoprecipitated with anti-Myc antibody and co-precipitation of p38MAPK was determined by immunoblotting. **(F)** The interaction of endogenous p38MAPK and KRS was also determined by co-immunoprecipitation. p38MAPK was immunoprecipitated with its specific antibody from A549 cells and co-precipitation of KRS was determined by immunoblotting. **(G)** GST or GST-KRS was reacted with purified p38MAPK in the presence of [γ-^{32}P] ATP and phosphorylation was determined by autoradiography. The activity of p38MAPK was confirmed by autophosphorylation. **(H)** The purified GST and GST-KRS were reacted with the protein extracts from A549 cells that were incubated in the presence of laminin with and without SB202190. The radioactivity of GST-KRS was determined as above. **(I)** A549 cells incubated in the combination of SB202190 and laminin and were fractionated into plasma membrane and cytosol, and the amounts of 67LR and KRS in each fraction were determined by immunoblotting.

Figure I-7. Determination of p38MAPK-induced phosphorylation site in KRS

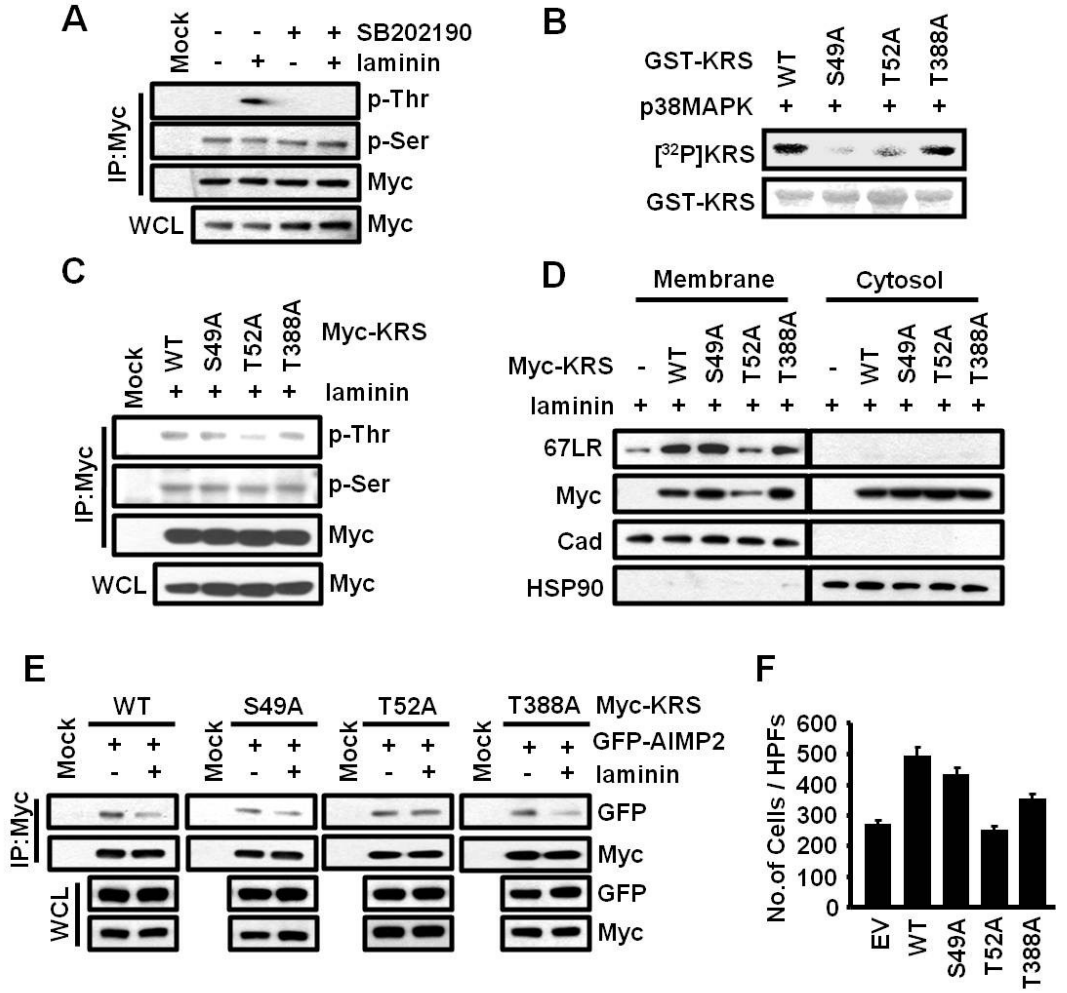

Figure I-7. Determination of p38MAPK-induced phosphorylation site in KRS. **(A)** A549 cells expressing Myc-KRS were incubated in the different combinations of SB202190 and laminin. Myc-KRS was immunoprecipitated and phosphorylation at threonine and serine was determined by anti-p-Thr and -p-Ser antibodies. **(B)** GST-KRS proteins containing each of S49A, T52A and T388A mutations were reacted with p38MAPK in the presence of [γ-^{32}P] ATP and phosphorylation was determined by autoradiography. **(C)** Each of Myc-KRS mutants was expressed in A549 cells and incubated in the presence of laminin. Myc-KRS was immunoprecipitated and subjected to immunoblotting with anti-p-Thr and -p-Ser antibodies. **(D)** The same cells as above

were fractionated into plasma membrane and cytosol, and the amounts of 67LR and KRS were determined by immunoblotting. **(E)** GFP-AIMP2 and each of KRS mutants were expressed in A549 cells in presence and absence of laminin. Myc-KRS was immunoprecipitated and co-precipitation of GFP-AIMP2 was determined by immunoblotting. **(F)** The effect of KRS mutant on migration via laminin was determined by using Transwell chamber assay. A549 cells were transfected with each of KRS mutants. The cells migrated through the membrane were counted and presented as bar graphs.

Figure I-8. Phosphorylation of KRS threonine 52 is too enough to membrane localization

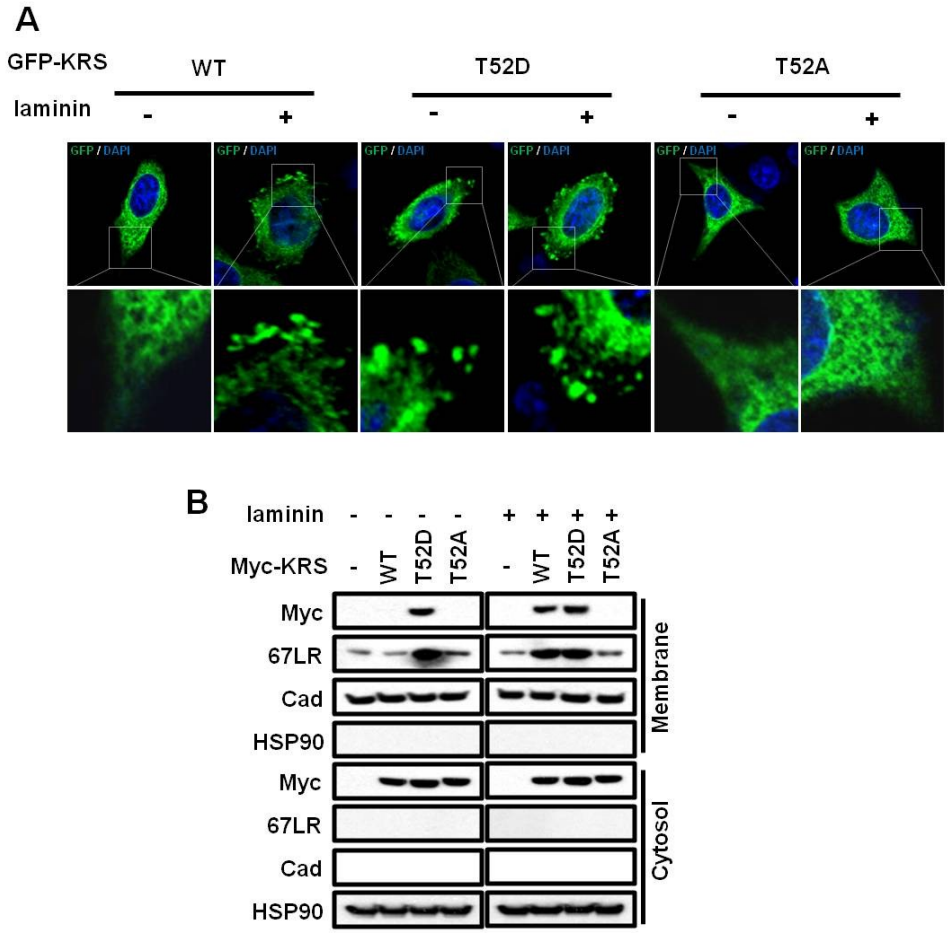

Figure I-8. Phosphorylation of KRS threonine 52 is too enough to membrane localization. **(A)** A549 cells transfected GFP-KRS wild type, T52D and T52A were treated laminin or not. Cellular localization of GFP-KRS was monitored by fluorescence microscopy. **(B)** The Myc-KRS wild type, T52D and T52A transfected A549 cells were fractionated into plasma membrane and cytosol after treatment with laminin, and the amounts of 67LR and Myc were determined by immunoblotting.

Figure I-9. Nedd4 is the specific E3 ligase of 67LR

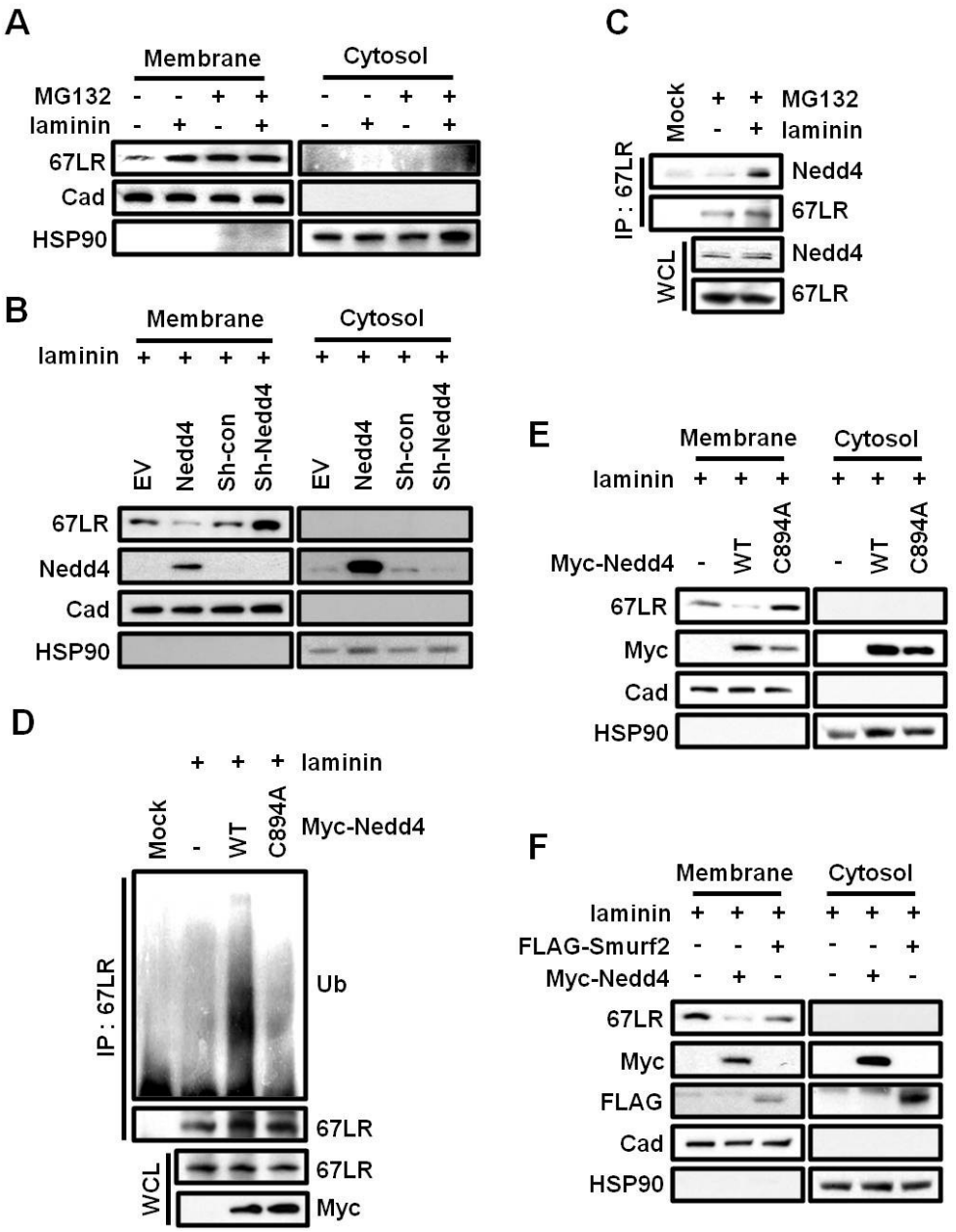

Figure I-9. Nedd4 is the specific E3 ligase of 67LR. **(A)** The laminin-untreated and -treated A549 cells were pre-incubated in the absence and presence of MG-132 (50μM, 4 h) and fractionated. Extracts from the two fractions were subjected to immunoblotting. **(B)** Nedd4 was increased and decreased by transfection with Nedd4 and sh-Nedd4,

respectively. Transfected A549 cells were treated with laminin and fractionated into plasma membrane and cytosol. 67LR and Nedd4 were detected by immunoblotting. **(C)** A549 cells pre-incubated with MG132 were treated with laminin or not. The endogenous 67LR was immunoprecipitated with anti-67LR antibody. Co-precipitates were detected by antibody against Nedd4. **(D)** A549 cells transfected with Myc-Nedd4 wild type or Myc-Nedd4 C894A were treated with laminin and MG132. Lysate from A549 cells was immunoprecipitated with anti-67LR antibody. Precipitates were subjected to SDS-PAGE. **(E)** Same cells as above were fractionated into cytosol and membrane. **(F)** A549 cells transfected with Myc-Nedd4 or FLAG-Smurf2 were treated with laminin and fractionated into cytosol and membrane. FLAG-Smurf2 was detected with anti-FLAG antibody.

Figure I-10. KRS inhibits Nedd4-mediated ubiquitination of 67LR

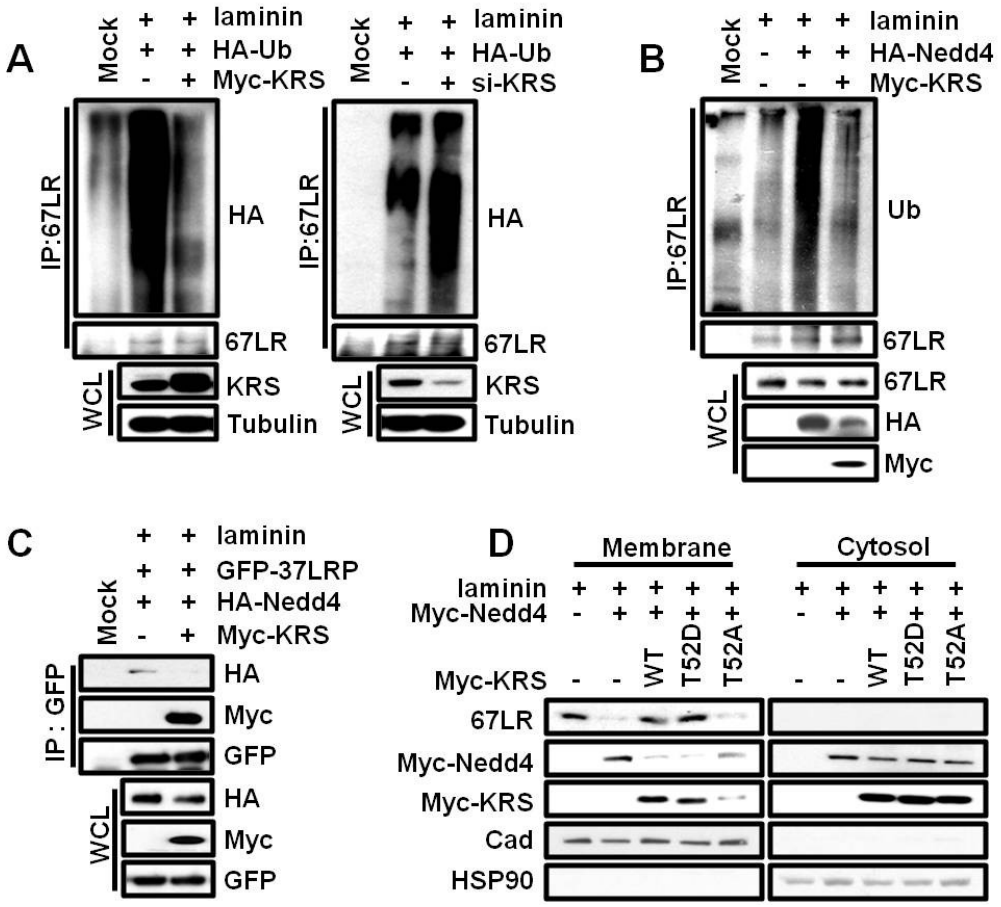

Figure I-10. KRS inhibits Nedd4-mediated ubiquitination of 67LR. **(A)** A549 cells transfected with HA-ubiquitin were incubated in the presence of laminin, and KRS expression was increased and suppressed by introduction of KRS and si-KRS, respectively. Extracts from each of the transfectants were precipitated with anti-67LR antibody, and the precipitates were separated by SDS-PAGE and subjected to immunoblotting with anti-HA antibody. **(B)** A549 cells transfected with the combination of HA-Nedd4 and Myc-KRS were lysed and precipitated with anti-67LR antibody. The precipitates were subjected to SDS-PAGE and immunoblotting with anti-Ub antibody. **(C)** A549 cells transfected with HA-Nedd4, GFP-37LRP and Myc-KRS were lysed and immunoprecipitated with anti-GFP antibody. Precipitates were separated by SDS-PAGE

and subjected to immunoblotting. **(D)** A549 cells were transfected with indicated pairs of Myc-Nedd4 and Myc-KRS T52 mutants. The transfected cells were separated into plasma membrane and cytosolic fractions.

Figure I-11. Proposed model for cell migration control of KRS via 67LR in plasma membrane

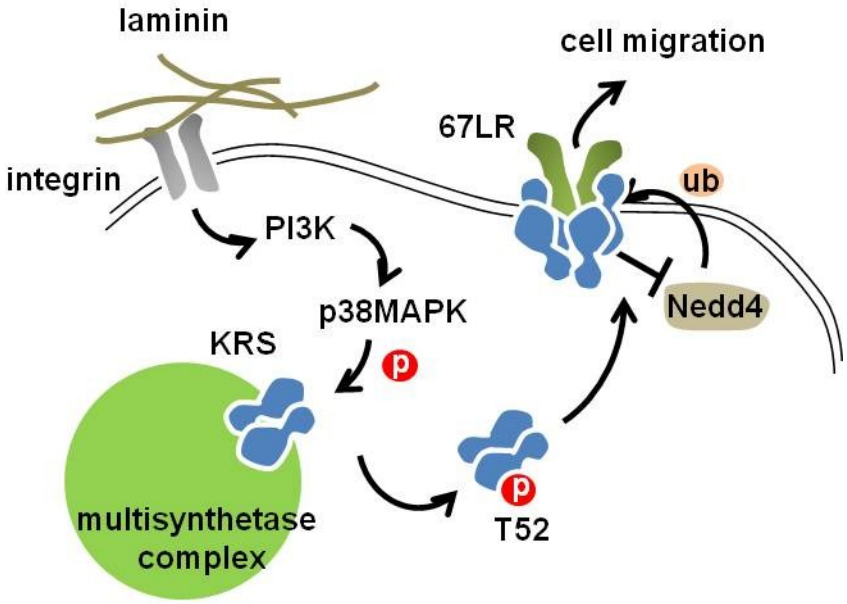

Figure I-11. Proposed model for cell migration control of KRS via 67LR in plasma membrane. Laminin binding to integrin can activate PI3K and its downstream p38MAPK which then introduces phosphorylation at T52 residue of KRS that is normally bound to MSC. The phosphorylated KRS dissociates from MSC and mobilized to plasma membrane. In the membrane, it binds to 67LR, preventing from Nedd4-mediated ubiquitination to 67LR to extend the membrane stability of 67LR. Thus, KRS binding to 67LR can enhance laminin-induced cell migration. Laminin signal can be also introduced via the pre-existing 67LR and the membrane trafficking of KRS can work as a positive feedback mechanism.

Table I-1. The phosphopeptides of KRS induced by p38MAPK.

Peptide	Precursor Mass (m/z)	Z	XC	DeltaCn	Phospho Site
QLSQApTAAATNHTTDNGVGPEEESVDPNQYYK	**1172.5127**	**3**	**4.93**	**0.08**	**52**
QLpSQATAAATNHTTDNGVGPEEESVDPNQYYK	**1172.5127**	**3**	**4.36**	**0.28**	**49**
VTYHPDGPEGQAYDVDFpTPPFR	**863.3758**	**3**	**4.29**	**0.41**	**388**

The phosphorylation sites predicted to be matched to the phosphopeptides of KRS identified by mass spectrometry are shown. The two phosphopeptides contain three potential phosphorylation sites at threonine 52, serine 49 and threonine 388.

Discussion

Here the membrane translocation and functional interaction of the two translational components in the plasma membrane was identified: KRS, an enzyme for protein synthesis, and laminin receptor whose precursor is a ribosomal subunit, p40, to induce laminin-dependent cell migration. Although it was conducted the most of the experiments in cancer cell lines, the laminin-induced membrane translocation of KRS and its positive effect on 67LR was found and cell migration were also confirmed in normal cells (data not shown), suggesting that the functional relationship between these two translational factors for cell migration should be generally applied. Perhaps, in the normal cells, the membrane translocation of KRS could be tightly controlled, but it could be out of control in cancer cells if KRS is either overexpressed or mutated. In this regard, it is worth noting that KRS is often highly expressed in cancer cells (13, 43-45). It is not yet clear why the cells recruit translational components to plasma membrane to control cell migration. One possibility is that the membrane localization of these factors may deplete them from the translational machinery, leading to the reduction of global translation. The energy saved from the reduction of translation can be then used for the cell migration.

Among the components of MSC, KRS is the most stable protein and required for the stability of other components (9), implying its potential to stabilize associated proteins. Although 37LRP showed the potential for the interaction with KRS (Figure I-2A, B), KRS appears to bind preferentially to 67LR in the plasma membrane (Figure I-2C). It is not yet understood how KRS undergoes conformational change to form a complex with 67LR in the membrane. Human KRS appears to exist as a homodimer that has a potential to form homo- or heterotetramer (33). Since 67LR is formed by the dimerization of 37LRP (46), KRS and 67LR may form $\alpha_2\beta_2$ or $\alpha_4\beta_2$ complex. The T52D mutation did not appear to change the homodimer formation of KRS (data not shown), implying that KRS may remain dimer after being phosphorylated at T52. However, further investigation is needed to determine the exact stoichiometry between the two proteins.

Post-translational modification was shown to be responsible for the control of association/dissociation of a few different components in MSC. For instance, phosphorylated EPRS is detached from MSC by IFN-gamma treatment for translational silencing of the target transcripts (47). GCN2-dependent phosphorylation of methionyl-tRNA synthetase (MRS) releases the bound tumor suppressor, AIMP3/p18 to repair DNA damage (48). Among the non-enzymatic components, phosphorylated AIMP2 is

translocated into nucleus upon DNA damage for the activation of p53 (49), and JNK-dependent phosphorylation of AIMP1 is involved in the control of its interaction with gp96 (50). These results indicate that MSC components, when dissociated from MSC, would respond specifically to different cellular stimuli through differential phosphorylation and execute their unique activities while they work together for protein synthesis when they are bound to MSC.

Although the biogenesis and physiological implication of 67LR are not yet completely understood, the increased level of 67LR has been acknowledged as a signature for metastatic cancer (19, 51-54). However, the regulator and molecular mechanism for the membrane stability of 67LR were not determined. Here it was identified KRS as a positive regulator for 67LR and its effect on cell migration. It has to be seen whether the effect of these two translational components on cell migration is also recapitulated in vivo and applied to the metastatic behavior of cancer.

Materials and methods

Cell culture and materials

A549, HeLa, HCT116, MCF7, WI-26 and HEK293 were purchased from American Type Culture Collection. Mouse mammary carcinoma 4T-1 cell line was kindly provided by Dr. Seong Jin Kim (Cha University). RPMI (for A549, HCT116 and 4T-1 cells) and Dulbecco's Modified Eagle Medium (for other cell lines) containing 10% fetal bovine serum and 1% antibiotics were used for cell cultivation. pcDNA3.1 encoding 37LRP was a kind gift from Dr. Hirofumi Tachibana (Kyushu University). Myc-tagged human KRS was cloned at the *Eco*RI/*Xho*I sites of pcDNA3. The cDNA fragments encoding the indicated peptides of GFP-tagged 37LRP were cloned at *Eco*RI/*Xho*I sites of pEGFP-C2. HA-tagged Nedd4 (Addgene plasmid 11426) and GFP-tagged ERK (Addgene plasmid 14747) (55) were purchased from Addgene. HA-tagged JNK and pcDNA3 encoding p38MAPK were a kind gift from Dr. Eui Ju Choi (Korea Univ.). Myc-tagged wild type and C894A Nedd4 were kindly provided by Dr. Byung-Gyu Kim (Kyungpook National Univ.). The clones for Myc-KRS N (1-219) and C (220-597) fragments were the kind gifts from Dr. Young Ho Jeon (KBSI). The cDNAs encoding Myc-KRS mutants at S49A, T52A, T388A and T52D were cloned using the

QuikChange® II (Agilent) following the manufacturer's instruction. Gene porter (GTS) and Lipofectamine 2000 (Invitrogen) were used as transfection reagent. Laminin (Engelbreth-Holm-Swarm murine sarcoma) was purchased from Sigma. The sequence for siRNAs targeting human KRS is shown as below: si-hKRS, GCU GUU UGU CAU GAA GAA AGA GAU

Cell migration assay

Cell migration was determined by using 24-well Transwell chambers with polycarbonate membranes (8.0 μm pore size, Costar) as described (13). A549 cells were suspended in serum-free RPMI and added to the top chamber at $1x10^5$ cells per well. Each of ECM (10 μg/ml, Sigma), laminin (10 μg/ml), collagen (10 μg/ml, Biomedical Technologies) and fibronectin (10 μg/ml, BD Biosciences) was coated on the membrane. To determine the effect of extracellular KRS, purified KRS at the indicated concentration was placed in the bottom chamber. To check the effect of phosphorylation of KRS on migration, alanine mutant transfected cells were used. The cells were allowed to migrate for 6 h at 37°C in a CO_2 incubator, fixed with 70% methyl alcohol in PBS for 30 min, washed with PBS three times, stained with hematoxylin (Sigma) for 10 min and washed with distilled water. After removing non-migrant cells from the top

face of the membrane with a cotton swab, the membranes were excised from the chamber and mounted with Gel Mount (Biomeda, Foster City, CA). The migrant cells (those attached to the bottom face of the membrane) were counted at three randomly selected scopes in high-power fields (x20).

Time-lapse fluorescence imaging

A549 cells were transfected with either GFP or GFP-KRS and incubated for 24 h. The cells were then replated on coverslips precoated with serum-containing culture medium for 6 h. Laminin or collagen was directly added to the medium just before live imaging using time-lapse microscopy (IX81-ZDC, Olympus) using a Coolsnap HQ/QL cold CCD digital camera (model of CoolSNAP-HQ2). Fluorescence from the cells positive for transfection (n = 10 for GFP-KRS cells with laminin, n = 7 for GFP-KRS cells with collagen, and n = 5 for GFP cells with laminin treatment) in CO_2-controlled chamber was time-lapsed for 50 min with 1 min intervals at 37^{o}C using MetaMorph software (Danaher Corporation). Images were analyzed for snap-pictures to cover images for 40 min using MetaMorph software.

Immunofluorescence staining

For the activated FAK staining, A549 cells were fixed in 3.8% paraformaldehyde for 5 min at room temperature, permeabilized with 0.05% Triton X-100 for 5 min, rinsed in PBS, and blocked in PBS containing 2% BSA for 30 min. Then, the cells were incubated with primary antibody against phospho-Y397 FAK for 1 h at room temperature. Actin was stained by using rhodamine phalloidin (Invitrogen). To confirm that the phosphorylation of KRS affects the localization in membrane, transfected A549 cells with GFP-KRS wild type, T52D and T52A were used. Transfected A549 cells were treated with laminin or not, then fixed with methyl alcohol and stained with DAPI. After washing with cold PBS, the samples were mounted. The mounted samples were visualized by fluorescent microscopy (BX51 fluorescent microscope, Olympus). For the staining of endogenous KRS and 67LR, A549 cells on a 9 mm coverslip were fixed with 70% methyl alcohol and washed briefly with cold PBS. After incubation with the blocking buffer containing 1% CAS, 3% BSA and 0.5% Triton X-100 for 30 min, the cells were incubated with the antibodies against KRS, and 67LR (MLuC-5, Santa Cruz) for 1 h that were conjugated with Alexa488 and 555 (Invitrogen), respectively. After washing with cold PBS for 30 min, the specimens were observed by laser-scanning microscopy.

Quantum dot analysis

To monitor the extracellularly exposed domain of KRS, KRS cDNA was inserted at *Eco*RI/*Sal*I sites of pEGFP-N3 and pEGFP-C2 (Clontech) to generate GFP fused to the C- and N-terminal ends of KRS, respectively. A549 cells transfected with pEGFP-N3, pEGFP-N3-KRS, pEGFP-C2 or pEGFP-C2-KRS were incubated in the absence and presence of laminin, rinsed with PBS, and incubated with anti-GFP antibody (Santa Cruz) at room temperature. After 1 h incubation, the cells were washed with PBS, treated with the biotinylated anti-mouse IgG antibody (eBioscience) and QD625-streptavidin conjugates (Invitrogen) for 1 h at room temperature. Finally, the immunostained-cells were rinsed with PBS. Image analysis of the immunostained cells was accomplished using a custom made hyperspectral single cell imaging cytometer. The setup and working principle of the imaging system were previously described (56, 57). The acquired cellular images were processed and analyzed using MetaMorph (Version 7.1.3.0, Molecular Devices).

Focal adhesion kinase assay

A549 cells transfected with EV or KRS for 48 h were incubated for 12 h in normal serum-containing culture medium and replated on the laminin-precoated (10 μg/ml)

culture dishes. The cells were detached, suspended with serum-free culture medium containing 1% BSA (Sigma), and rolled-over (60 rpm in CO_2 incubator) for 1 h to nullify the basal signaling activity. The cells were either kept in suspension or reseeded onto the laminin-precoated culture dishes containing the replating medium and incubated in CO_2 incubator for 2 h. The cells were harvested and the proteins were extracted for Western blot analysis with the primary antibodies against phospho-Y397FAK, phospho-Y925FAK, FAK (Abcam, Cambridge), KRS (Abcam) and tubulin (Sigma).

Zymography

A549 cells transfected with si-control and -KRS or EV and the Myc-KRS were incubated for 48 and 24 h, respectively, and seeded ($1x10^5$ cells/well). After starving the cells in serum-free RPMI for 2 h, laminin (10 μg/ml) was added and incubated for 24 h. The culture medium (20 μl) was mixed with 5xFOD buffer (0.125 M Tris-HCl, pH 6.8, 4% SDS, 20% glycerol and 0.01% bromophenol blue) and subjected to 10% SDS-PAGE containing 1mg/ml gelatin. The gel was washed with 2.5% Triton X-100 twice 20 min per washing, then with distilled water twice 20 min per washing, and incubated with the reaction buffer (50 mM Tris-HCl, pH 7.5, 10 mM $CaCl_2$, 150 mM NaCl, 1 μM

$ZnCl_2$, 1% Triton X-100 and 0.002% sodium azide) for 24 h at 37^{o}C. The gel was washed with distilled water, stained with Coomassie blue R250, and then destained with 35% methanol.

Yeast two-hybrid analysis

The cDNA encoding human KRS was obtained by PCR with the forward and backward primers containing EcoRI and XhoI sites, respectively. The product was digested with *EcoR*I and *Xho*I, and ligated to the corresponding sites of pEG202 (for the construction of LexA-fusion proteins). Likewise, the cDNAs for AIMP1/p43, AIMP2/p38 and 37LRP were inserted into pJG4-5 (for the construction of B42-fusion proteins). The cDNA encoding human 37LRP was kindly provided by Dr. Barbara J. Ballermann (University of Alberta). The positive interaction was determined by the formation of blue colonies on the X-gal-containing yeast medium.

Immunoprecipitation

A549 cells were lysed with 20 mM Tris-HCl (pH 7.4) buffer containing 150 mM NaCl, 0.5% Triton X-100, 0.1% SDS, and protease inhibitor (Calbiochem). The protein extracts were incubated with normal IgG and protein G agarose for 2 h, and then

centrifuged to remove nonspecific IgG binding proteins. It was mixed the supernatants with purified anti-KRS antibody, incubated the mixture for 2 h at 4^{o}C with agitation, added protein A agarose, and centrifuged. After washing the precipitates with the cold lysis buffer three times, the precipitates were dissolved in the SDS sample buffer and separated by SDS-PAGE. To determine the binding of KRS and laminin receptor in different cell fractions, it was transfected Myc-tagged KRS and separated plasma membrane and cytosolic fractions using Proteoextract kit (Calbiochem), following the manufacturer's instruction. To analyze protein levels, extracts from the cells were separated by 10% SDS-PAGE. Anti-LR antibody (Abcam, ab2508) was used for simultaneous immunoblotting of 37LRP and 67LR, unless specified. Antibodies for HSP90 and pan-cadherin were purchased from Santa Cruz.

***In vitro* binding assay**

Human 37LRP/p40 was prepared by *in vitro* translation in the presence of [^{35}S] methionine, and mixed with each of GST, GST-KRS and -WRS. GST proteins were precipitated with glutathione-Sepharose and 37LRP co-precipitated with GST proteins was detected by autoradiography. To determine the domains of laminin receptor involved in the interaction with KRS, the DNA fragments encoding the indicated

domains of 37LRP were isolated by PCR and expressed as GFP fusion proteins. They were then mixed with GST-KRS and precipitated with glutathione-Sepharose. Co-precipitates of the laminin receptor fragments were determined by Western blotting with antibody against GFP.

Flow cytometry

To determine the laminin-induced surface exposure of KRS and MRS, A549 cells transfected with Myc-KRS or Myc-MRS were detected with anti-Myc antibody. For quantification of 67LR on cell surface, $1x10^6$ cells were incubated with IgG or anti-LR antibody (MLuC5, 1 μg) recognizing extracellular domain of 67LR and then with FITC secondary antibody. After washing with PBS, the samples were scanned by FACS. The antibodies against integrin α2 (Chemicon, 1 μg), α3 (GeneScript, 1 μg), α4 (Chemicon, 1 μg), α5 (Chemicon, 1 μg), α6 (Chemicon, 1 μg), β4 (58) and αvβ5 (Chemicon, 1 μg) were used to determine the effect of KRS on surface exposure of integrins.

Pulse-chase experiment

HEK293 cells transfected with si-KRS or si-control (Invitrogen) were then incubated with methionine-free medium for 1 h. Then, [^{35}S] methionine (50 μCi/ml) was added

and incubated for 1 h. After washing off the radioactive methionine with fresh medium, 67LR was immunoprecipitated with its specific antibody (Santa Cruz), separated by 12% SDS-PAGE and subjected to autoradiography using BAS (FLA-3000, Fujifilm).

Fatty acylation

To see the effect of KRS on fatty acylation of laminin receptor, A549 cells with different expression levels of KRS were washed three times with PBS, starved with serum-free medium for 4 h, and then pulsed for 2 h in medium containing 0.1 mCi/ml [^{3}H] palmitic acid. The cells were washed three times with cold PBS, and incubated with laminin in serum-free medium for 1 h. Laminin receptor was immunoprecipitated with antibody against laminin receptor (Abcam). The radioactivities of the precipitates were measured by a liquid scintillation counter (Wallac).

***In vitro* kinase assay**

A549 cells were incubated with SB202190 (20 μM, Calbiochem) or LY294002 (20 μM, Calbiochem) for 4 h, and treated with laminin for 1 h. The cells were washed with cold PBS three times and lysed by sonication in the kinase buffer containing 20 mM Tris-HCl, pH 7.5, 15 mM $MgCl_2$, 1 mM EGTA, 0.1 mM DTT, 1 mM Na_3VO_4, 0.5 mM NaF,

0.1 mM β-glycerophosphate and 0.1 mM Sodium pyrophosphate. After purified GST-KRS and GST were pre-incubated with cold ATP (250 μM) on ice for 10 min, mixed with the protein extract (250 μg) or p38MAPK (Cell Science) and [γ-^{32}P] ATP 10 μCi (3000 Ci/mmol) in the kinase buffer, incubated at 30^{o}C for 30 min, and stopped by the addition of the SDS sample buffer. The proteins in the reaction mixture were separated by SDS-PAGE and autoradiographed (FLA-3000, FUJIFILM).

Mass spectrometry

Coomassie-stained KRS phosphorylated by recombinant p38MAPK was in-gel digested with trypsin (Promega) and analyzed by capillary column LC-tandem MS analysis to map the peptides and identify phosphopeptides. The experiments were done using LTQ-Orbitrap MS systems (ThermoFinnigan, San Jose, CA) equipped with nanospray ionization sources. Data were acquired in data-dependent mode to simultaneously record full-scan mass and CID spectra with MSA (Multi-stage activation). For peptide mapping, the CID spectra were compared to the sequence of human KRS using Sequest (Bioworks). To identify phosphopeptides and specific phosphorylation sites, CID spectra were searched for the peptides that contain pSer, pThr or pTyr modifications by a combination of database searches and by plotting neutral loss chromatograms to show

characteristic loss of phosphate group.

Ubiquitination assay

A549 cells transfected with the indicated plasmids were pre-incubated with MG132 (50 μM) and cultivated in the presence of laminin. 67LR was immunoprecipitated with anti-LR antibody (MLuC5) and the precipitates were separated by SDS-PAGE for immunoblotting.

RT-PCR

Total RNAs were extracted from A549 cells that were dose dependently transfected with KRS or treated laminin time dependently using RNeasy mini kit (QIAGEN). 1 μg of RNA was used for RT-PCR with dNTP, random hexamer and MMLV in 20 μl reaction, and 1 μl of cDNA was used for PCR with appropriate primers using PCR PreMix (BIONEER). The sequences for the primers specific to 37LRP, KRS, GAPDH and actin are shown as following; 37LRP: CCG CTC GAG ATG TCC GGA GCC CTT GAT GTC CTG and CCG GGA TCC TTA AGA CCA GTC AGT GGT TGC TCC, KRS: CAA TGC CCA TGC CCC AGC CA and ACC CCA CCC TTC CGG CGA AT, GAPDH:

TTT GGT CGT ATT GGG CGC CTG and CCA TGA CGA ACA TGG GGG CAT,

Actin: CCT TCC TGG GCA TGG AGT CCT and GGA GCA ATG ATC TTG ATC TT.

References

1. Guo, M., Schimmel, P., and Yang, X. L. (2010) Functional expansion of human tRNA synthetases achieved by structural inventions. *FEBS Lett* **584**, 434-442
2. Park, S. G., Ewalt, K. L., and Kim, S. (2005) Functional expansion of aminoacyl-tRNA synthetases and their interacting factors: new perspectives on housekeepers. *Trends Biochem Sci* **30**, 569-574
3. Park, S. G., Schimmel, P., and Kim, S. (2008) Aminoacyl tRNA synthetases and their connections to disease. *Proc Natl Acad Sci U S A* **105**, 11043-11049
4. Kim, S., You, S., and Hwang, D. (2011) Aminoacyl-tRNA synthetases and tumorigenesis: more than housekeeping. *Nat Rev Cancer* **11**, 708-718
5. Lee, S. W., Kang, Y. S., and Kim, S. (2006) Multi-functional proteins in tumorigenesis: Aminoacyl-tRNA synthetases and translational components. *Current Proteomics* **3**, 15
6. Park, S. G., Choi, E. C., and Kim, S. (2010) Aminoacyl-tRNA synthetase-interacting multifunctional proteins (AIMPs): a triad for cellular homeostasis. *IUBMB Life* **62**, 296-302
7. Lee, S. W., Cho, B. H., Park, S. G., and Kim, S. (2004) Aminoacyl-tRNA synthetase complexes: beyond translation. *J Cell Sci* **117**, 3725-3734
8. Han, J. M., Kim, J. Y., and Kim, S. (2003) Molecular network and functional implications of macromolecular tRNA synthetase complex. *Biochem Biophys Res Commun* **303**, 985-993
9. Han, J. M., Lee, M. J., Park, S. G., Lee, S. H., Razin, E., Choi, E. C., and Kim, S. (2006) Hierarchical network between the components of the multi-tRNA synthetase complex: implications for complex formation. *J Biol Chem* **281**, 38663-38667
10. Ray, P. S., Arif, A., and Fox, P. L. (2007) Macromolecular complexes as depots for releasable regulatory proteins. *Trends Biochem Sci* **32**, 158-164
11. Halwani, R., Cen, S., Javanbakht, H., Saadatmand, J., Kim, S., Shiba, K., and Kleiman, L. (2004) Cellular distribution of Lysyl-tRNA synthetase and its interaction with Gag during human immunodeficiency virus type 1 assembly. *J Virol* **78**, 7553-

7564

12. Yannay-Cohen, N., Carmi-Levy, I., Kay, G., Yang, C. M., Han, J. M., Kemeny, D. M., Kim, S., Nechushtan, H., and Razin, E. (2009) LysRS serves as a key signaling molecule in the immune response by regulating gene expression. *Mol Cell* **34**, 603-611

13. Park, S. G., Kim, H. J., Min, Y. H., Choi, E. C., Shin, Y. K., Park, B. J., Lee, S. W., and Kim, S. (2005) Human lysyl-tRNA synthetase is secreted to trigger proinflammatory response. *P Natl Acad Sci USA* **102**, 6356-6361

14. Roesli, C., Borgia, B., Schliemann, C., Gunthert, M., Wunderli-Allenspach, H., Giavazzi, R., and Neri, D. (2009) Comparative analysis of the membrane proteome of closely related metastatic and nonmetastatic tumor cells. *Cancer Res* **69**, 5406-5414

15. Yan, W., Lee, H., Deutsch, E. W., Lazaro, C. A., Tang, W., Chen, E., Fausto, N., Katze, M. G., and Aebersold, R. (2004) A dataset of human liver proteins identified by protein profiling via isotope-coded affinity tag (ICAT) and tandem mass spectrometry. *Mol Cell Proteomics* **3**, 1039-1041

16. Yan, W., Lee, H., Yi, E. C., Reiss, D., Shannon, P., Kwieciszewski, B. K., Coito, C., Li, X. J., Keller, A., Eng, J., Galitski, T., Goodlett, D. R., Aebersold, R., and Katze, M. G. (2004) System-based proteomic analysis of the interferon response in human liver cells. *Genome Biol* **5**, R54

17. Ardini, E., Pesole, G., Tagliabue, E., Magnifico, A., Castronovo, V., Sobel, M. E., Colnaghi, M. I., and Menard, S. (1998) The 67-kDa laminin receptor originated from a ribosomal protein that acquired a dual function during evolution. *Mol Biol Evol* **15**, 1017-1025

18. Auth, D., and Brawerman, G. (1992) A 33-kDa polypeptide with homology to the laminin receptor: component of translation machinery. *Proc Natl Acad Sci U S A* **89**, 4368-4372

19. Nelson, J., McFerran, N. V., Pivato, G., Chambers, E., Doherty, C., Steele, D., and Timson, D. J. (2008) The 67 kDa laminin receptor: structure, function and role in disease. *Biosci Rep* **28**, 33-48

20. Wewer, U. M., Taraboletti, G., Sobel, M. E., Albrechtsen, R., and Liotta, L. A. (1987) Role of laminin receptor in tumor cell migration. *Cancer Res* **47**, 5691-5698

21. Donaldson, E. A., McKenna, D. J., McMullen, C. B., Scott, W. N., Stitt, A. W.,

and Nelson, J. (2000) The expression of membrane-associated 67-kDa laminin receptor (67LR) is modulated in vitro by cell-contact inhibition. *Mol Cell Biol Res Commun* **3**, 53-59

22. Kim, W. H., Lee, B. L., Jun, S. H., Song, S. Y., and Kleinman, H. K. (1998) Expression of 32/67-kDa laminin receptor in laminin adhesion-selected human colon cancer cell lines. *Br J Cancer* **77**, 15-20

23. Nikles, D., Vana, K., Gauczynski, S., Knetsch, H., Ludewigs, H., and Weiss, S. (2008) Subcellular localization of prion proteins and the 37 kDa/67 kDa laminin receptor fused to fluorescent proteins. *Biochim Biophys Acta* **1782**, 335-340

24. Yang, X. W. H., Flores, L. M., Li, Q. L., Zhou, P. C., Xu, F. H., Krop, I. E., and Hemler, M. E. (2010) Disruption of Laminin-Integrin-CD151-Focal Adhesion Kinase Axis Sensitizes Breast Cancer Cells to ErbB2 Antagonists. *Cancer Res* **70**, 2256-2263

25. Suh, H. N., and Han, H. J. (2010) Laminin regulates mouse embryonic stem cell migration: involvement of Epac1/Rap1 and Rac1/cdc42. *Am J Physiol Cell Physiol* **298**, C1159-1169

26. Schlaepfer, D. D., and Mitra, S. K. (2004) Multiple connections link FAK to cell motility and invasion. *Curr Opin Genet Dev* **14**, 92-101

27. Grisaru-Granovsky, S., Salah, Z., Maoz, M., Pruss, D., Beller, U., and Bar-Shavit, R. (2005) Differential expression of protease activated receptor 1 (Par1) and pY397FAK in benign and malignant human ovarian tissue samples. *Int J Cancer* **113**, 372-378

28. Brunton, V. G., Avizienyte, E., Fincham, V. J., Serrels, B., Metcalf, C. A., 3rd, Sawyer, T. K., and Frame, M. C. (2005) Identification of Src-specific phosphorylation site on focal adhesion kinase: dissection of the role of Src SH2 and catalytic functions and their consequences for tumor cell behavior. *Cancer Res* **65**, 1335-1342

29. Givant-Horwitz, V., Davidson, B., and Reich, R. (2005) Laminin-induced signaling in tumor cells. *Cancer Lett* **223**, 1-10

30. Rho, S. B., Kim, M. J., Lee, J. S., Seol, W., Motegi, H., Kim, S., and Shiba, K. (1999) Genetic dissection of protein-protein interactions in multi-tRNA synthetase complex. *Proc Natl Acad Sci U S A* **96**, 4488-4493

31. Kim, J. Y., Kang, Y. S., Lee, J. W., Kim, H. J., Ahn, Y. H., Park, H., Ko, Y. G.,

and Kim, S. (2002) p38 is essential for the assembly and stability of macromolecular tRNA synthetase complex: implications for its physiological significance. *Proc Natl Acad Sci U S A* **99**, 7912-7916

32. Quevillon, S., Robinson, J. C., Berthonneau, E., Siatecka, M., and Mirande, M. (1999) Macromolecular assemblage of aminoacyl-tRNA synthetases: identification of protein-protein interactions and characterization of a core protein. *J Mol Biol* **285**, 183-195

33. Guo, M., Ignatov, M., Musier-Forsyth, K., Schimmel, P., and Yang, X. L. (2008) Crystal structure of tetrameric form of human lysyl-tRNA synthetase: Implications for multisynthetase complex formation. *Proc Natl Acad Sci U S A* **105**, 2331-2336

34. Landowski, T. H., Dratz, E. A., and Starkey, J. R. (1995) Studies of the structure of the metastasis-associated 67 kDa laminin binding protein: fatty acid acylation and evidence supporting dimerization of the 32 kDa gene product to form the mature protein. *Biochemistry* **34**, 11276-11287

35. Buto, S., Tagliabue, E., Ardini, E., Magnifico, A., Ghirelli, C., van den Brule, F., Castronovo, V., Colnaghi, M. I., Sobel, M. E., and Menard, S. (1998) Formation of the 67-kDa laminin receptor by acylation of the precursor. *J Cell Biochem* **69**, 244-251

36. Barczyk, M., Carracedo, S., and Gullberg, D. (2010) Integrins. *Cell Tissue Res* **339**, 269-280

37. Nguyen, B. P., Gil, S. G., and Carter, W. G. (2000) Deposition of laminin 5 by keratinocytes regulates integrin adhesion and signaling. *J Biol Chem* **275**, 31896-31907

38. Xia, Y., and Karin, M. (2004) The control of cell motility and epithelial morphogenesis by Jun kinases. *Trends Cell Biol* **14**, 94-101

39. Fujimura, Y., Yamada, K., and Tachibana, H. (2005) A lipid raft-associated 67 kDa laminin receptor mediates suppressive effect of epigallocatechin-3-O-gallate on Fc epsilon RI expression. *Biochem Bioph Res Co* **336**, 674-681

40. Lafont, F., and Simons, K. (2001) Raft-partitioning of the ubiquitin ligases Cbl and Nedd4 upon IgE-triggered cell signaling. *P Natl Acad Sci USA* **98**, 3180-3184

41. Yasuda, J., Nakao, M., Kawaoka, Y., and Shida, H. (2003) Nedd4 regulates egress of Ebola virus-like particles from host cells. *J Virol* **77**, 9987-9992

42. Rotin, D., and Kumar, S. (2009) Physiological functions of the HECT family of ubiquitin ligases. *Nat Rev Mol Cell Biol* **10**, 398-409

43. Lukk, M., Kapushesky, M., Nikkila, J., Parkinson, H., Goncalves, A., Huber, W., Ukkonen, E., and Brazma, A. (2010) A global map of human gene expression. *Nat Biotechnol* **28**, 322-324

44. Hippo, Y., Taniguchi, H., Tsutsumi, S., Machida, N., Chong, J. M., Fukayama, M., Kodama, T., and Aburatani, H. (2002) Global gene expression analysis of gastric cancer by oligonucleotide microarrays. *Cancer Res* **62**, 233-240

45. Sun, L., Hui, A. M., Su, Q., Vortmeyer, A., Kotliarov, Y., Pastorino, S., Passaniti, A., Menon, J., Walling, J., Bailey, R., Rosenblum, M., Mikkelsen, T., and Fine, H. A. (2006) Neuronal and glioma-derived stem cell factor induces angiogenesis within the brain. *Cancer Cell* **9**, 287-300

46. Jamieson, K. V., Wu, J., Hubbard, S. R., and Meruelo, D. (2008) Crystal structure of the human laminin receptor precursor. *J Biol Chem* **283**, 3002-3005

47. Arif, A., Jia, J., Mukhopadhyay, R., Willard, B., Kinter, M., and Fox, P. L. (2009) Two-site phosphorylation of EPRS coordinates multimodal regulation of noncanonical translational control activity. *Mol Cell* **35**, 164-180

48. Kwon, N. H., Kang, T., Lee, J. Y., Kim, H. H., Kim, H. R., Hong, J., Oh, Y. S., Han, J. M., Ku, M. J., Lee, S. Y., and Kim, S. (2011) Dual role of methionyl-tRNA synthetase in the regulation of translation and tumor suppressor activity of aminoacyl-tRNA synthetase-interacting multifunctional protein-3. *Proc Natl Acad Sci U S A* **108**, 19635-19640

49. Han, J. M., Park, B. J., Park, S. G., Oh, Y. S., Choi, S. J., Lee, S. W., Hwang, S. K., Chang, S. H., Cho, M. H., and Kim, S. (2008) AIMP2/p38, the scaffold for the multi-tRNA synthetase complex, responds to genotoxic stresses via p53. *Proc Natl Acad Sci U S A* **105**, 11206-11211

50. Kim, G., Han, J. M., and Kim, S. (2010) Toll-like receptor 4-mediated c-Jun N-terminal kinase activation induces gp96 cell surface expression via AIMP1 phosphorylation. *Biochem Biophys Res Commun* **397**, 100-105

51. Narumi, K., Inoue, A., Tanaka, M., Isemura, M., Shimo-Oka, T., Abe, T., Nukiwa, T., and Satoh, K. (1999) Inhibition of experimental metastasis of human

fibrosarcoma cells by anti-recombinant 37-kDa laminin binding protein antibody. *Jpn J Cancer Res* **90**, 425-431

52. Menard, S., Tagliabue, E., and Colnaghi, M. I. (1998) The 67 kDa laminin receptor as a prognostic factor in human cancer. *Breast Cancer Res Treat* **52**, 137-145

53. Castronovo, V. (1993) Laminin receptors and laminin-binding proteins during tumor invasion and metastasis. *Invasion Metastasis* **13**, 1-30

54. Liotta, L. A., Rao, N. C., Barsky, S. H., and Bryant, G. (1984) The laminin receptor and basement membrane dissolution: role in tumour metastasis. *Ciba Found Symp* **108**, 146-162

55. Yung, Y., Yao, Z., Aebersold, D. M., Hanoch, T., and Seger, R. (2001) Altered regulation of ERK1b by MEK1 and PTP-SL and modified Elk1 phosphorylation by ERK1b are caused by abrogation of the regulatory C-terminal sequence of ERKs. *J Biol Chem* **276**, 35280-35289

56. Naoghare, P. K., Ki, H. A., Paek, S. M., Tak, Y. K., Suh, Y. G., Kim, S. G., Lee, K. H., and Song, J. M. (2010) Simultaneous quantitative monitoring of drug-induced caspase cascade pathways in carcinoma cells. *Integr Biol (Camb)* **2**, 46-57

57. Naoghare, P. K., Kim, M. J., and Song, J. M. (2008) Uniform threshold intensity distribution-based quantitative multivariate imaging cytometry. *Anal Chem* **80**, 5407-5417

58. Gagnoux-Palacios, L., Dans, M., van't Hof, W., Mariotti, A., Pepe, A., Meneguzzi, G., Resh, M. D., and Giancotti, F. G. (2003) Compartmentalization of integrin alpha6beta4 signaling in lipid rafts. *J Cell Biol* **162**, 1189-1196

Chapter Ⅱ

Tumor Suppressor AIMP2 Regulates Smad7-Smurf2-Mediated Negative Regulation of TGF-β Signaling

Running title: AIMP2 enhances TGF-β signaling via controlling negative feedback

Keywords: ARS-interacting multifunctional protein 2, Smurf2, Smad7, TGF-β receptor I, FBP, TGF-β signal

Abbreviations list

AIMP2: ARS-interacting multifunctional protein2

MSC: Multi-tRNA synthetase complex

KRS: Lysyl-tRNA synthetase

EV: Empty vector

si-con: si-control

WCL: Whole cell lysate

Abstract

ARS-interacting multifunctional protein 2 (AIMP2) is a scaffolding protein required for the formation of macromolecular tRNA synthetase complex. AIMP2 also plays pivotal roles as a tumor suppressor to regulate cell growth and death. Here, the functional significance of AIMP2 in TGF-β signaling was investigated. AIMP2 enhances TGF-β signaling and facilitates TGF-β-mediated cell cycle arrest. Upon TGF-β signal, AIMP2 is phosphorylated by p38MAPK and then translocated into the nucleus. While, in the nucleus, AIMP2 directly binds to Smurf2-Smad7 complex and activates Smurf2 E3 ubiquitin ligase that targets FUSE binding protein 1 (FBP1), a transcriptional activator of c-myc, AIMP2 stabilizes TGF-β receptor through nuclear activation and degradation of Smurf2. Thus, this work suggests the novel activity of AIMP2 as a mediator of TGF-β signaling and a component of negative feedback loop of TGF-β signaling pathway.

Introduction

TGF-β signaling pathway is involved in the regulation of diverse cellular functions, including cell proliferation, differentiation, migration and apoptosis (1, 2). Alteration of TGF-β signaling can lead to human diseases such as fibrosis and cancer (3-5). TGF-β signaling is initiated by binding of TGF-β to type II receptor. Activated type II receptor by interaction of TGF-β recruits and phosphorylates the type I receptor, which propagates the signal via phosphorylation of Smad proteins. Then phosphorylated Smad2 and Smad3 (R-Smad) form the complex with Smad4 (Co-Smad) and translocate into the nucleus to regulate gene transcription (6). Duration and stability of TGF-β signaling is tightly regulated via negative feedback loop. Negative feedback loop of TGF-β signaling is composed of Smad7 (I-Smad) (7) and Smad ubiquitin regulatory factors 2 (Smurf2), HECT type E3 ubiquitin ligase (8, 9). To terminate the signal, Smurf2 is activated by interaction of Smad7 in nucleus. The Smad7-Smurf2 complex is subsequently targeted to active TGF-β receptor I in the plasma membrane (10). N-terminal region of Smad7 helps the association between HECT domain of Smurf2 and UbcH7, E2 conjugating enzyme (11). Upon association of the Smad7-Smurf2 complex with TGF-β receptor I, both Smad7 and TGF-β receptor I are subjected to ubiquitination

for proteosomal degradation (12). The turnover of TGF-β receptor I drives the termination of TGF-β signaling and inhibits the excess proceeding of signal.

Aminoacyl-tRNA synthetases (ARSs) are housekeeping enzymes that ligate the amino acids to their cognate tRNAs. In eukaryotes, nine different ARSs form the macromolecular complex, multi-tRNA synthetase complex (MSC), with the three auxiliary components, AIMP1, AIMP2, and AIMP3 (13). The AIMPs facilitate the union of the MSC (14). In addition to scaffolding function of AIMPs, they also play the non-canonical functions (15). AIMP1 is secreted as a cytokine for regulating angiogenesis (16), immune response (17) and has the glucose-like function (18). AIMP3 is revealed as tumor suppressor through the activation of p53 via interaction with ATM/ATR (19) and is involved the aging phenotype (20). AIMP2 induces cell death by activation of p53 (21) and degradation of TRAF2 (22) in response to DNA damage and TNF-α signal, respectively. Reduction of AIMP2 in multi-organ carcinogenesis mouse model provides enhanced susceptibility to tumor formation, proving AIMP2 as a haploinsufficient tumor suppressor (23). Upon TGF-β stimulation, AIMP2 is translocated into the nucleus, binds to FBP1, a transcriptional activator of c-myc, and enhances ubiquitination and degradation of FBP1, resulting in reduction of c-myc transcription (24). However, the molecular details of AIMP2 nuclear translocation and

FBP1 degradation, and the role of AIMP2 in TGF-β signaling pathway have been unknown. Here the functional significance and working mechanism of AIMP2 in the regulation of TGF-β signaling pathway was investigated.

Results

AIMP2 enhances TGF-β signal

Since AIMP2 facilitates the degradation of FBP by TGF-β signal (24), it was investigated whether AIMP2 is involved in TGF-β signaling. To determine the role of AIMP2 in TGF-β signaling pathway, the phosphorylation of Smad2, TGF-β signal mediator, was checked up. The phosphorylation of Smad2 in AIMP2-knockdowned HeLa cells using si-AIMP2 was analyzed. When AIMP2 was downregulated, declined phosphorylation of Smad2 was observed (Figure II-1A). When AIMP2 was overexpressed in HeLa cells, drastically increased phosphorylation of Smad2 was observed than when AIMP2 was not overexpressed (Figure II-1B). Also, it was compared the response of Smad2 phosphorylation in mouse embryonic fibroblasts (MEFs) from $AIMP2^{+/+}$ and $AIMP2^{-/-}$ mice. The phosphorylated duration of Smad2 was decreased by the depletion of AIMP2 (Figure II-1C, left). Next, the expression of AIMP2 was rescued in knockout MEF cells and monitored the phosphorylation of Smad2. Through adding AIMP2 in $AIMP2^{-/-}$ MEF cells, the amounts of phosphorylated Smad2 was recovered as similar as wild type MEF cells, suggesting the critical role of AIMP2 in TGF-β signaling (Figure II-1C, right). To confirm the effect of AIMP2 on

TGF-β signaling, it was checked TGF-β-mediated transcription of target promoter, SBE, by luciferase assay. In condition of declined AIMP2, the decreased activity of SBE was observed (Figure II-1D). While AIMP2 was overexpressed, opposite result, enhancement of reporter activity was observed (Figure II-1E). For monitoring the effect of AIMP2 on TGF-β-mediated gene activation, the AIMP2 recovery experiment was repeated in AIMP2$^{-/-}$ MEF cells. The reduced luciferase activity of SBE was observed in AIMP2$^{-/-}$ MEF cells, but the activity was rescued by recovery of AIMP2 in the same cells (Figure II-1F).

TGF-β-mediated phosphorylation of AIMP2 is required for nuclear localization

To understand the enhancement of TGF-β signal by AIMP2, the molecular behavior of AIMP2 was investigated upon TGF-β signaling. Previous report described that AIMP2 is phosphorylated by UV damage and moves to nucleus from cytosol (21). So it was tested whether TGF-β signal-mediated phosphorylation of AIMP2 is happened by 2D electrophoresis. The spot of AIMP2 was mobilized by treatment of TGF-β1 and shifted spots were removed upon treating alkaline phosphatase, implying the TGF-β signal-mediated phosphorylation of AIMP2 (Figure II-2A). Also cells were transfected with Myc-AIMP2 and incubated in medium with TGF-β1 or without TGF-β1. The

precipitated Myc-AIMP2 was subjected to SDS-PAGE and immunoblotting with antibody against p-serine, -threonine, -tyrosine. When TGF-β1 was treated, the phosphorylation of AIMP2 at serine residue was observed (Figure II-2B). Next it was checked up which kinase phosphorylates AIMP2. Since the TGF-β signal is mediated by p38MAPK and JNK (25), the phosphorylation of AIMP2 was monitored by 2D electrophoresis after SB202190 or SP600125, inhibitor of p38MAPK and JNK, respectively, was treated. When SB202190 was pretreated, TGF-β signal-mediated phosphorylation of AIMP2 was not observed (Figure II-3A). But phosphorylation of AIMP2 was not affected by pretreatment of SP600125 (Figure II-3B). p38MAPK-mediated phosphorylation of AIMP2 was also confirmed by using anti-p-ser antibody. When SB202190 were pretreated, the TGF-β-mediated phosphorylation of AIMP2 was not observed (Figure II-2C). But pretreatment of SP600125 did not affect the phosphorylation of AIMP2, suggesting that p38MAPK specifically phosphorylates AIMP2 (Figure II-3C). To check whether p38MAPK actually phosphorylates AIMP2, *in vitro* kinase assay was performed in the presence of [γ-^{32}P] ATP. It was observed that p38MAPK activated by treating with TGF-β1 directly phosphorylates purified AIMP2 (Figure II-2D). Also the interaction of AIMP2 to p38MAPK was checked. The endogenous binding of p38MAPK to AIMP2 was confirmed by immunoprecipitation

(Figure II-3D) and pull down assay shows direct binding between AIMP2 and p38MAPK (Figure II-3E). So it was concluded that p38MAPK phosphorylates AIMP2 on serine residue by TGF-β signal. Next, it was investigated which serine residue of AIMP2 is the phosphorylation site. Phosphorylation site of AIMP2 was predicted from website, NetPhos 2.0 server. As a result, serine 156, 157 and 160 were predicted as potent phosphorylation sites. AIMP2 mutants containing S156A, S157A, S160A and S157A/S160A, which serine 157, 160 is simultaneously double mutated to alanine, were generated. AIMP2 mutants were subjected to *in vitro* kinase assay using activated p38MAPK. Through *in vitro* kinase assay, the phosphorylation of S156A was ablated and another mutants were phosphorylated as wild type AIMP2 (Figure II-2E). TGF-β signal-mediated phophosrylation of AIMP2 was not observed in 293T cells expressed S156A mutant (Figure II-2F). To investigate whether the phosphorylation actually affects the TGF-β signal-dependent translocation of AIMP2, it was monitored TGF-β signal-mediated localization of AIMP2. Through cellular fractionization, it was observed that S156A mutant expressed cells could not move to nucleus upon treating TGF-β1 (Figure II-2G, middle). In case of S156D mutant that can mimic the phosphorylation on serine 156, it was showed the constitutively increased nuclear residence of AIMP2 although TGF-β1 was not treated (Figure II-2G, bottom). The

localization of AIMP2 mutants was monitored by immumofluoresence staining when the TGF-β signal was treated or not. Upon treating TGF-β1, nuclear foci of GFP-AIMP2 wild type were observed, but GFP-S156A mutants did not (Figure II-2H, middle). The residence of GFP-S156D mutants in nucleus was basally monitored when TGF-β1 was treated or not (Figure II-2H, bottom). Combined together, phosphorylation of AIMP2 on serine 156 via p38MAPK leads nuclear translocation of AIMP2 from cytosol.

AIMP2 binds to Smad7

To investigate how AIMP2 enhances TGF-β signal, the binding between AIMP2 and Smads, regulating components of TGF-β signal, was screened. Each FLAG-tagged Smad1, 2, 3, 5 (R-Smad), 6 and 7 (I-Smad) was introduced into 293T cells with Myc-AIMP2 and the cells were treated with TGF-β1. The cells were lysed and immunoprecipitated with anti-Myc antibody. Through immunoprecipitation, it was monitored that Smad7 is specifically precipitated with AIMP2 (Figure II-4A). Further investigation of the interaction between AIMP2 and Smad7 by yeast two-hybrid assay was confirmed. As same as the result of immunoprecipitation, AIMP2 formed the colony with Smad7, not Smad2 and 3, in leucine-depleted media (Figure II-5). It was

checked up whether the interaction between AIMP2 and Smad7 is direct. Through *in vitro* pull down assay using GST-AIMP2 and radioactively synthesized Smad7, it was determined that AIMP2 directly binds to Smad7 (Figure II-4B). Next, the endogenous interaction of AIMP2 to Smad7 was monitored. Through endogenous immunoprecipitation with anti-AIMP2 antibody, it was observed that endogenous AIMP2 binds to Smad7 (Figure II-4C). Since the expression of Smad7 is induced by TGF-β signal in nucleus, it was checked whether interaction of two molecules is induced and where is the cellular localization of interaction. To confirm the induction and localization of binding, HeLa cells expressed Myc-AIMP2 were pretreated with MG132 and treated with TGF-β1 as time dependent manner. After the cells were fractionized into cytosol and nucleus, each fraction was immunoprecipitated with anti-Myc antibody. The amounts of co-precipitated Smad7 with AIMP2 were time dependently induced by TGF-β signal in nucleus (Figure II-4D). It was determined the binding region of the two proteins. Smad7 was divided into two domains, N-terminal domain (NTD) and PY-motif (N), and MH2 domain (C) (Figure II-4E, bottom). GFP-Smad7 wild type (WT), N and C mutants were overexpressed with Myc-AIMP2 in 293T cells. Through co-immunoprecipitation with anti-Myc antibody, it was observed that AIMP2 binds to MH2 domain of Smad7 (Figure II-4E, upper). Conversely, to map

the binding region of AIMP2 to Smad7, three deletion mutants (1-83aa, 84-225aa and 226-320aa) of AIMP2 were used. The region of AIMP2 containing 84-225 amino acids was co-immunoprecipitated with Smad7 (Figure II-4F). To elucidate the correct binding region of two proteins, 84-225 amino acids region of AIMP2 were further divided into four fragments. Through pull down assay, it was confirmed that Smad7 preferentially binds to 156-191 amino acids region of AIMP2 (Figure II-4G). Combined together, all the binding data shows the middle region of AIMP2 directly binds to MH2 domain of Smad7 in nucleus as TGF-β signal dependent manner.

AIMP2 forms the ternary complex with Smad7 and Smurf2

After Smad7 is induced by TGF-β signal, Smad7 binds to Smurf2 for forming the negative feedback complex (10). So it was determined whether AIMP2 is comprised in negative feedback complex of TGF-β signal. 293T cells expressed Myc-AIMP2, FLAG-Smurf2 and GFP-Smad7 were treated with TGF-β1 and immunoprecipitated with anti-Myc antibody. Smad7 and Smurf2, components of negative feedback complex, were precipitated with AIMP2 (Figure II-6A). The same cells were subjected to immunoprecipitation with anti-GFP antibody for precipitating Smad7, one of the negative feedback complex. Smurf2 and AIMP2 were also precipitated with Smad7

(Figure II-6B), suggesting that Smad7 and Smurf2 form the ternary complex. Since AIMP2 is comprised of TGF-β signal negative feedback complex via binding to Smad7, it was checked up whether AIMP2 increases the interaction between Smad7 and Smurf2. When AIMP2 was overexpressed, it was observed the increased binding between Smad7 and Smurf2 by immunoprecipitation (Figure II-6C). Also the same result was obtained by pull down assay. When AIMP2 was increased as dose dependent manner, the interaction between Smurf2 and Smad7 was enhanced and AIMP2 was also precipitated together with Smurf2 as same pattern as Smad7 (Figure II-6D). Through *in vitro* pull down assay, it was concluded that the increased interaction of Smad7 to Smurf2 via AIMP2 is direct effect, not other molecular effect. Since Smurf2 is exported by binding with Smad7 in nucleus (10), it was checked whether AIMP2 affects the translocation of negative feedback complex of TGF-β signal. HeLa cells overexpressed AIMP2 were pretreated with MG132 and treated with TGF-β1 as time dependent manner. The cells were fractionized to cytosol and nucleus. When AIMP2 was overexpressed, nuclear export of Smad7 and Smurf2 was failed and accumulated amounts of them in nucleus were increased (Figure II-6E). Since the exported negative feedback complex binds to TGF-β receptor I for stop the signal (11), it was checked whether the interaction between TGF-β receptor I and Smad7 is affected by AIMP2.

Through the immunoprecipitation, it was confirmed that co-precipitated amounts of Smad7 with TGF-β receptor I were declined when AIMP2 was overexpressed (Figure II-6F). All the data shows that AIMP2 enhances the interaction between Smurf2 and Smad7, resulting the accumulation of negative feedback complex in nucleus.

AIMP2 enhances auto-ubiquitination of Smurf2

If Smurf2 fails to export to cytosol and accumulates in nucleus, the auto-ubiquitination of Smurf2 is processed with Smad7, leading to ubiquitination-mediated turnover (10, 26). Since AIMP2 inhibits the export of Smad7 and Smurf2, it was monitored whether AIMP2 leads the turnover of Smurf2. The expression level of Smurf2 and Smad7 was compared in $AIMP2^{+/+}$ and $AIMP2^{-/-}$ MEF cells. AIMP2 knockout caused the enhanced expression of Smurf2 and Smad7, but the expression of TGF-β receptor I was downregulated (Figure II-7A). The ectopic expression of AIMP2 in HeLa cells showed the declined expression of Smurf2 and Smad7, but the expression of TGF-β receptor I was increased (Figure II-7B, left). Opposite result was obtained when AIMP2 was knockdowned by using specific si-RNA (Figure II-7B, right). Next, the protein stability of Smurf2 was checked up through pulse chase analysis. Overexpression of AIMP2 ablated the stability of Smurf2 (Figure II-7C) and the stability of Smurf2 was sustained

when AIMP2 was knockdowned (Figure II-7D). Since the accumulated Smurf2 in nucleus is subjected to auto-ubiquitination (10), it was investigated whether the altered stability of Smurf2 via AIMP2 is caused by ubiquitination. The amounts of ubiquitinated Smurf2 were increased in AIMP2 overexpressing 293T cells (Figure II-7E). AIMP2-downregulated 293T cells showed the declined ubiquitination of Smurf2 (Figure II-7F).

AIMP2 inhibits Smad7-mediated degradation of TGF-β receptor I

Since the positive relationship between AIMP2 and TGF-β receptor I was monitored in the cells modified the expression of AIMP2 (Figure II-7A, B) and AIMP2 controls the stability of Smurf2, specific E3 ligase of TGF-β receptor I, it was investigated whether AIMP2 affects the stabilization of TGF-β receptor I. The stability of TGF-β receptor I was checked by the pulse chase assay. When AIMP2 is increased, the sustained stability of TGF-β receptor I was observed (Figure II-7G). AIMP2-downregulated cells showed the opposite results (Figure II-7H). Since the turnover of TGF-β receptor I is mediated by ubiquitination, it was tried to observe whether the expression of AIMP2 actually affects the ubiquitination of TGF-β receptor I. The ubiquitinated amounts of TGF-β receptor I were diminished when ectopic AIMP2 was expressed (Figure II-7I). Also,

opposite result was observed in AIMP2-decreased condition (Figure II-7J). Because the ubiquitination of TGF-β receptor I is controlled by binding of Smad7, inhibitory Smad (27), it was checked whether AIMP2 affects the Smad7-mediated turnover of TGF-β receptor I. Smad7-dependent turnover of TGF-β receptor I was recovered by overexpression of AIMP2 (Figure II-7K). Since AIMP2 controls the accumulation of Smad7 in nucleus, it was determined whether nuclear translocation of AIMP2 affects Smad7 dependent-turnover of TGF-β receptor I by using serine 156 mutants of AIMP2. S156A mutant failed to recovery the expression of TGF-β receptor I as wild type, but S156D mutant showed the similar effect as wild type (Figure II-7K). Also, to check whether AIMP2 affects Smad7-mediated regulation of TGF-β signal, SBE-luciferase assay was tried. In HeLa cells expressed S156A mutant, the effect of recovery as wild type on Smad7-mediated suppression of activity was not observed, but S156D was as similar as wild type (Figure II-7L).

Smurf2 works as a E3 ligase of FBP via AIMP2

Since nuclear accumulation of Smuf2 leads it to work as the E3 ligase of nuclear other targets (10). It was previously reported that AIMP2 downregulated the expression of FBP in nucleus (24). Since AIMP2 leads the accumulation of Smurf2 in nucleus, it was

investigated whether Smurf2 has the possibility to work as E3 ligase of FBP. First, the endogenous interaction between Smurf2 and FBP was determined by immunoprecipitation. The endogenous Smurf2 is co-immunoprecipitated with FBP (Figure II-8A). Previous report showed the 84-225aa peptide region of AIMP2 binds to FBP (24). To check whether the binding region of AIMP2 to Smad7 and FBP is overlapped, the interaction region of AIMP2 to FBP was further determined. Pull down assay revealed that 84-155aa region of AIMP2 preferentially binds to FBP (Figure II-8B). Since E3 ligase binds to substrate for delivery of ubiquitin (28), it was checked whether TGF-β signal induces the interaction between FBP and Smurf2. 293T cells expressed FLAG-Smurf2 were pretreated with MG132 and cultivated in the absence or presence of TGF-β1. After immunoprecipitation using anti-FBP antibody, co-precipitated amounts of Smurf2 were detected. The treatment of TGF-β1 increased the interaction between Smurf2 and FBP (Figure II-8C). To determine whether AIMP2 enhances the binding of Smurf2 to FBP, Myc-AIMP2 was introduced into 293T cells expressed FLAG-Smurf2 and treated with MG132 and TGF-β1. Through the immunoprecipitation, it was observed that AIMP2 enhanced the binding of Smurf2 to FBP and AIMP2 was also bound to FBP when the interaction between Smurf2 and FBP was increased (Figure II-8D). It was speculated that AIMP2 could play a role of adaptor

in Smurf2-mediated ubiquitination of FBP. To identify the function of AIMP2 as adaptor in degradation of FBP, it was monitored the expression of FBP in HeLa cells which is transfected with FLAG-Smurf2, GFP-Smad7 and Myc-AIMP2. The declined expression of FBP was not observed by just ectopic expression of Smurf2 and Smad7, but adding of AIMP2 with Smurf2 and Smad7 caused drastic turnover of FBP (Figure II-8E). If the degradation of FBP was mediated by Smurf2, E3 ligase, ubiquitination of FBP should be observed. So, it was determined the amounts of ubiquitinated FBP as same condition as above. The ubiquitnation assay showed the enhanced ubiquitination of FBP in condition of simultaneous overexpression with Smurf2, Smad7 and AIMP2 (Figure II-8F). Taken together, all the data shows the relationship between Smurf2 and FBP is E3 ligase and substrate, respectively, and AIMP2 might work as a adaptor of binding between Smurf2 and FBP.

AIMP2 enhances TGF-β signal-mediated suppression of proliferation

Since TGF-β signal is known to suppress the proliferation (3) and AIMP2 works as positive regulator of TGF-β signal via the suppression of negative feedback, it was checked whether AIMP2-mediated enhancement of TGF-β signal consequently induces inhibition of proliferation. Through the thymidine incorporation assay, TGF-β signal-

dependent suppression of proliferation was not observed in AIMP2$^{-/-}$ MEF cells (Figure II-9A). The result as similar as AIMP2$^{-/-}$ MEF cells was monitored when AIMP2 was knockdowned by using AIMP2 specific si-RNA in HeLa cells (Figure II-9B). Conversely, opposite result was observed in AIMP increased condition. The TGF-β signal-mediated suppression of proliferation was accelerated by ectopic expression of AIMP2 (Figure II-9C). Also, the cell cycle of AIMP2$^{-/-}$ MEF cells was analyzed upon treating TGF-β1 compared to AIMP2$^{+/+}$ MEF cells by using flow cytometry. Portion of G0/G1 phase in cell cycle was increased upon treating TGF-β1 in AIMP2$^{+/+}$ MEF cells, but, in AIMP2$^{-/-}$ MEF cells, TGF-β signal-dependent increase of G0/G1 phase in cell cycle was not observed (Figure II-9D). The same result was also observed in knockdowned cells using si-AIMP2. While control cells showed increase of G1 phase in cell cycle upon treating TGF-β1, the enhancement of it was not observed in AIMP2 transiently knockdowned cells (Figure II-9E). To check whether nuclear traslocation of AIMP2 affects TGF-β signal dependent-inhibition of proliferation, the proliferation was monitored in HeLa cells expressed AIMP2 phosphorylation mutants through thymidine incorporation assay. As expected, HeLa cells expressed AIMP2 wild type and S156D mutant enhanced TGF-β signal-mediated inhibition of proliferation, but it could not observe the wild type effect in case of S156A mutant cell line (Figure II-9F).

Taken together, the phosphorylation of AIMP2 on serine 156 by p38MAPK drives the nuclear translocation of AIMP2. AIMP2 forms the ternary complex with Smad7 and Smurf2, negative feedback molecule of TGF-β signal, in nucleus. AIMP2 bound to negative feedback complex leads the accumulation of the complex and the auto-ubiquitination of Smurf2 in nucleus. Accumulated Smurf2 via AIMP2 in nucleus also works as E3 ligase of FBP, which is strong transcription enhancer of c-myc, resulting in the downregulation of c-myc. Also the degradation of Smurf2 and Smad7 via AIMP2 contributes the stabilization of TGF-β receptor I and enhances the TGF-β signal. Consequently, turnover of FBP via Smurf2 and stabilization of TGF-β receptor I via the nuclear translocation of AIMP2 cause the growh arrest of the cells (Figure II-10).

Figure II-1. AIMP2 facilitates the TGF-β signal

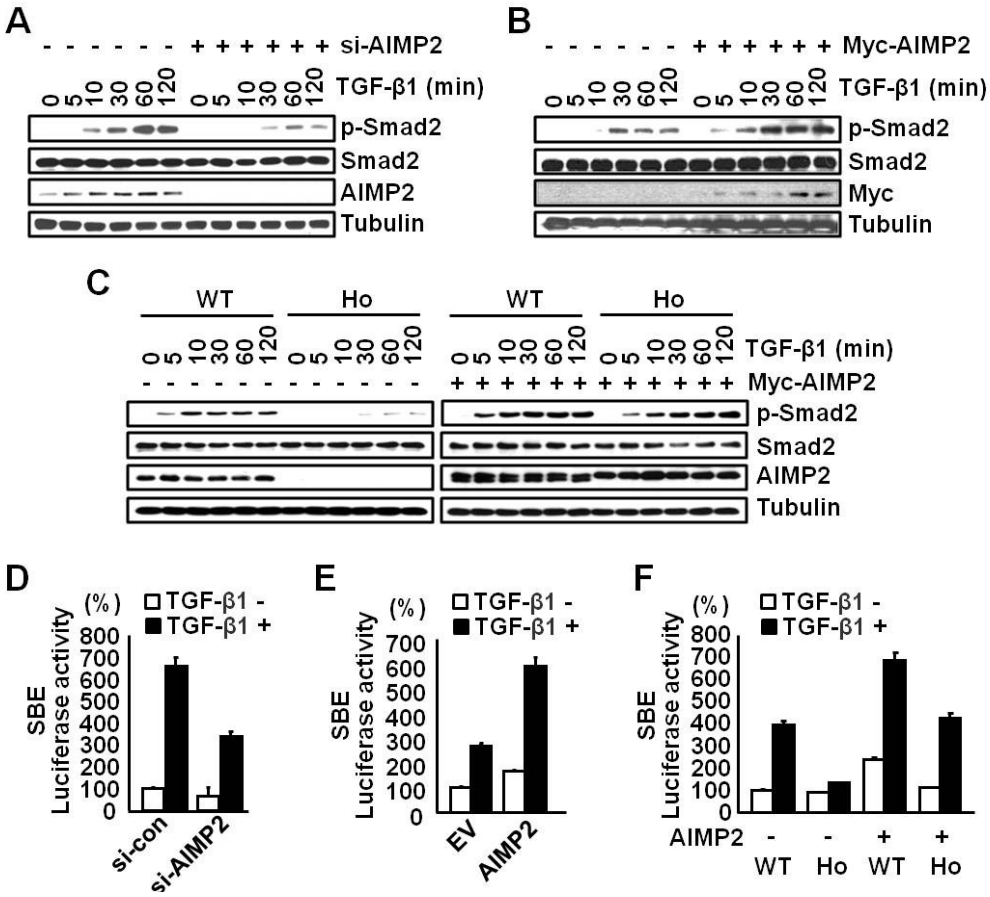

Figure II-1. AIMP2 facilitates the TGF-β signal. **(A, B)** To monitor whether AIMP2 affects to TGF-β signal, AIMP2 was knockdownded and overexpressed into HeLa cells by using AIMP2 specific si-RNA (A) and Myc-AIMP2 (B), respectively, and the cells were treated with TGF-β1 time dependently. The cells were lysed and subjected to SDS-PAGE. Amounts of phosphorylated Smad2 were detected with anti-p-Smad2 antibody. Tubulin was used as loading control. **(C)** Myc-AIMP2 or EV was introduced into $AIMP2^{+/+}$ and $AIMP2^{-/-}$ mouse embryonic fibroblast (MEF) cells. Extracts from the cells treated wih TGF-β1 time dependently were subjected to immunoblottting. The amounts of p-Smad2 was determined as above. **(D, E)** AIMP2 knockdowned (D) or overexpressed (E) HeLa cells were transfected with SBE-luciferase gene and treated with TGF-β1. The cells were subjected to luciferase assay. **(F)** EV or Myc-AIMP2 was

overexpressed into AIMP2$^{+/+}$ and AIMP2$^{-/-}$ MEF cells which expressed SBE-luciferase gene. TGF-β1 treated MEF cells were analyzed as above.

Figure II-2. Phosphorylation of AIMP2 is required for nuclear translocation

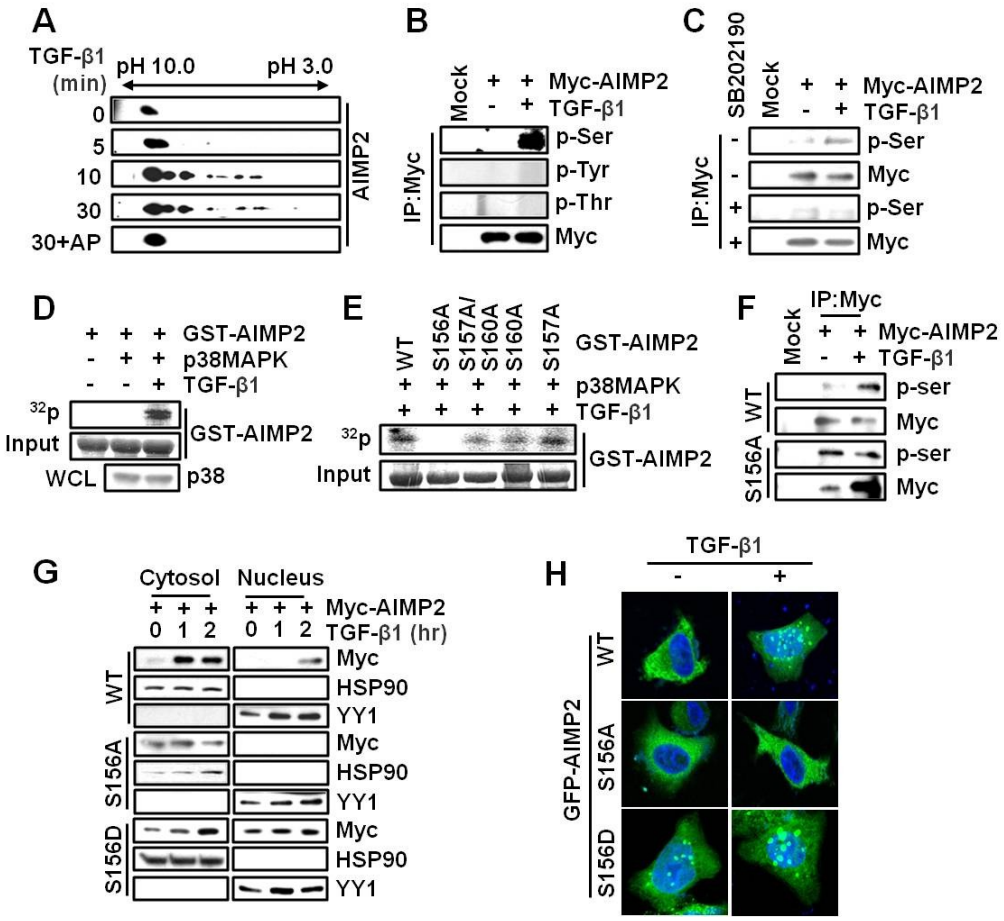

Figure II-2. Phosphorylation of AIMP2 is required for nuclear translocation. **(A)** HeLa cells were treated with TGF-β1 time dependently and the each cell was subjected to two dimensional electrophoresis. Isoelectrically separated AIMP2 was detected by using anti-AIMP2 antibody. Alkaline phosphatase (AP) were treated to lysates incubated with TGF-β1 for 30min. **(B)** 293T cells expressing Myc-AIMP2 were treated with TGF-β1 or not. AIMP2 was immunoprecipitated with anti-Myc antibody and phosphorypation of AIMP2 was detected by anti-p-Ser, p-Tyr and p-Thr antibody. **(C)** Myc-AIMP2 introduced 293T cells were incubated in different combination of SB2020190 and TGF-β1. The immunoprecipitated AIMP2 was subjected to SDS-PAGE. Phosphorylation was detected with anti-p-Ser antibody. **(D)** GST-AIMP2 was subjected to *in vitro* kinase

assay with [γ-^{32}P] ATP and p38MAPK. p38MAPK is prepared by immunoprecipitation in HeLa cells cultured in the presence or absence of TGF-β1. Phosphorylation was determined by autoradiography. **(E)** GST-AIMP2 containing S156A, S157A/S160A, S160A and S157A mutations was reacted with activated p38MAPK and [γ-^{32}P] ATP, and phosphorylation was detected by autoradiography. **(F)** Myc-AIMP2 wild type (WT) and S156A mutant was expressed into 293T cells. The cells were treated with TGF-β1 and the amounts of phosphorylated AIMP2 was detected as above. **(G)** HeLa cells introduced Myc-AIMP2 wild type (WT), S156A and S156D were treated with TGF-β1 time dependently and seperated into cytosol and nucleus fraction. The amounts of AIMP2 in each fraction were detected with using anti-AIMP2 antibody. **(H)** GFP-AIMP2 wild type (WT), S156A and S156D expressed HeLa cells were treated with TGF-β1. Nuclear AIMP2 was monitored with GFP using confocal microscopy.

Figure II-3. p38MAPK phosphorylates AIMP2

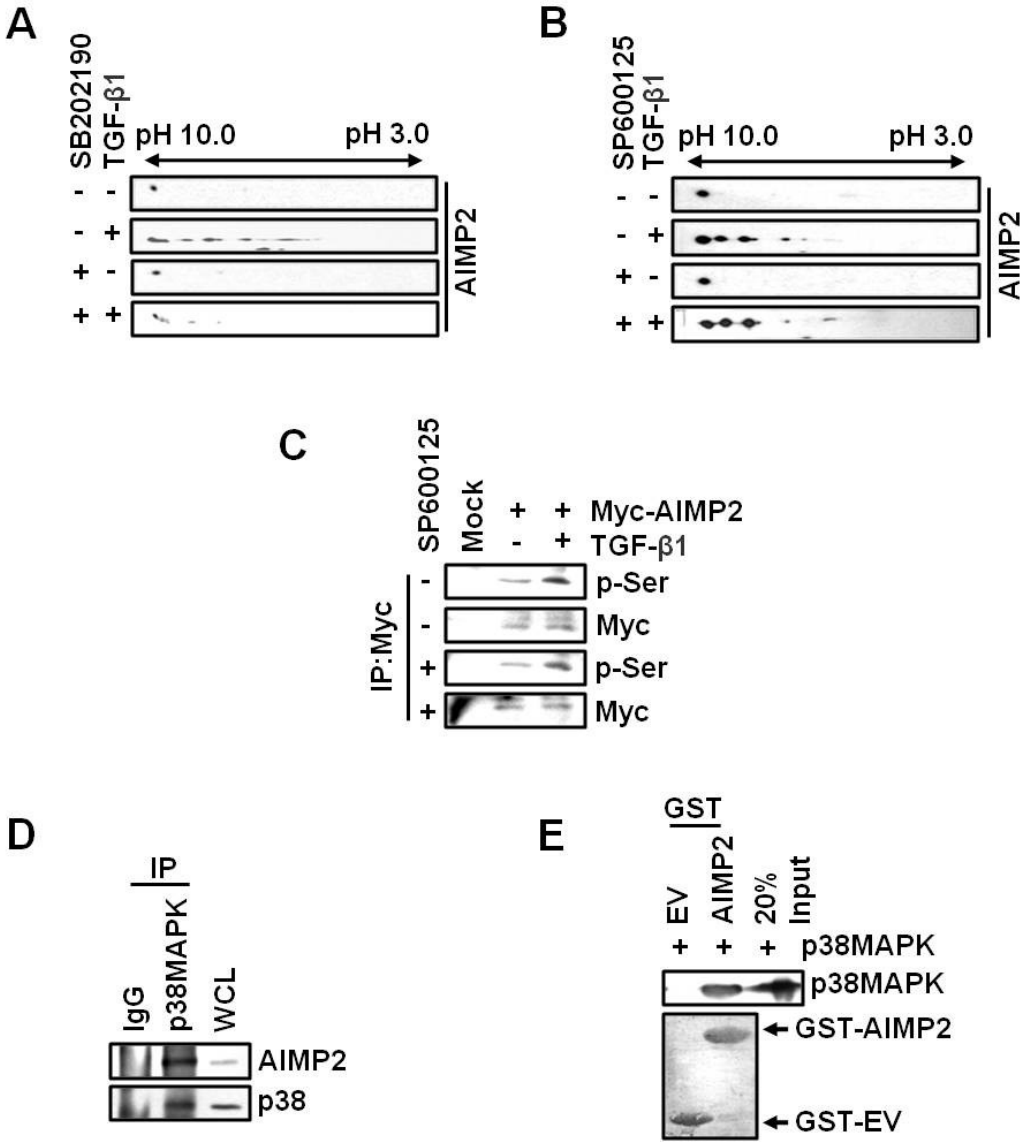

Figure II-3. p38MAPK phosphorylates AIMP2. **(A, B)** SB202190 (A), SP600125 (B) and TGF-β1 were treated to HeLa cells in different combination. Harvested cells were subjected to two dimensional electrophoresis. Isoelectrically moved AIMP2 was detected with anti-AIMP2 antibody. **(C)** The different combination of SB2020190 and TGF-β1 were treated into Myc-AIMP2 expressed 293T cells. Myc-AIMP2 was immunoprecipitated by anti-Myc antibody and the immunoprecipitates were subjected

to SDS-PAGE. Anti-p-Ser antibody was used for detecting phosphorylation of AIMP2. **(D)** Extracts from HeLa cells treated with TGF-β1 were immunoprecipitated by using anti-p38MAPK antibody. Co-precipitated AIMP2 with p38MAPK was determined by anti-AIMP2 antibody. **(E)** The cell lysates expressed p38MAPK was mixed with GST-AIMP2 and pull downed with glutathione-Sepharose beads. The amounts of precipitated p38MAPK were detected by Western blotting with anti-p38MAPK antibody.

Figure II-4. Interaction between AIMP2 and Smad7

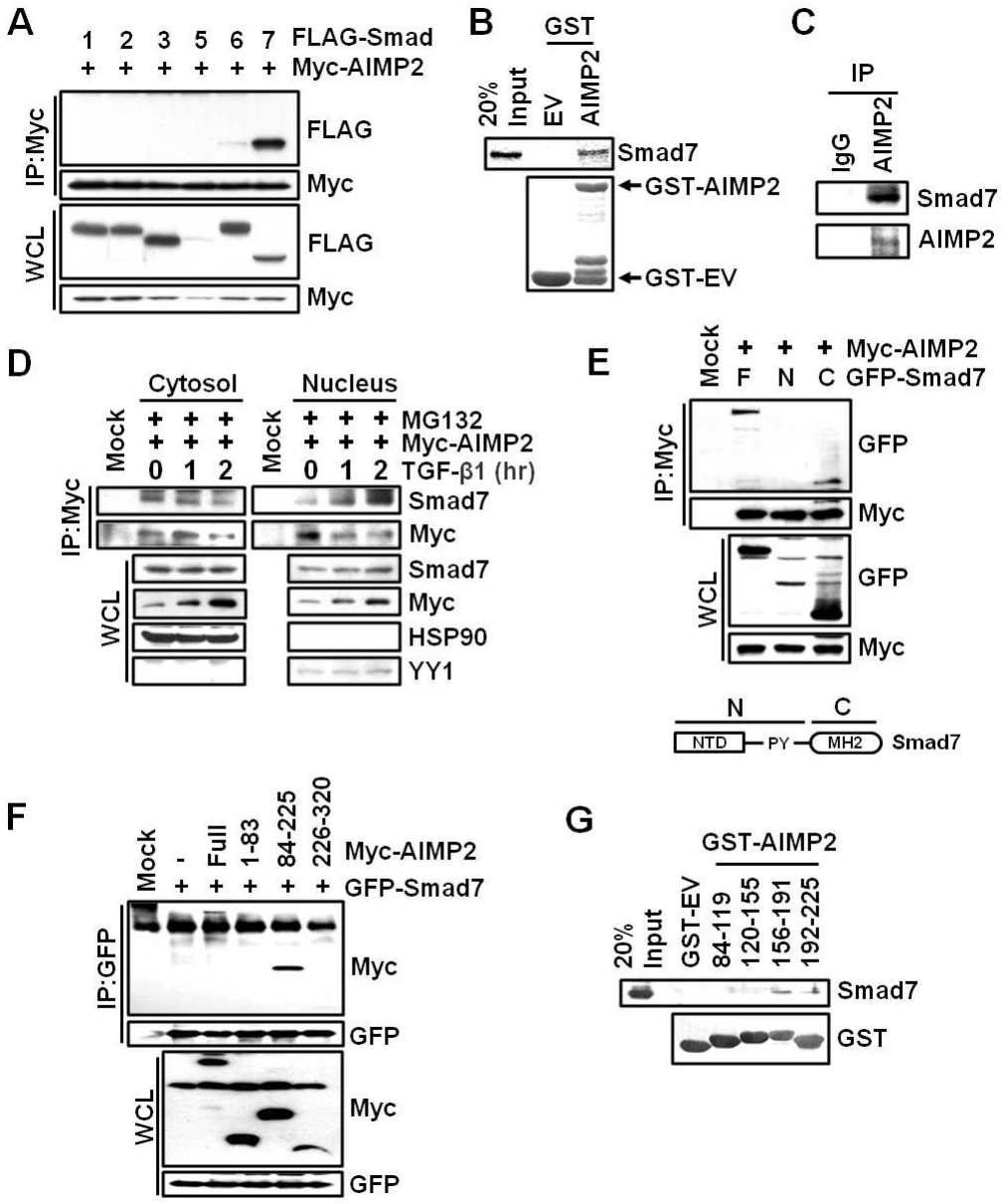

Figure II-4. Interaction between AIMP2 and Smad7. **(A)** Myc-tagged AIMP2 and each FLAG-tagged Smad (Smad1, Smad2, Smad3, Smad5, Smad6 and Smad7) were expressed into 293T cells and treated with TGF-β1. Each cells were lysed and immuniprecipitated witn anti-Myc antibody. Precipitates were separated to SDS-PAGE. Co-precipitates with AIMP2 were detected with anti-FLAG antibody. **(B)** GST-AIMP2

was reacted with Smad7 synthesized by *in vitro* translation in the presence of [^{35}S] methionine and subjected to pull-down with glutathione-Sepharose beads. Co-precipitated Smad7 was detected by autoradiography. **(C)** Endogenous AIMP2 was immunoprecipitated with anti-AIMP2 antibody in TGF-β1 treated HeLa cells. Precipitates were separated by SDS-PAGEC and subjected to Western blotting with anti-Smad7 antibody. **(D)** Myc-AIMP2 transfected HeLa cells were pre-incubated and treated with MG132 and TGF-β1, respectively. The cells were fractionated into cytosol and nucleus and each fraction was immunoprecipitated with anti-Myc antibody. Co-precipitated Smad7 was monitored by Western blotting. **(E)** 293T cells expressed Myc-AIMP2 were transfected with deletion mutants of GFP-Smad7, Full length (F), N-terminus (N) and C-terminus (C). Co-precipitated deletion mutants of Smad7 with AIMP2 were analyzed by immunoprecipitation. The arrangement of domains in Smad7 were showed (bottom). **(F)** Deletion mutants of Myc-AIMP2, Full length, 1-83, 84-225 and 226-320 amino acids, were overexpressed into GFP-Smad7 expressed 293T cells. The cells were lysed and subjected to immunoprecipitation with anti-GFP antibody. Precipitates were separated in an SDS-PAGE and immunoblotted with anti-Myc and -GFP antibody. **(G)** GST proteins containing 84-119, 120-155, 156-191 and 192-225 amino acids region of AIMP2 were purified. Each purified GST protein was incubated with extracts from HeLa cells and pulled down with glutathione-Sepharose beads. The precipitated Smad7 was detected by Western blotting using anti-Smad7 antibody.

Figure II-5. AIMP2 specifically binds to Smad7

Figure II-5. AIMP2 specifically binds to Smad7. Plasmids encoding B42-AIMP2 was introduced into yeast cells which is transformed with Lex-Smad2, -Smad3, -Smad7, KRS and EV. The cell growth was observed in a leucine-depleted medium. Lysyl tRNA synthetase (KRS) and empty vector (EV) were used for, positive and negative control, respectively, about interaction of AIMP2.

Figure II-6. Ternary complex formation of AIMP2 with negative feedback complex of TGF-β signal

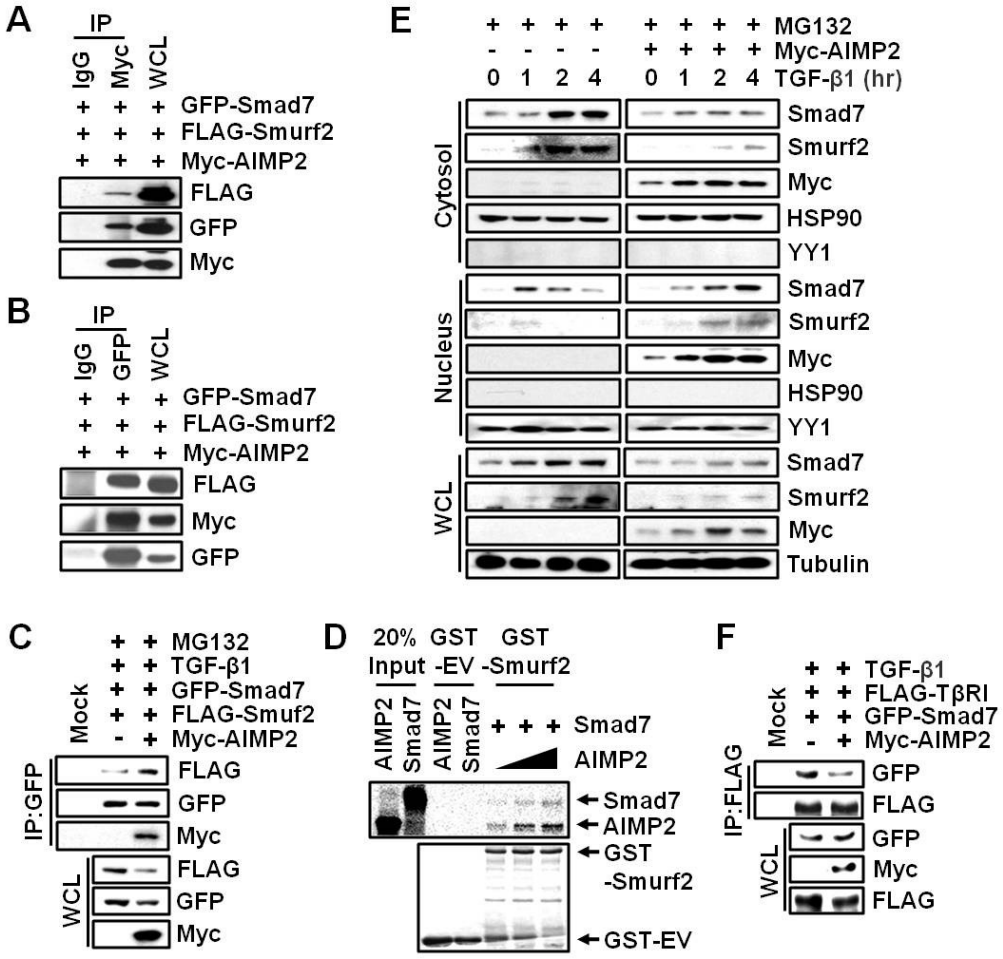

Figure II-6. Ternary complex formation of AIMP2 with negative feedback complex of TGF-β signal. **(A, B)** GFP-Smad7, FLAG-Smurf2 and Myc-AIMP2 were introduced into the 293T cells and treated with TGF-β1. The cells were immunoprecipitated with anti-Myc (A) and -GFP (B) antibody for precipitating of AIMP2 and Smad7, respectively. Each precipitates was separated by SDS-PAGE and immunonblotting with specific antibody. **(C)** The indicated combinatory overexpressed 293T cells were treated with MG132 and TGF-β1. Anti-GFP antibody was used for immunoprecipitation of Smad7. The amounts of co-precipitated Smurf2 were detected by western blotting. **(D)** Smad7 and AIMP2 were prepared by *in vitro* translation with [^{35}S] methionine. GST-

Smurf2 was mixed with prepared Smad7 and AIMP2 in different combination. GST-Smurf2 was precipitated with glutathione-Sepharose beads. Co-precipitated AIMP2 and Smad7 with Smurf2 were determined by autoradiography. **(E)** EV and Myc-AIMP2 transfected HeLa cells were pre-incubated with MG132 and treated time dependently with TGF-β1. The cells were subjected to fractionization and lysis for preparing cytosol and nucleus, and cell extracts, respectively. Each fraction and lysates was subjected to SDS-PAGE. HSP90, YY1 were used as loading control of cytosol and nucleus, respectively. **(F)** The cells transfected with indicated plasmids were immunoprecipitated with anti-FLAG antibody for precipitating TGF-β receptor I. The precipitates were separated with SDS-PAGE and immunobloted with specific antibody.

Figure II-7. AIMP2 enhances auto-ubiquitination of Smurf2

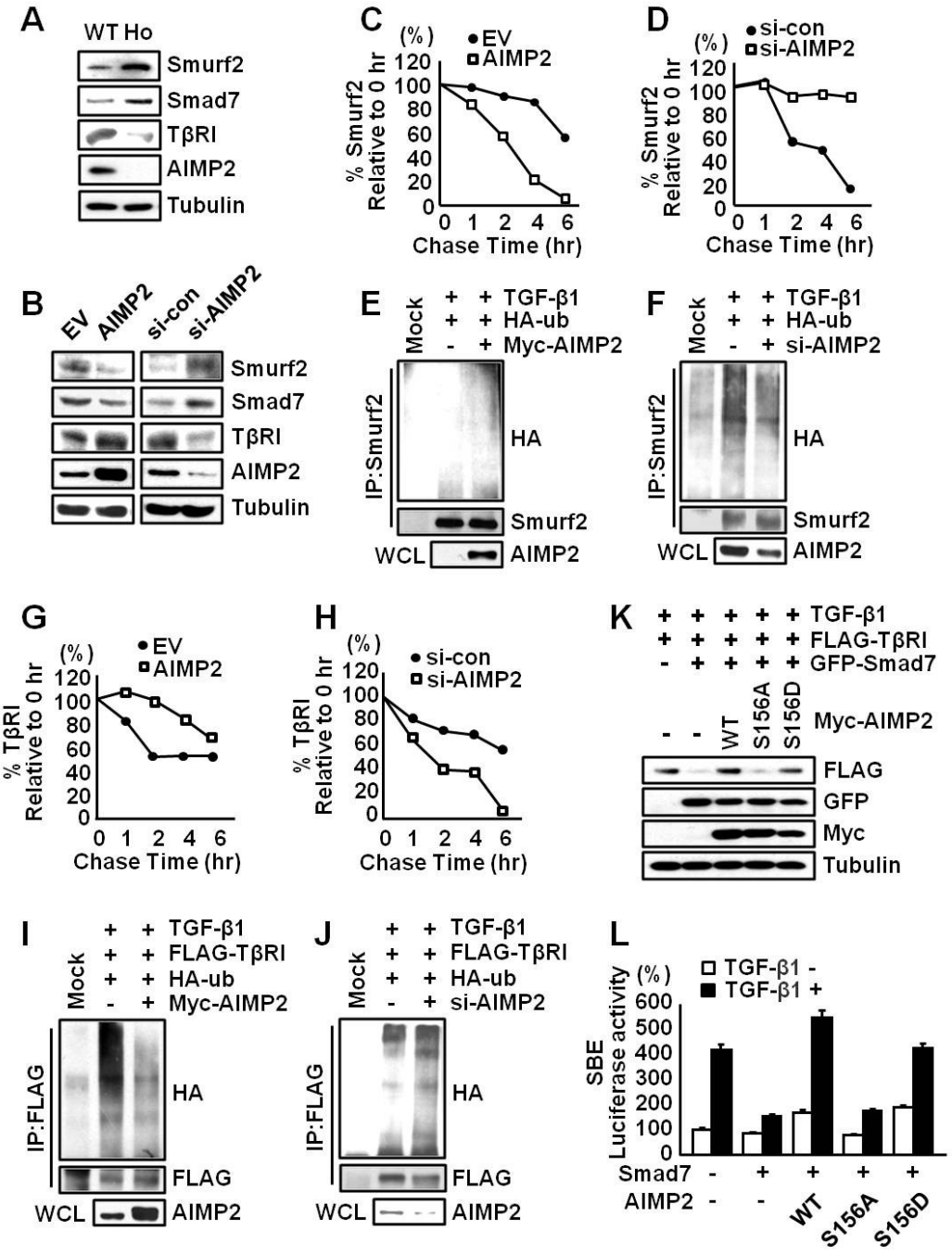

Figure II-7. AIMP2 enhances auto-ubiquitination of Smurf2. **(A)** The expression of Smurf2, Smad7 and TGF-β receptor I (TβRI) in AIMP2$^{-/-}$ MEF cells were compared to them in AIMP2$^{+/+}$ MEF cells. MEF cell extracts were subjected to SDS-PAGE and

analyzed by Western blotting using anti-Smurf2, -Smad7, -TβRI and -AIMP2 antibody. **(B)** AIMP2 were overexpressed (left) and knockdowned (right) in HeLa cells. The cells were lyzed and the expression of Smurf2, Smad7 and TGF-β receptor I was determined as above. **(C, D)** AIMP2 overexpressed (C) and knockdowned (D) HeLa cells were incubated in the presence of [^{35}S] methionine. Smruf2 was immunoprecipitated with anti-Smurf2 antibody, separated by SDS-PAGE, and autoradiographed. **(E, F)** HA-ub was introduced into 293T cells transfected as above. The cells were pre-treated and incubated with MG132 and TGF-β1, respectively. The lysates were precipitated with anti-Smurf2 antibody and the amounts of ubiquitinated Smurf2 was detected by using anti-HA antibody. **(G, H)** HeLa cells were transfected for overexpression (G) and knockdown (H) of AIMP2. The cells were labeled with [^{35}S] methionine. Immunoprecipitation of TGF-β receptor I was subjected for determining the amounts of radioactive TGF-β receptor I. **(I, J)** 293T cells were modified by transfection with Myc-AIMP2 and si-AIMP2 for overexpression and downregulation of AIMP2. FLAG-TGF-β receptor I and HA-ub were expressed into the each cell. Each cell treated with MG132 and TGF-β1 were immunoprecipitated with anti-FLAG antibody. **(K)** Indicated combination of FLAG-TGF-β receptor I, GFP-Smad7 and Myc-AIMP2 was used for monitoring of Smad7-mediated turnover of TGF-β receptor I. Extracts form transfected 293T cells were subjected to SDS-PAGE and immunobloted with specific antibody. **(L)** Myc-AIMP2, Smad7 and SBE-luciferase gene was transfceted into the HeLa cells as indicated combinatory manner and the cells were incubated with media with or without TGF-β1. The cells were subjected to luciferase assay.

Figure II-8. Smurf2 functions as E3 ligase of FBP via AIMP2

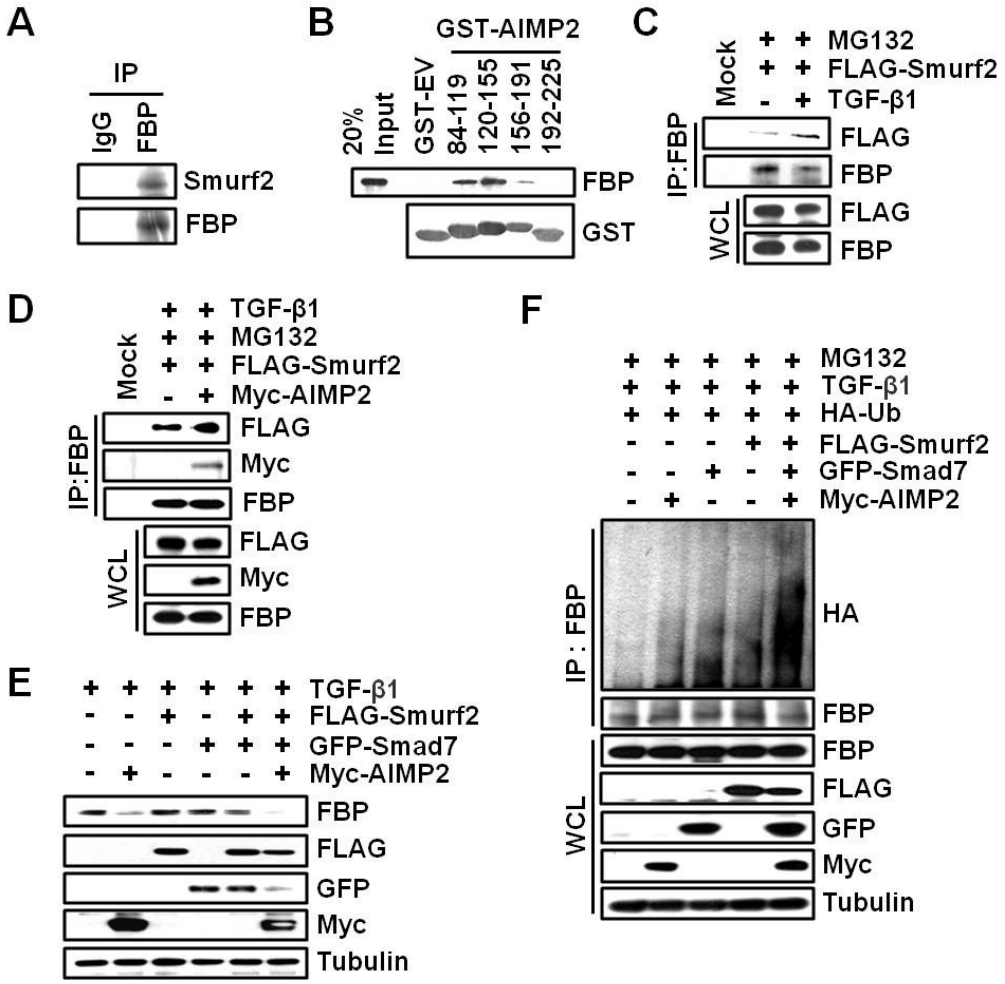

Figure II-8. Smurf2 functions as E3 ligase of FBP via AIMP2. **(A)** HeLa cells were treated with TGF-β1 and immunoprecipitated with anti-FBP antibody. Co-precipitated endogenous Smurf2 with FBP was detected with anti-Smurf2 antibody. **(B)** Extracts from HeLa cells were reacted with GST proteins containing amino acid region of AIMP2 84-119, 120-155, 156-191 and 192-225. Mixture was subjected to precipitation with glutathione-Sepharose beads. Co-precipitated GST protein was detected Western blotting using anti-FBP antibody. **(C)** FLAG-Smurf2 introduced 293T cells were pre-incubated with MG132 and cultured in medium with or without TGF-β1. Each cells was lysed and immunoprecipitated with anti-FBP antibody. Co-precipitated Smurf2 was detected by immunoblotting using anti-FLAG antibody. **(D)** FLAG-Smurf2 introduced

293T cells were overexpressed with EV or Myc-AIMP2. The cells were treated with MG132 and TGF-β1. Cells were immunoprecipitated with anti-FBP antibody and subjected to SDS-PAGE. **(E)** FLAG-Smurf2, GFP-Smad7 and Myc-AIMP2 introduced HeLa cells in different combinations were treated with TGF-β1. Extracts from the cells were separated by SDS-PAGE and subjected to Western blotting with specific antibody. **(F)** HA-ub was introduced into the same cells as above. The cells were subjected to immunoprecipitation using anti-FBP antibody and SDS-PAGE. The amounts of ubiquitinated FBP were determined by immunoblotting using anti-HA antibody.

Figure II-9. AIMP2 increases TGF-β signal-mediated cell cycle arrest

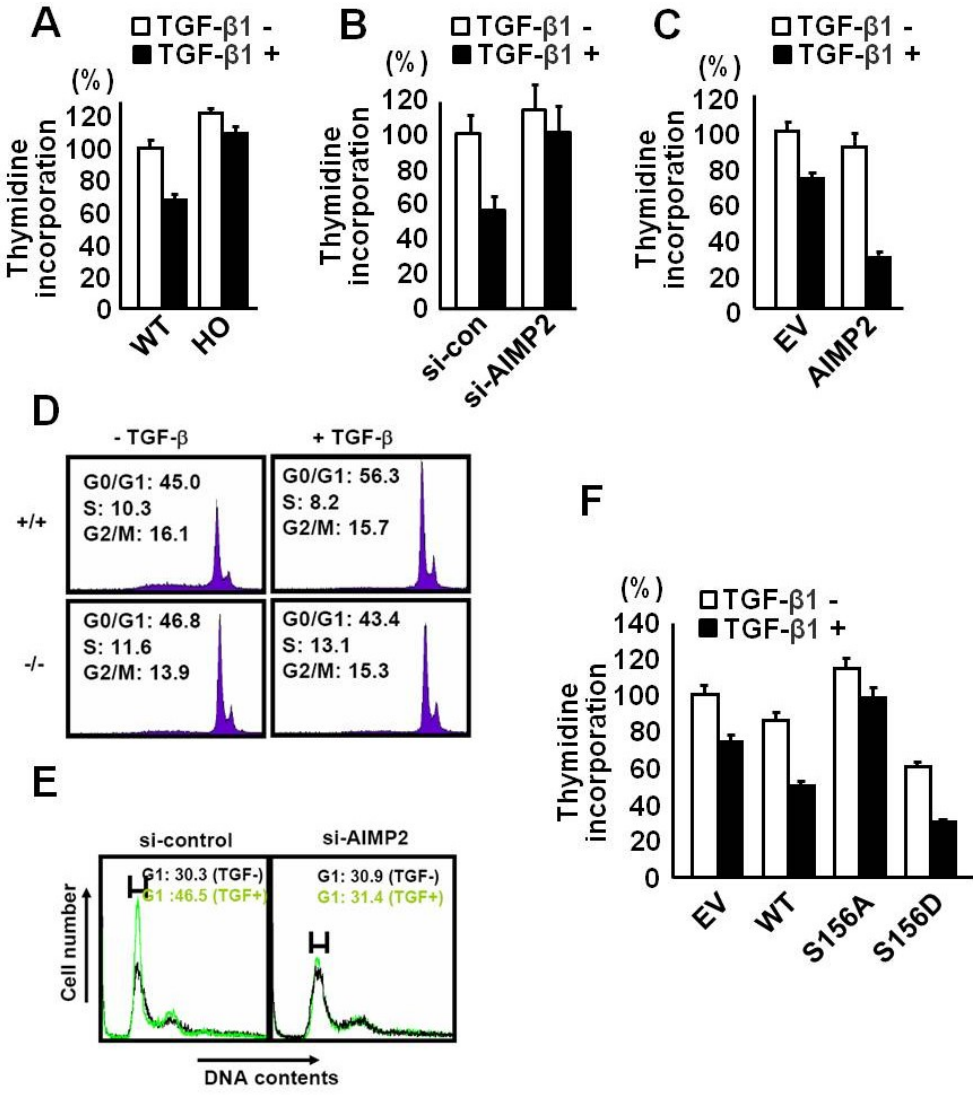

Figure II-9. AIMP2 increases TGF-β signal-mediated cell cycle arrest. **(A-C)** TGF-β dependent proliferation was checked in AIMP2 MEF (A), knockdowed (B) and overexpressed (C) HeLa cells by thymidine incorporation assay. Each cell was treated with TGF-β1 and incubated in medium with [^{3}H] thymidine. Proliferation was observed by detecting the radioactivity. **(D)** TGF-β signal-mediated cell cycle in AIMP2$^{-/-}$ MEF cells were compared to them in AIMP2$^{+/+}$ MEF cells. MEF cells were treated with TGF-β1 and monitored cell cycle by FACS analysis. **(E)** The effect of AIMP2 on TGF-β signal-mediated cell cycle was monitored in AIMP2 knockdownd HeLa cells by FACS

analysis as above. **(F)** AIMP2 wild type (WT), S156A and S156D mutants were expressed into HeLa cells. The cells were treated or not with TGF-β1 and cultivated in media containing [^{35}H] thymidine. Proliferation was determined by detecting the radioactivity.

Figure II-10. Schematic summary of AIMP2-mediated enhancement of TGF-β signal

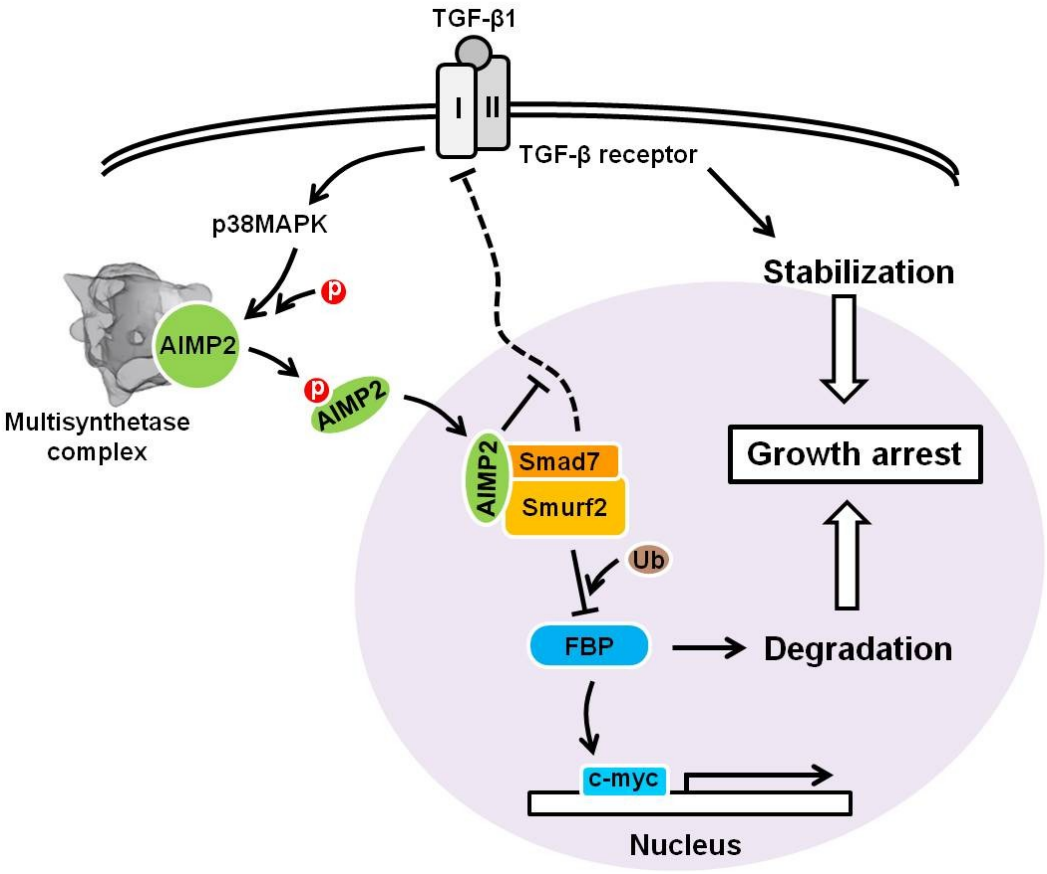

Figure II-10. Schematic summary of AIMP2-mediated enhancement of TGF-β signal. Upon TGF-β signal, activated p38MAPK-mediated phosphorylation of AIMP2 at serine 156 residue leads to nuclear translocation of it. In nucleus AIMP2 forms the ternary complex with Smad7 and Smurf2, negative feedback molecules of TGF-β signal. Ternary complex is accumulated in nucleus and degraded with FBP, novel target of Smurf2, by Smuf2-mediated auto-ubiquitination. AIMP2-mediated accumulation of Smurf2 and Smad7 leads to increase of TGF-β signal, resulting the augment of TGF-β signal-dependent cell cycle arrest and cell death.

Discussion

Negative feedback is critical for maintaining the cellular homeostasis. So, fine regulating of negative feedback is important to survival or death of cells. Also, ruin of negative feedback is the cause of disease, specifically cancer (31, 32). Negative feedback of TGF-β signal is the important on TGF-β signal-mediated cell cycle arrest, proliferation and apoptosis (8). Irregular control of TGF-β signal via abnormal negative feedback is observed in many cancers (9, 33). Here it was identified that AIMP2, scaffolding protein of multisynthetase complex (MSC), controls the negative feedback of TGF-β signal. TGF-β signal-mediated phosphorylation of AIMP2 via p38MAPK drives AIMP2 to nuclear translocation from cytosol. In nucleus, AIMP2 forms the ternary complex with Smad7 and Smuf2, negative feedback molecules of TGF-β signal, and AIMP2 in ternary complex inhibits the nuclear export of them. The accumulated Smurf2 is subjected to auto-ubiquitination and also ubiquitinates the novel nuclear target, FBP. Auto-ubiquitination of Smurf2 via AIMP2 in nucleus leads the stabilization of TGF-β receptor I, resulting in the augment of TGF-β signaling. Also Smurf2-mediated degradation of FBP causes downregulation of c-myc, implying the suppression of proliferation (Figure II-10).

Tumor suppressive effect of AIMP2 is related with various signals (23). Upon UV signal, AIMP2 translocates into nucleus to activate p53 and drives to cell death (21). AIMP2 also inhibits the proliferation through TNF-α signal-mediated degradation of TRAF2 (22). AIMP2 facilitates the turnover of c-myc via ubiquitination of FBP, transcriptional regulator of c-myc (24). Also, it was unveiled AIMP2 enhances TGF-β signal in normal, cancer and mouse embryonic fibroblast cell lines. These mean that the role of AIMP2 on regulation of TGF-β signal is commonly meaningful in physiological and pathological condition. In normal environment, it was speculated that AIMP2 inhibits the approach of pre-existed, not induced, Smad7 and Smurf2 to TGF-β receptor I. These functions of AIMP2 make the TGF-β signal transduction well in early TGF-β signal period prior to the induction of Smad7

It was showed that AIMP2 is phosphorylated and translocated to nucleus by TGF-β signal. Phosphorylation is the important post translational modification to control the molecular function. In addition to canonical scaffolding function of AIMP2 in MSC, AIMP2 is phosphorylated by TGF-β signal for non-canonical function. The utilization of AIMP2 via phophorylation for fine tuning of TGF-β signal means that AIMP2 is significant molecule in TGF-β signal. Previous report showed that AIMP2 is phosphorylated by UV damage for translocation into nucleus (21). Combined together,

phosphorylation of AIMP2 is critical for non-canonical function, especially translocation from cytosol. The identification of phosphorylation site by UV is the further task for comprehension of the translocation of AIMP2.

For efficient translation, 9 ARSs form the MSC with three non-enzymatic factors, AIMPs. Among 3 AIMPs, AIMP2 specifically makes the MSC stable via interaction with associated ARSs in MSC. AIMP2-mediated augmentation of binding with associated molecule is also adapted to the interaction between TRAF2 and c-IAP1 for degradation of TRAF2 (22). Interestingly, AIMP2 also stabilizes the complex of TGF-β signal negative feedback, Smad7 and Smurf2, via enhancing the interaction. So, AIMP2 dependent-stabilization of associated molecule via interaction is the critical for AIMP2 mediated-control of various signaling pathway.

c-myc is the critical oncogene in progression and development of cancer, and its enhanced expression is well reported (34). So, control of c-myc is the target of efficient cancer therapy (34). Previously it was reported AIMP2 downregulates c-myc via facilitating the ubiquitination of FBP, transcriptional regulator of c-myc (24). Although degradation of FBP is increased by AIMP2, how AIMP2 regulates the ubiquitination of FBP in nucleus is not clear by this time. In this paper, I elucidate the detailed degradation mechanism of FBP. Accumulated Smurf2 in nucleus via AIMP2 works as

E3 ligase of FBP and AIMP2 enhances the interaction of FBP to Smurf2, substrate and E3 ligase, respectively.

AIMP2, also known potent tumor suppressor, facilitates the TGF-β signal through the stabilization of TGF-β receptor I via inhibiting negative feedback. I suggest that AIMP2 is a novel member of TGF-β signal, implying TGF-β signal-mediated tumor suppressor.

Materials and methods

Cell culture and materials

293T and HeLa cells were purchased from American Type Culture Collection. AIMP2 knockout mouse embryonic fibroblasts (MEF) were isolated from 12.5 - 14.5 day embryos. Dulbecco's Modified Eagle Medium containing 10% fetal bovine serum and 1% antibiotics were used for cell cultivation. Myc-tagged human AIMP2 was cloned at the EcoRI/XhoI sites of pcDNA3.0. FLAG-tagged TGF-β receptor I, FLAG-tagged Smad1, Smad2, Smad3, Smad5, Smad6, Smad7 and GFP-tagged Smad7 wild type, N-terminal fragment, C-terminal fragment were kind gifts from Dr. Seong Jin Kim (Cha Univ.). FLAG-tagged Smurf2 was kindly gifted from Dr. Suk-Chul Bae (Chungbuk National Univ.). Myc-, GFP- and GST-tagged AIMP2 containing point mutation of serine 156, 157 and 160 were cloned using the QuikChange® Ⅱ (Agilent), following the manufacturer's instruction. The siRNA targeting AIMP2 was designed as the sequence of AGAGCUUGCAGAGACAGGUUAGACU. The cells were separated to cytosol and nucleus fractions using Proteoextract kit (Calbiochem), following the manufacturer's instruction. TGF-β1 (5ng/ml) was purchased from R&D Systems. MG132 were purchased from Calbiochem. SB202190, SP600125 and anti-FLAG antibody were

purchased from Sigma-Aldrich. Antibodies against AIMP2 was purchased from Abcam. Anti-p-Smad2 and -Smad2 antibodies were purchased from Cell signaling. The other antibodies using in this study were purchased from Santa Cruz Biotechnology.

Immunoprecipitation

The cells were lysed with 50 mM Tris-HCl (pH 7.4) buffer containing 100 mM NaCl, 0.5% Triton X-100, 0.05% SDS, 10% glycerol, 1 mM EDTA and protease inhibitor (Calbiochem). To remove the nonspecific IgG bound proteins, protein extracts were incubated with normal IgG and protein agarose for 2 h and then centrifuged. The supernatants were mixed with specific antibody, incubated the mixture for 4 h at 4^{o}C with gentle agitation, added protein agarose. After agitation, precipitates were washed with the cold lysis buffer three times, and precipitates were dissolved in the SDS sample buffer and subjected to SDS-PAGE.

***In vitro* binding assay**

To detect the direct interaction, GST-proteins were mixed with proteins prepared by *in vitro* translation (Promega) in the presence of [^{35}S] methionine (PerkinElmer) or cell extract in PBS for 6 h at 4^{o}C. After incubation, mixed GST-proteins were precipitated

with glutathione-Sepharose beads and washed with cold PBS three times. Co-precipitates with GST-proteins were subjected to SDS-PAGE. The separated precipitates were detected by autoradiography using using BAS (FLA-3000, Fujifilm) and analyzed by Multi-Gauge program (V3.0, Fujifilm) or Western blotting with specific antibody.

Flow cytometry analysis

To determine the effect of AIMP2 on TGF-β-mediated cell cycle, $AIMP2^{+/+}$, $AIMP2^{-/-}$ MEF cells and AIMP2 knockdowned HeLa cell lines were incubated in TGF-β1 contained 0.5% serum containing medium for 12 h. After incubation, harvested cells were fixed with 70% ethanol for 1 h at 4^{o}C and washed twice with cold PBS. The cells were stained with propidium iodide (50 μg/ml), 0.1% sodium citrate, 0.3% NP40 and RNaseA (50 μg/ml) for 40 min, and subjected to flow cytometry (FACSCalibur, Becton-Dickinson). For each sample, 20,000 cells were analyzed using Cell Quest Pro software.

Pulse-chase assay

The cells were incubated with methionine-free medium for 1 h. Then, [^{35}S] methionine (50 μCi/ml) was added and incubated for 1 h. After washing off the radioactive methionine with fresh medium, the cells cultivated in complete medium for 4 h were

harvested at the time interval. Target proteins were immunoprecipitated with specific antibody, and precipitates were subjected to SDS-PAGE. Autoradiography detected by using BAS (FLA-3000, Fujifilm) was quantified by Multi-Gauge program (V3.0, Fujifilm) and visualized as bar graph.

Ubiquitination assay

The cells were pre-incubated with MG132 for 4 h (50 μM), and treated with TGF-β1. The cells were lysed with 50 mM Tris-HCl (pH 7.4) buffer containing 100 mM NaCl, 0.5% Triton X-100, 0.1% SDS, 10% glycerol, 1 mM EDTA and protease inhibitor (Calbiochem). The interesting proteins were immunoprecipitated with specific antibody and subjected SDS-PAGE for immunoblotting to determine the amounts of ubiquitinated protein.

***In vitro* kinase assay**

p38MAPK was prepared by immuneprecipitation using anti-p38MAPK antibody in TGF-β1-treated cells. Purified GST-tagged AIMP2 was pre-incubated (30 min, 4°C) with immunoprecipitated p38MAPK in buffer containing 50 mM Tris-HC1 (pH 7.3), 100 mM NaC1, 10 mM MnC12, 10%(vol/vol) glycerol, 5 mM dithiothreitol, and 0.05%

Triton X-100. After pre-incubation, reaction was carried out in the presence of [γ-^{32}P] ATP 10 μCi (3000 Ci/mmol) at 28°C for 20 min and stopped by the addition of the SDS sample buffer. The proteins in the reaction mixture were separated by SDS-PAGE and autoradiographed (FLA-3000, FUJIFILM).

Thymidine incorporation

HeLa cells introduced by using transfection with Myc-AIMP2 and si-AIMP2 were treated with TGF-β1 for 12 h. AIMP2$^{+/+}$ and AIMP2$^{-/-}$ MEF cells were cultivated in medium with TGF-β1 for 12 h. Each cell was incubated with 1 μCi/ml of [^{3}H] thymidine for 4 h. The incorporated thymidine was measured by liquid scintillation counter (Wallac). Counted radioactivity was presented as bar graph. The experiments were repeated independently at three times.

Reporter gene assay

HeLa cells expressed pSBE-lux were transfected with Myc-AIMP2 or si-AIMP2 to overexpress or suppress the expression of AIMP2, respectively. Also, pSBE-lux was introduced into AIMP2$^{+/+}$ and AIMP2$^{-/-}$ MEF cells. The cells were treated with TGF-β1 for 24 h. Luciferase activity was measured by using Luciferase Assay System following

the manufacturer's protocol (Promega, USA). Determined activity was showed as a bar graph and the experiments were repeated independently at three times.

Two-dimensional electrophoresis

HeLa cells were treated with TGF-β1 time dependently. The cells were lysed in 2D-lysis buffer containing 7 M urea, 2 M thiourea, 1% ASB-14, 40 mM Tris, and 2% tributylphosphine. Alkaline phosphatase was added in the extracts for 4 h. Cell lysates were loaded onto immobilized pH gradient strip gels (linear pH gradient 7–10, 7 cm). Isoelectric focusing was performed at 4,000 V until the total volt-hours reached 15 kV-hours by using a PROTEAN isoelectric focusing cell (Bio-Rad). After two-step equilibration with 375 mM Tris-HCl (pH 8.8), 6 M urea, 2% SDS, 20% glycerol, 2% DTT, and 2.5% iodoacetamide, the immobilized pH gradient strips were embedded on top of 12% SDS/PAGE gels and sealed with 1% agarose. Proteins were separated by SDS-PAGE and detected by immunoblotting with using anti-AIMP2 antibody.

Immunofluorescence staining

HeLa cells were expressed with GFP-AIMP2 wild type, S156A and S156D mutants. Each transfected cells were treated with TGF-β1 for 2 h and then washed briefly with

cold PBS. After incubation with the blocking buffer, 1% CAS, for 30 min and mounted with mounting solution containing DAPI (ImmunoBioScience Corp.). The mounted samples were observed by confocal laser-scanning microscopy.

Yeast two-hybrid analysis

It is obtained the cDNA encoding human KRS by PCR with the primers containing *EcoR*I and *Xho*I sites. The product was digested and sub-cloned into pJG4-5 vector (for the construction of B42-fusion proteins) via *EcoR*I and *Xho*I sites. As above, cDNAs of Smad2, Smad3, Smad7, lysyl-tRNA synthetase (KRS) were introduced into pEG202 (for the construction of LexA-fusion proteins). The cDNA encoding Smad2, Smad3, Smad7 was kindly gifted from Seong Jin Kim (Cha Univ.) Each clone was tranfromed into yeast cells as pair of pJG4-5 and pEG202. Interaction was detected by growth in leucine-depleted medium. KRS was used as positive control for analysis.

References

1. Siegel, P. M., and Massague, J. (2003) Cytostatic and apoptotic actions of TGF-beta in homeostasis and cancer. *Nat Rev Cancer* **3**, 807-821
2. Massague, J. (2000) How cells read TGF-beta signals. *Nat Rev Mol Cell Biol* **1**, 169-178
3. Massague, J. (2008) TGFbeta in Cancer. *Cell* **134**, 215-230
4. Ikushima, H., and Miyazono, K. (2010) TGFbeta signalling: a complex web in cancer progression. *Nat Rev Cancer* **10**, 415-424
5. Meulmeester, E., and Ten Dijke, P. (2011) The dynamic roles of TGF-beta in cancer. *J Pathol* **223**, 205-218
6. Massague, J., and Chen, Y. G. (2000) Controlling TGF-beta signaling. *Genes Dev* **14**, 627-644
7. Hayashi, H., Abdollah, S., Qiu, Y., Cai, J., Xu, Y. Y., Grinnell, B. W., Richardson, M. A., Topper, J. N., Gimbrone, M. A., Jr., Wrana, J. L., and Falb, D. (1997) The MAD-related protein Smad7 associates with the TGFbeta receptor and functions as an antagonist of TGFbeta signaling. *Cell* **89**, 1165-1173
8. Itoh, S., and ten Dijke, P. (2007) Negative regulation of TGF-beta receptor/Smad signal transduction. *Curr Opin Cell Biol* **19**, 176-184
9. Izzi, L., and Attisano, L. (2004) Regulation of the TGFbeta signalling pathway by ubiquitin-mediated degradation. *Oncogene* **23**, 2071-2078
10. Wiesner, S., Ogunjimi, A. A., Wang, H. R., Rotin, D., Sicheri, F., Wrana, J. L., and Forman-Kay, J. D. (2007) Autoinhibition of the HECT-type ubiquitin ligase Smurf2 through its C2 domain. *Cell* **130**, 651-662
11. Ogunjimi, A. A., Briant, D. J., Pece-Barbara, N., Le Roy, C., Di Guglielmo, G. M., Kavsak, P., Rasmussen, R. K., Seet, B. T., Sicheri, F., and Wrana, J. L. (2005) Regulation of Smurf2 ubiquitin ligase activity by anchoring the E2 to the HECT domain. *Mol Cell* **19**, 297-308
12. Kavsak, P., Rasmussen, R. K., Causing, C. G., Bonni, S., Zhu, H., Thomsen, G. H., and Wrana, J. L. (2000) Smad7 binds to Smurf2 to form an E3 ubiquitin ligase that

targets the TGF beta receptor for degradation. *Mol Cell* **6**, 1365-1375

13. Park, S. G., Ewalt, K. L., and Kim, S. (2005) Functional expansion of aminoacyl-tRNA synthetases and their interacting factors: new perspectives on housekeepers. *Trends Biochem Sci* **30**, 569-574

14. Han, J. M., Lee, M. J., Park, S. G., Lee, S. H., Razin, E., Choi, E. C., and Kim, S. (2006) Hierarchical network between the components of the multi-tRNA synthetase complex: implications for complex formation. *J Biol Chem* **281**, 38663-38667

15. Kim, S., You, S., and Hwang, D. (2011) Aminoacyl-tRNA synthetases and tumorigenesis: more than housekeeping. *Nat Rev Cancer* **11**, 708-718

16. Park, S. G., Kang, Y. S., Ahn, Y. H., Lee, S. H., Kim, K. R., Kim, K. W., Koh, G. Y., Ko, Y. G., and Kim, S. (2002) Dose-dependent biphasic activity of tRNA synthetase-associating factor, p43, in angiogenesis. *J Biol Chem* **277**, 45243-45248

17. Ko, Y. G., Park, H., Kim, T., Lee, J. W., Park, S. G., Seol, W., Kim, J. E., Lee, W. H., Kim, S. H., Park, J. E., and Kim, S. (2001) A cofactor of tRNA synthetase, p43, is secreted to up-regulate proinflammatory genes. *J Biol Chem* **276**, 23028-23033

18. Park, S. G., Kang, Y. S., Kim, J. Y., Lee, C. S., Ko, Y. G., Lee, W. J., Lee, K. U., Yeom, Y. I., and Kim, S. (2006) Hormonal activity of AIMP1/p43 for glucose homeostasis. *Proc Natl Acad Sci U S A* **103**, 14913-14918

19. Park, B. J., Kang, J. W., Lee, S. W., Choi, S. J., Shin, Y. K., Ahn, Y. H., Choi, Y. H., Choi, D., Lee, K. S., and Kim, S. (2005) The haploinsufficient tumor suppressor p18 upregulates p53 via interactions with ATM/ATR. *Cell* **120**, 209-221

20. Oh, Y. S., Kim, D. G., Kim, G., Choi, E. C., Kennedy, B. K., Suh, Y., Park, B. J., and Kim, S. (2010) Downregulation of lamin A by tumor suppressor AIMP3/p18 leads to a progeroid phenotype in mice. *Aging Cell* **9**, 810-822

21. Han, J. M., Park, B. J., Park, S. G., Oh, Y. S., Choi, S. J., Lee, S. W., Hwang, S. K., Chang, S. H., Cho, M. H., and Kim, S. (2008) AIMP2/p38, the scaffold for the multi-tRNA synthetase complex, responds to genotoxic stresses via p53. *Proc Natl Acad Sci U S A* **105**, 11206-11211

22. Choi, J. W., Kim, D. G., Park, M. C., Um, J. Y., Han, J. M., Park, S. G., Choi, E. C., and Kim, S. (2009) AIMP2 promotes TNFalpha-dependent apoptosis via ubiquitin-mediated degradation of TRAF2. *J Cell Sci* **122**, 2710-2715

23. Choi, J. W., Um, J. Y., Kundu, J. K., Surh, Y. J., and Kim, S. (2009) Multidirectional tumor-suppressive activity of AIMP2/p38 and the enhanced susceptibility of AIMP2 heterozygous mice to carcinogenesis. *Carcinogenesis* **30**, 1638-1644

24. Kim, M. J., Park, B. J., Kang, Y. S., Kim, H. J., Park, J. H., Kang, J. W., Lee, S. W., Han, J. M., Lee, H. W., and Kim, S. (2003) Downregulation of FUSE-binding protein and c-myc by tRNA synthetase cofactor p38 is required for lung cell differentiation. *Nat Genet* **34**, 330-336

25. Zhang, Y. E. (2009) Non-Smad pathways in TGF-beta signaling. *Cell Res* **19**, 128-139

26. Bonni, S., Wang, H. R., Causing, C. G., Kavsak, P., Stroschein, S. L., Luo, K., and Wrana, J. L. (2001) TGF-beta induces assembly of a Smad2-Smurf2 ubiquitin ligase complex that targets SnoN for degradation. *Nat Cell Biol* **3**, 587-595

27. Hanyu, A., Ishidou, Y., Ebisawa, T., Shimanuki, T., Imamura, T., and Miyazono, K. (2001) The N domain of Smad7 is essential for specific inhibition of transforming growth factor-beta signaling. *J Cell Biol* **155**, 1017-1027

28. Nalepa, G., Rolfe, M., and Harper, J. W. (2006) Drug discovery in the ubiquitin-proteasome system. *Nat Rev Drug Discov* **5**, 596-613

29. Wang, J., Han, W., Zborowska, E., Liang, J., Wang, X., Willson, J. K., Sun, L., and Brattain, M. G. (1996) Reduced expression of transforming growth factor beta type I receptor contributes to the malignancy of human colon carcinoma cells. *J Biol Chem* **271**, 17366-17371

30. Zeng, Q., Phukan, S., Xu, Y., Sadim, M., Rosman, D. S., Pennison, M., Liao, J., Yang, G. Y., Huang, C. C., Valle, L., Di Cristofano, A., de la Chapelle, A., and Pasche, B. (2009) Tgfbr1 haploinsufficiency is a potent modifier of colorectal cancer development. *Cancer Res* **69**, 678-686

31. Nakamura, M., Kitaura, J., Enomoto, Y., Lu, Y., Nishimura, K., Isobe, M., Ozaki, K., Komeno, Y., Nakahara, F., Oki, T., Kume, H., Homma, Y., and Kitamura, T. (2011) Transforming growth factor-beta-stimulated clone-22 is a negative-feedback regulator of Ras / Raf signaling: Implications for tumorigenesis. *Cancer Sci*

32. Lee, M. H., Mabb, A. M., Gill, G. B., Yeh, E. T., and Miyamoto, S. (2011) NF-

kappaB induction of the SUMO protease SENP2: A negative feedback loop to attenuate cell survival response to genotoxic stress. *Mol Cell* **43**, 180-191

33. Kleeff, J., Ishiwata, T., Maruyama, H., Friess, H., Truong, P., Buchler, M. W., Falb, D., and Korc, M. (1999) The TGF-beta signaling inhibitor Smad7 enhances tumorigenicity in pancreatic cancer. *Oncogene* **18**, 5363-5372

34. Albihn, A., Johnsen, J. I., and Henriksson, M. A. (2010) MYC in oncogenesis and as a target for cancer therapies. *Adv Cancer Res* **107**, 163-224

국문초록

암 세포 증식과 이동에서의 Lysyl-tRNA Synthetase 와 Aminoacyl-tRNA Synthetase-Interacting Multi-functional Protein2 의 역할 규명

Aminoacyl-tRNA synthetases (ARSs)는 단백질 합성과정 중 tRNA 에 상보적인 아미노산을 결합시켜주는 효소이다. 이 중 9 개의 ARS 는 multi-tRNA synthetase complex (MSC)를 형성하며, 이 밖에도 MSC 안에는 효소의 활성을 갖지 않으면서 MSC 골격 유지에 중요한 AIMP (Aminoacyl-tRNA synthetase interacting multifunctional protein) 1, 2, 3 으로 명명된 보조인자가 포함되어 있다. Lysine 을 $tRNA^{Lys}$ 에 전달해주는 Lysyl-tRNA synthetase (KRS)는 MSC 안에서 AIMP2 와 강하게 결합하고 있다.

Lysyl-tRNA synthetase (KRS)는 ribosome 구성요소 중 하나인 p40/37LRP 의 dimer 형태인 67kDa laminin receptor (67LR)와 세포막에서 결합하여 세포 이동에 중요한 역할을 하게 된다. 67LR 은 세포이동과 암전이의 주요인자로 보고되어있다. 본 연구는 KRS 를 통한 67LR 의 안정화가 일반 세포의 경우 세포이동을 촉진하며, 암세포의 경우 암세포의 이동을 촉진시켜 암 전이를 돕는 작용을 한다는 것을 규명하였다. Laminin

신호가 전달되면 KRS 는 52 번 threonine 잔기에 인산화가 일어난 후 MSC 에서 분리되어 세포막으로 이동하게 된다. 세포막으로 이동한 KRS 는 67LR 과 결합하여 E3 ligase 중 하나인 Nedd4 에 의한 67LR 의 분해를 저해하고 67LR 의 안정화에 기여한다.

KRS 와 강한 결합을 하는 AIMP2 는 KRS 와 반대로 TGF-β 신호에 의해 암 세포 증식 억제 인자로써 작용한다. TGF-β 신호는 세포 증식을 억제하는 신호이다. 본 연구는 AIMP2 가 TGF-β 신호를 촉진시키고, c-myc 의 발현을 감소시킴으로써 세포의 증식 및 분열을 억제하여 항암기능을 나타냄을 규명하였다. TGF-β 신호가 전달되면 AIMP2 는 156 번 serine 잔기의 인산화를 통해 핵 안으로 들어가게 된다. 핵 안에서 AIMP2 는 TGF-β 신호의 억제인자로 알려져 있는 Smurf2-Smad7 complex 의 분해를 촉진시킴으로써 TGF-β 수용체의 안정성을 증가시킨다. 또한 이 분해과정을 이용하여 AIMP2 는 암 유발인자인 c-myc 의 상위인자인 FBP 를 분해시켜 c-myc 의 발현 또한 감소시킨다.

앞의 2 가지 연구를 통해 MSC 내에서 상호작용하는 KRS 와 AIMP2 가 암 세포 이동 (KRS)과 암 세포 성장 억제 (AIMP2)의 상반된 기능을 수행한다는 사실을 규명하였다. 위의 연구를 통해 KRS 와 AIMP2 는

암 전이와 증식을 조절할 수 있는 암 치료의 혁신적 표적으로서의 가치를 지님을 알 수 있다.

주요어: Lysyl-tRNA synthetase (KRS)/ Laminin 수용체/ Laminin 신호/ 세포이동/ AIMP2/ TGF-β 신호/ TGF-β 수용체/ Smurf2-Smad7/ FBP/ 세포증식

학번: 2007-30945